Design and Performance Improvement of Electrically Small Feeds for Prime Focus Reflectors

By

Mohammad Qudrat-E-Maula

A thesis submitted to the Faculty of Graduate Studies of
The University of Manitoba
in partial fulfilment of the requirements of the degree of

DOCTOR OF PHILOSOPHY

DEPARTMENT OF ELECTRICAL AND COMPUTER ENGINEERING
UNIVERSITY OF MANITOBA
WINNIPEG, MANITOBA, CANADA

Abstract

In this thesis, two new types of electrically small feed antennas, slotted circular waveguide feeds, and microstrip dipole feeds are designed and studied for prime focus reflectors. The existing electrically small feeds used in prime focus reflectors exhibit some limitations such as asymmetrical radiation patterns, complex integration with microwave devices, requirement of struts support, and high cost. The design of these two new kinds of feeds is of particular interest since they provide symmetrical radiation pattern, and are low profile, easy to fabricate, simpler to mount on the reflector system, and low cost.

Circular waveguide feeds have been a good choice for prime focus reflector systems. The main drawback of these feeds is that the E- and H-plane radiation patterns are not equal in small diameter apertures, and hence the reflector efficiency is low. In this report, an attempt is made to equalize the radiation patterns of these feeds, by slotting their wall at the open-end. Even though radiation pattern equalization is possible with these feeds, the efficiency remains still low. Therefore, chokes are introduced with the slotted waveguide feeds to improve the radiation characteristics as well as the efficiency. Slotted circular waveguides with a cavity is also studied, where slots are used as additional parameters, to equalize their radiation patterns, and hence increase the efficiency.

In the second part of the thesis, microstrip dipole feeds are studied because of their light weight, low aperture blockage and ease of assembly on the reflector system. These feeds are designed for backward radiation and thus eliminate strut support. Parametric studies are conducted to improve the input impedance, miniaturize the antenna, and design for dual frequency operation. All these feeds have unequal E- and H-plane radiation patterns. Therefore, they are candidates for elliptical reflector system.

To improve the pattern equalization of microstrip dipole feeds, the dipole arms are modified. Two techniques are used for this purpose, bending microstrip dipole arms, or adding corrugations. In the bent microstrip dipole case, the design is suitable for narrow band operation. In order to improve the input impedance while equalizing the radiation patterns, a corrugated microstrip dipole is designed and investigated. Satisfactory performance is obtained.

All feed examples studied in this thesis are fabricated and experimentally evaluated for the input impedance match and performance on a reflector. Satisfactory results are obtained.

Acknowledgments

I would like to express my sincere gratitude to my supervisor Professor Lotfollah Shafai for giving me the opportunity to work on this project. His patience, constant encouragement and supports are invaluable to me throughout this thesis work. I would also like to thank the members of my examining committee, Dr. Behzad Kordi, and Dr. Wooil M. Moon from the University of Manitoba and Dr. Safieddin Safavi-Naeini from University of Waterloo.

I would like to thank Dr. Syeed Iftekhar Reza Latif, and Dr. Alireza Foroozesh for their comments and insights. Many thanks go to all my friends and colleagues in the EM group who were really helpful to me throughout this research, with deep and valuable discussions and suggestions. Special thanks to Cory Smit for fabricating the antennas, Brad Tabachnick for the antenna measurements, and Shelly Girardin for her extensive helps, whenever it was needed, during my studies at the university.

I would especially like to thank my parents for their encouragement in my quest for higher education and also my wife for her continuous support to finish the thesis successfully.

Dedication

To my parents

Table of Contents

List of Tables

List of Figures

List of Symbols

θ_0	aperture angle or subtended half angle
ϕ	azimuth angle
$\boldsymbol{\eta}_c$	cross-polarization efficiency
D	diameter of the reflector
θ	elevation angle
ε_{eff}	effective dielectric constant
E	electric field
f	focal length of the reflector
fr	frequency of the antenna
ε_0	free space permittivity
G	gain of the antenna
$\boldsymbol{\eta}_g$	gain factor
$\boldsymbol{\eta}_i$	illumination efficiency
Z_{in}	input impedance of transmission line
$\boldsymbol{\eta}_0$	intrinsic impedance
H	magnetic field
d	phase center location; from the waveguide face (waveguide case) or from the co-axial feed point of the feed line (microstrip case)

$\boldsymbol{\eta}_p$	phase efficiency
Ψ	phase angle of radiated field
Γ	reflection coefficient
ε_r	relative dielectric constant
μ_r	relative permeability
S_{11}	return loss
$\boldsymbol{\eta}_s$	spillover efficiency
λ_0	wavelength in free space
λ_d	wavelength in the dielectric substance
k	wave number

Chapter 1

Introduction

1.1 Overview

Reflector antennas have been used since the discovery of the radio waves by Hertz in 1887 [1]. It evolved during the World War II, when numerous radar applications were developed. During 1950s, further modifications to these antennas were made possible due to the development of microwave communication systems and utilization of radio telescopes in astronomy. Along with these developments, reflectors were simultaneously employed at earth stations in the USA, Canada, UK, France and other countries [2]. Reflector antennas are also used in remote sensing [3], RADAR [4], or military applications [5]. All these applications require efficient feeds, if the benefit of the reflector antennas is to be realised. Therefore, continuous efforts have been made to develop more sophisticated feed designs.

A reflector antenna consists of a primary feed, to radiate electromagnetic wave and a curved reflecting surface in order to collimate these waves over a larger secondary aperture. The feed, being located at the focal point of the reflector, acts as a point source

and produces spherical waves which are reflected by the parabolic surface into a plane wave. Therefore, it provides a uniform phase distribution over the reflector aperture.

Reflector antennas can be of different types based on the location of feeds used in the antenna. The simplest form of a reflector antenna is the prime focus reflector, with a feed located at its focal point. Another type of reflector antennas is dual reflector system, where the primary feed is located near the rear of the main reflector, and a small sub-reflector is used in front of it for illumination. Aperture blockage caused either by the primary feed in a prime focus reflector or by the sub-reflector in a dual reflector system, reduces the electrical performance of these types. The other type of reflector antenna is called the offset reflector, where the geometry of the reflector is asymmetric and its feed is located outside the main beam. As the geometry is asymmetric, the reflector is less straightforward than the previous symmetric cases, and various effects due to the asymmetry must be considered.

The feed is the essential part of any reflector system. In dual reflector system, it is large in size, having aperture diameters of three to eight wavelengths. However, in prime focus reflectors, that use a single parabolic reflector, the feed is small [6].

Various electrically small feeds are used in the prime focus reflector system. Their common criterion is their small aperture diameter which is less than three wavelengths. The main categories of the feeds are: dipole feeds, waveguide feeds, horns feeds, and microstrip feeds [6]-[7]. Dipole feeds are the oldest among these, and generally the size is 0.5 λ_0, where λ_0 is the wavelength in free space. Thus, aperture blocking is usually at a minimum with this kind of feeds, and the feeds are easy to fabricate. However, their beamwidths in principal planes are unequal, and may be used with reflectors having

elliptical aperture. Waveguide feeds can be used satisfactorily as an antenna feed, since they provide good reflector illumination and are also easy to fabricate. However, for small diameter waveguides, radiation patterns at different planes are not equal, that cause low illumination efficiency. They also require struts support to mount on the reflector. The horn feeds are another category of small feeds. The horn is used to control the radiating aperture size. It is difficult to excite a large diameter waveguide so that only a single mode is generated. In horn, the throat serves as a filter device, allowing only a single mode to be propagated freely to the aperture. The important design considerations of the horn feeds are the impedance characteristics and the efficient illumination of the reflector. They also require struts support and are costly to fabricate. Another category of the feeds is the microstrip feed, which has a simple structure, can be low cost and easy to integrate with other circuitry. The major advantage of microstrip feeds is that they have smaller axial length because of their planar configuration, as compared to waveguide or horn feeds. However, they have disadvantages of unequal beamwidths, high cross-polarization and low efficiency.

Therefore, all above feeds have their merits and demerits. The factors that might be relevant to the choice of feeds are mainly pattern symmetry, peak cross-polarization level, efficiency, bandwidth and input impedance. There are other aspects, which may also be significant such as the size, volume, and weight. Other than the electrical properties, the mechanical issues are also important for the feed design, such as, the mounting on the reflector and associated implementation cost. Therefore, in practice one or more of these factors will influence the selection of a feed for a particular application.

In this thesis, we will explore two different kinds of feeds, slotted circular waveguide feeds and microstrip dipole feeds. Their electrical and mechanical properties will be investigated and improved.

1.2 Objective of the Thesis

The motivation of this research evolved from the desire to design electrically small feed antennas with improved performance characteristics for prime focus reflectors. The primary advantages of these reflectors are their low cost and high performance with a well design feed. Therefore, it is necessary to design a feed with good radiation characteristics, that can be fabricated easily and at low cost.

Two different types of feed categories are selected for this purpose. One is slotted circular waveguide feeds, where slots are added as an additional parameter with the circular waveguide feeds. Therefore, investigations are carried out on slotted circular waveguide feeds in order to contribute further to the knowledge and understanding of these antennas. The goals related to this area of research are summarized as follows:

- Design and investigate small circular waveguide (0.35 λ_0) feeds with open ended slots, in both E- and H-planes.
- Identify the slot parameters on waveguide feed performance.
- Design and investigate slotted circular waveguide feeds with choke(s).
- Design and investigate slotted circular waveguide feeds with a cavity.
- Design and investigate cavity feeds with a quarter wavelength choke in presence of the slots.

- Determine the gain factor, the phase center location of all feeds, and study their stability over the frequency band.
- Fabricate and measure all feeds performance in the laboratory and compare with simulation results.

The second category of the feeds is the microstrip dipole feeds, which are a new backward radiating feeds. The primary advantages are low profile, simple structure, low cost, easy of fabrication and mount with RF circuits. The goals related to this area of research are summarized as follows:

- Design and investigate microstrip dipole feeds for backward radiation.
- Characterize and improve the input parameters of the feed.
- Determine the gain factor and phase center of the feed, and study their stability over its frequency band.
- Investigate techniques for improving radiation pattern symmetry of the feed.
- Investigate the effects of various parameters of the feeds on its performance.
- Investigate the miniaturization techniques.
- Design and investigate the dual frequency operation of the feed.
- Fabricate all these feeds in the laboratory and compare their measured performance with simulation results.

Microstrip dipole feed has unequal radiation patterns, which is useful as a feed for reflector with elliptical aperture. However, modified microstrip dipole feeds are designed and investigated for the radiation pattern equalization, which is useful as a feed for reflector with circular aperture. The goals related to this area of research are summarized as follows:

- Investigate techniques for equalizing the E- and H-plane radiation patterns.
- Design a bent microstrip dipole feed for pattern equalization.
- Improving the feed performance with additional dipole-reflectors.
- Investigate and design a corrugated microstrip dipole feed for pattern equalization.
- Determine the gain factor and phase center of all these feeds, and study their stability over the frequency band.
- Fabricate all these feeds in the laboratory and compare their measured performance with simulation results.

1.3 Organization of the Thesis

The first two chapters introduce the topic; motivation of the work; review previous works and provide necessary background information. Chapter 1 is the introduction to the reflector feeds and objective of the research. A review of criteria for feed design, phase center concept and literature review are included in Chapter 2, which provides useful information for feed design and analysis.

Slotted circular waveguide feeds are discussed in Chapter 3. Circular waveguides with slots equalize the E- and H-plane radiation patterns of small diameter feeds. However, they have limitations in improving the gain factor of the feeds. Therefore, slotted circular waveguide feeds with a single choke are introduced, which improve the gain factor. They also retain the pattern equalization of the E- and H-plane. For further improvement of the gain factor, slotted circular waveguide feeds with multiple chokes are

discussed in this chapter. Slotted circular waveguide feeds with a cavity are also investigated. They have a sector shape radiation patterns with broad beamwidths, which is useful for deep reflectors.

Microstrip dipole feeds are studied in chapter 4, which is another type of feed for prime focus reflectors. They are designed for backward radiation that eliminates the need for strut support. The impedance bandwidth is improved by modifying the feed transmission line. The feed shows slight pattern asymmetry, which is improved by changing the dipole arm lengths. The effect of substrate is also discussed. The size reduction of the feed is possible by slotting the dipole arms, which is investigated in this chapter. In some applications, dual band operation is needed and therefore, dual band microstrip dipole feeds are also designed and studied.

In chapter 5, microstrip dipole feeds with modified dipole arms are introduced, to equalize the radiation pattern beamwidths. Two techniques are used for this purpose. First, the bent dipole arms with a single dipole-reflector are used to achieve the radiation patterns symmetry. However, the back lobe level is high for this case. Therefore, dual dipole-reflectors are used to improve the back lobe level. Second, the corrugated microstrip dipole feed is used for pattern equalization, which also improves the input impedance of the feed.

The summary and contribution of the research are discussed in chapter 6, where the directions for future research are also provided.

Chapter 2

Background Study

2.1 Introduction

The most important factor that determines the overall performance of a prime focus reflector antenna system is the feed, which is located at the focal point of the reflector. It usually comes in many different shapes and sizes, ranging from simple dipoles and waveguides to horns, microstrip antennas or traveling wave antennas. The choice of feed antenna is often a complex decision and is based on reflector parameters. One of the requirements of the feed is that it must be small compared to the wavelength and should give a spherical phase front, which is from a distance it must appear as though the energy is radiated from a point source. To illuminate adequately the entire reflector area, the radiation from the feed must be directed towards the reflector. Also, the field should be of such a nature that after reflection the waves must be properly polarized. Therefore, it is necessary to know all features of a feed before its design. In the following sub-section we discuss the important features of electrically small feeds.

2.2 Important Features of Small Feeds

2.2.1 Characteristics of Small Feeds

The performance of a prime focus reflector is mainly controlled by its feed. Achieving a maximum efficiency from the reflector antenna requires a close control of the amplitude, phase and polarization of the feed. They are discussed below.

2.2.1.1 Radiation Pattern

It is well known that a transmitting or receiving antenna will not detect energy uniformly in all directions. This directional selectivity of an antenna is characterized in terms of its radiation pattern, which is a plot of the relative strength of radiated field as a function of the angular parameters, in the form of the elevation angle θ, and azimuth angle ϕ, for a constant radius r. To completely define the antenna's radiation characteristics, it would be necessary to measure or calculate the amplitude, phase and polarization of the radiated fields over the surface of a sphere, at every frequency of operation. However, in practical applications for a y-polarized antenna, the principal E-plane ($\phi = 90^0$), H-plane ($\phi = 0^0$) and the cross-polarization ($\phi = 45^0$) patterns are used to measure the radiation characteristics. Fig 2.1 shows the radiation pattern of a feed antenna where the principal E- and H-plane patterns are symmetric up to 90^0 with a cross-polarization level of -35 dB at 45^0 plane.

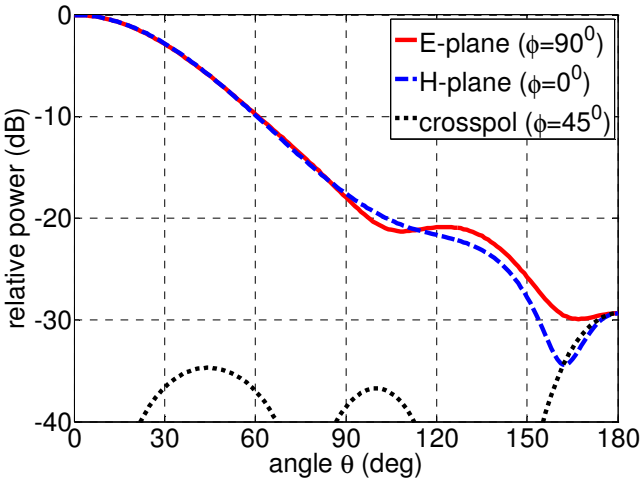

Fig. 2.1 Radiation pattern of a feed antenna.

2.2.1.2 Polarization

The polarization of an antenna in a given direction is defined as the polarization of the wave radiated by the antenna. The polarization of a radiated wave describes the shape and orientation of the electric field vectors as a function of time. There are three different polarizations for a plane wave signal and these are the linear polarization, the circular polarization and the elliptical polarization. Most communication systems use either liner (vertical or horizontal) or circular (RHC-right hand circular or LHC-left hand circular) polarization. However, linear polarization antenna is easy to fabricate and inexpensive. In this study liner polarization is used. The linear polarized field is divided into two parts: co-polarization component, which is wanted and cross-polarization component, which is unwanted in the antenna applications.

In order to achieve polarization purity of the reflector antenna, it is necessary to keep the cross-polarization level low. This requirement needs significant efforts to develop feed antennas that will give low cross-polarization. There are three different definitions for cross polarization in literature, but Ludwig's third definition is the most useful one. According to his third definition [8], for a y-polarized field,

$$E_{co}(\theta,\phi) = E.\hat{y} = E.\left(\hat{\theta}\sin\phi + \hat{\phi}\cos\phi\right), \quad \theta = 0^0 \tag{2.1}$$

$$E_{cross}(\theta,\phi) = E.\hat{x} = E.\left(\hat{\theta}\cos\phi - \hat{\phi}\sin\phi\right) \tag{2.2}$$

Similarly, for a x-polarized field,

$$E_{co}(\theta,\phi) = E.\hat{x} = E.\left(\hat{\theta}\cos\phi - \hat{\phi}\sin\phi\right), \quad \theta = 0^0 \tag{2.3}$$

$$E_{cross}(\theta,\phi) = E.\hat{y} = E.\left(\hat{\theta}\sin\phi + \hat{\phi}\cos\phi\right) \tag{2.4}$$

where,

$$E = E_\theta\hat{\theta} + E_\phi\hat{\phi} \tag{2.5}$$

Therefore, for a y-polarized field, the co- and cross-polarization components of the E-field can be written as,

$$E_{co}(\theta,\phi) = E_\theta\sin\phi + E_\phi\cos\phi \tag{2.6}$$

$$E_{cross}(\theta,\phi) = E_\theta\cos\phi - E_\phi\sin\phi \tag{2.7}$$

The property of a circular symmetric antenna is that both $E_\theta(\theta,\phi)$ and $E_\phi(\theta,\phi)$ functions are the multiplication of two independent functions of θ and ϕ, in the forms of $E_\theta = f(\theta)\sin\phi$ and $E_\phi = g(\theta)\cos\phi$.

therefore,

$$E_{cross} = f(\theta)\sin\phi\cos\phi - g(\theta)\sin\phi\cos\phi \tag{2.8}$$

$$E_{cross} = \sin\phi\cos\phi[f(\theta) - g(\theta)] \quad (2.9)$$

at $\phi = 45^0$, Therefore, the above equation is,

$$E_{cross} == \frac{1}{2}[f(\theta) - g(\theta)] \quad (2.10)$$

The result shows that for zero cross-polarization both magnitude and phase of E and H-plane radiation patterns must be equal.

2.2.1.3 Input impedance

Impedance characteristics are very important for any type of antenna. It is a simple concept, which relates the voltage and current at the input of the antenna. The real part of an antenna's impedance represents power that is either radiated away or absorbed within the antenna. The imaginary part of the impedance represents power that is stored in the near field of the antenna (non-radiated power). An antenna with real input impedance (zero imaginary part) is said to be resonant.

Input impedance can also be characterized by the reflection coefficient, Γ or S_{11} parameter of the scattering matrix of the antenna. Reflection coefficient is defined as the amplitude of the reflected voltage wave, normalized to the amplitude of the incident voltage wave, and can be written as,

$$\Gamma = \frac{Z_L - Z_0}{Z_L + Z_0} \quad (2.11)$$

Here, Z_L is the load impedance and Z_0 is the characteristic impedance of the transmission line. When the load is mismatched, not all of the available power from the source is delivered to the load. This 'loss' is called the return loss R_l, and is defined (in dB) as, $R_l = -20\log|\Gamma|$ dB. As an example, for a perfect matched load, $\Gamma = 0$, the

return loss is ∞ dB or $S_{11} = -\infty$ dB (no reflected power), whereas, for a complete mismatch, $|\Gamma| = 1$ and return loss is 0 dB or $S_{11} = 0$ dB.

The input impedance influences the feed design, and so should be computed as part of the complete design process. It is generally a function of frequency. Thus the antenna will be matched to the interconnecting transmission line and other associated equipment, only within a bandwidth. The input impedance of an antenna depends on many factors including its geometry, method of excitation and its proximity to surrounding objects.

2.2.2 Performance Criteria of Small Feeds

The design of feed antennas depends on the radiation and impedance characteristics. However, the feed performance with a reflector is the most important factor. There are two important performance criteria that are used to evaluate the feed with a reflector. First is the performance of feeds and the second is their stability within the frequency band. In the following subsection, we will discuss these criteria.

2.2.2.1 Performance of Feeds

The antenna efficiency depends on the gain of the reflector, which is defined as [9]-[10]:

$$G = \frac{4\pi A}{\lambda_0^{\,2}}\eta = \frac{(\pi d)^2}{\lambda_0^{\,2}}\eta \tag{2.12}$$

where,

A is the area of the antenna aperture,
d is the diameter of the prime focus reflector,
λ_0 is the wavelength in free space,
η is the efficiency.

For prime focus reflectors, the gain is related to the efficiency or gain factor of the antenna. It is a useful measure of how well the feed antenna makes use of the reflector aperture. The gain factor of a prime focus reflector antenna can be defined as [6]:

$$\eta_g = cot^2\left(\frac{\theta_0}{2}\right)\frac{\left[\int_0^{\theta_0}\{f(\theta)+g(\theta)\}\tan\left(\frac{\theta}{2}\right)d\theta\right]^2}{\int_0^{\pi}\{|f(\theta)|^2+|g(\theta)|^2\}sin\theta d\theta} \tag{2.13}$$

where, $f(\theta)$ and $g(\theta)$ are the principal E- and H-plane patterns of the feed, and θ_0 is the reflector aperture angle.

The gain factor of a reflector is made up of four separate efficiencies. These are the spillover efficiency η_s, the illumination efficiency η_i, the cross-polarization efficiency η_c and the phase efficiency η_p and can be written as:

$$\eta_g = \eta_s \times \eta_i \times \eta_c \times \eta_p \tag{2.14}$$

The spillover efficiency is a measure of how much energy spills past the edge of the reflector. Radiation from a feed that is not intercepted by the reflector is a reason for some power loss, and hence reductions in the antenna gain. This loss is called the spillover loss, which doesn't contribute to the main beam. Thus the spillover efficiency $\boldsymbol{\eta}_s$ is the ratio of the power intercepted by the reflector to the total power radiated by the feed and is given by [11]-[12]:

$$\eta_s = \frac{\int_0^{\theta_0}\{|f(\theta)|^2+|g(\theta)|^2\}sin\theta d\theta}{\int_0^{\pi}\{|f(\theta)|^2+|g(\theta)|^2\}sin\theta d\theta} \tag{2.15}$$

All areas of a reflector should be illuminated with equal energy from the feed. However, the edges of the reflector are further away from the focus than its center, and for this reason more energy is required at the edges than at the center. Therefore, the

radiation patterns of the feed usually taper off toward the outer edge of the reflector and illuminate with a lower intensity, and this loss is called illumination loss. Thus, illumination efficiency $\boldsymbol{\eta}_{\mathrm{i}}$ is the ratio of the actual feed power pattern that illuminates a reflector over the desired feed power pattern. It can be expressed in the form [11]-[12]:

$$\eta_i = 2cot^2\left(\frac{\theta_0}{2}\right)\frac{\left[\int_0^{\theta_0}\{|f(\theta)| + |g(\theta)|\}\tan\left(\frac{\theta}{2}\right)d\theta\right]^2}{\int_0^{\theta_0}\{|f(\theta)| + |g(\theta)|\}^2 sin\theta d\theta} \tag{2.16}$$

The phase efficiency is a measure of the phase error across the reflector caused by the non-uniform phase of the feed radiation patterns. Therefore, this efficiency is due to the phase errors in the co-polar field and it is defined as [11]-[12]:

$$\eta_P = \frac{\left[\int_0^{\theta_0}\{f(\theta) + g(\theta)\}\tan\left(\frac{\theta}{2}\right)d\theta\right]^2}{\left[\int_0^{\theta_0}\{|f(\theta)| + |g(\theta)|\}\tan\left(\frac{\theta}{2}\right)d\theta\right]^2} \tag{2.17}$$

The cross-polarization efficiency is a measure of the proportion of the total energy that is contained in the cross-polar pattern. It measures the amount of power lost in the cross-polar radiation pattern. Therefore, it is defined as the power of the co-polar field relative to the total power and expressed as [11]-[12]:

$$\eta_c = \frac{1}{2}\frac{\int_0^{\theta_0}\{|f(\theta)| + |g(\theta)|\}^2 sin\theta d\theta}{\int_0^{\theta_0}\{|f(\theta)|^2 + |g(\theta)|^2\} sin\theta d\theta} \tag{2.18}$$

The phase efficiency and the cross-polarization efficiency are very small for well designed feeds and reflectors. If the feed is located with its phase center at the focal point of the reflector, the phase efficiency is normally high, typically better than -0.1 dB [13].

Other than these efficiencies, there are other factors that reduce the overall efficiency of the prime focus reflector. These are [14] :

i) Aperture blockage - In prime focus reflector, the feed is located in front of its aperture. Therefore, the feed structure and its support struts block some of the beam. In small diameter reflectors, where the size of the feed is comparable with the size of the reflector, this can reduce the efficiency significantly.

ii) Shape errors - random surface errors in the shape of the reflector reduce the efficiency.

2.2.2.2 Frequency Stability

Generally, a feed antenna may be designed at one specific frequency. However, its performance will change within a frequency band. Thus the frequency characteristics of a feed refers to the manner in which its performance varies over a given frequency band. The performance can be accessed by the shape of radiation patterns, the beamwidths, the peak cross-polarization level, the back lobe level and the input impedance of the feed antenna, all of which need to be investigated within the frequency band of the feed.

2.2.3 Phase Center of Small Feeds

Phase centre is defined as a point in z-axis from which, when emitted, far-field phase-fronts or, correspondingly, group-delay fronts are spherical. That is, the phase value is constant in a certain angular area of interest when measured with respect to the coordinate system whose origin is in the phase center.

The phase center is also significant as it is the point from which the antenna radiation appears to originate. The knowledge of the phase center location is important in feed antenna applications, because for parabolic reflectors, the feed must be located at its

focus, which means the feed phase center must coincide with the reflector focal point. In most feeds, there is a phase center region rather than a single phase center point, because the radiation consists of a summation of spherical waves which emanate from the aperture. However, the phase center location should remain reasonably constant in order to minimize the phase variation over the radiation sphere of the feed.

In 1956, David Carter studied the phase center of microwave antennas and developed formulas for reflector antennas [15]. Rusch and Potter have defined the phase center as the origin of a sphere with a best nearly constant phase variation in a least square sense [16]. Manila (1982) studied the role of the antenna phase center in geodetic measurements based on satellite systems [17]. A practical method of determining the phase centers of the feed antennas has been presented in [18], where the phase center has been obtained as the location along the focal axis of the reflector system that maximizes the feed efficiency. This paper locates the phase center, within a small distance of a trial point, which causes small aperture phase error. However, it is generally difficult to locate the phase center of a wide angle feed, which is generalized by Rao and Shafai [19].

2.2.3.1 Phase Center Determination

The phase center of a feed antenna is defined as the origin of a sphere, over which the phase of the radiated field is nearly constant in the principle ϕ =0°, and 90° planes. Fig. 2.2 shows the geometry for calculating the phase center, where O (0, 0, 0) is the origin of the coordinates, and O′ (0, 0, d) is the phase center location of the antenna. Here, R is the distance from the origin to the far field point, r is the distance from the phase center

location to the same observation point and d is the distance from origin to the phase center location. Both R and r are much larger than d and can be considered parallel.

The radiated far field of the feed can be expressed as [20]-[21],

$$E(R,\theta,\phi) = |f(\theta,\phi)|\frac{e^{-jkR}}{R}e^{j\Psi(\theta,\phi)} \tag{2.19}$$

where $f(\theta,\phi)$ is the amplitude pattern, $\Psi(\theta,\phi)$ is the phase angle of the radiated field. The phase of a radiated field is determined by *-jkR* plus phase of the far field function and must be independent of the origin of the (θ,ϕ).

Using the Fraunhofer approximations, we can make the following approximations -

in denominator $R \approx r$

in exponential $R \approx r + r_0.\hat{r}$

Therefore, the radiated far field of (2.19) at the new phase reference point O′ becomes,

$$E(R,\theta,\phi) = |f(\theta,\phi)|\frac{e^{-jk(\mathrm{r}+r_0.\hat{r})}}{r}e^{j\Psi(\theta,\phi)} \tag{2.20}$$

or,

$$E(R,\theta,\phi) = |f(\theta,\phi)|\frac{e^{-jkr}}{r}\frac{e^{-jk(r_0.\hat{r})}}{r}e^{j\Psi(\theta,\phi)} \tag{2.21}$$

or,

$$E(R,\theta,\phi) = |f(\theta,\phi)|\frac{e^{-jkr}}{r}e^{j(\Psi(\theta,\phi)-kr_0.\hat{r})} \tag{2.22}$$

It is assumed that because of the symmetry, the phase center will move on the Z-axis. Therefore, $r_0.\hat{r} = kdcos\theta$.

$$E(R,\theta,\phi) = |f(\theta,\phi)|\frac{e^{-jkr}}{r}e^{j(\Psi(\theta,\phi)-kdcos\theta))} \tag{2.23}$$

Therefore if the phase variation at O′ is Ψ_d, then the general expression is,

$$\Psi_d(\theta,\phi) = \Psi(\theta,\phi) - kdcos\theta \tag{2.24}$$

Now the location of the phase center d, is the distance where phase variation $\Psi_d(\theta,\phi)$ of the co-polar pattern in the principal planes is minimum. This can be done by calculating phase variation with changing d, by trial and error using the above equation.

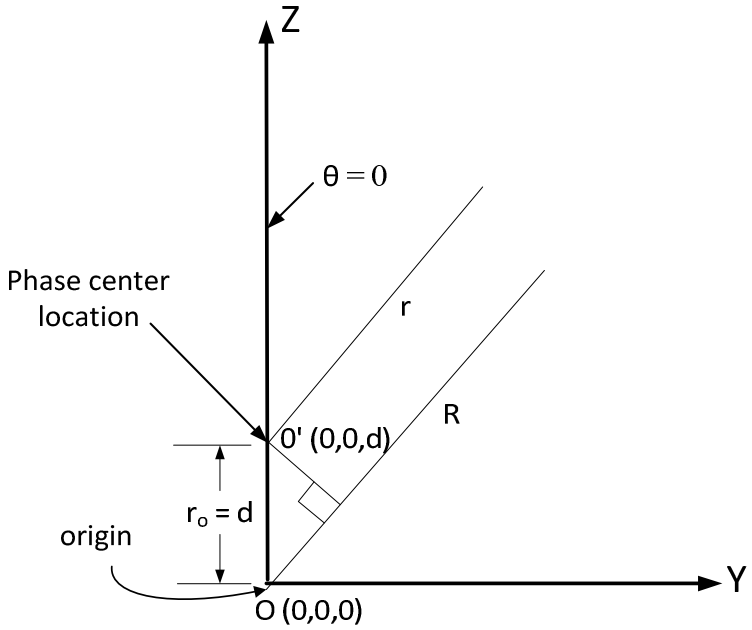

Fig. 2.2 Geometry and co-ordinate system to find the phase center location; assuming phase center movement is in the z direction.

The phase center location for the E-plane d_E and H-plane d_H are different, as the phase variation of the two principal planes are different. Therefore, a global phase center d_c is taken, where phase variations of the two planes seem to be minimized and that is the global phase center of the feed. Another procedure to find the global phase center is to calculate d_E and d_H separately and then taking the average $d_{avg} = \frac{(d_E+d_H)}{2}$.

2.3 Literature Review

Different types of electrically small feed antennas are used in prime focus reflectors [6]-[7]. Among these feeds, circular waveguide feeds, dipole feeds and microstrip feeds are discussed below, as they are the candidates for the research in this thesis.

2.3.1 Circular Waveguide Feeds

Historically circular waveguide is used as a feed for the prime focus reflector antennas [12]. It has very simple configuration though its performance as a feed is low. One of the important parameters of a circular waveguide feed is its radius, as the beamwidth, cross-polarization level and back lobe level depend on it. For waveguides with a small radius, the E-plane pattern provides a wider beamwidth than the H-plane, which becomes reversed for large radii, where the H-plane provides a wider beamwidth than the E-plane [22]. The wall thickness of the waveguide is another important parameter, since the currents of the end surface of the wall and diffraction effects alter the radiation patterns. James et al. [23] studied extensively the effects of the wall thickness, which was also verified by Shafai et al. [22]. According to James et al. [24], for circular waveguides with small radius, the cross-polarization of the antenna is small for small wall thicknesses, compare to large wall thicknesses.

To indicate the characteristics of the circular waveguide as a feed for parabolic reflector antennas, its performance with the reflector antenna was considered. Shafai et al. [22] calculated the spillover efficiency, the illumination efficiency and the gain factor

for different f/D ratios for a circular waveguide with different radii, and their result showed that the gain factor and spillover efficiency improve with increasing radius.

The phase center location of the feed is also important, since the phase center of the feed and the focal point of the reflector must be coincident with each other. It is evident that, for near cut-off waveguides, the location of the phase center depends strongly on the aperture angle (subtended half angle). As the waveguide diameter increases, the phase center, for an angular range of less than 50^0, moves to the waveguide aperture. Beyond 50^0, the phase center is initially in front of the waveguide open end, but moves inside the waveguide for radius 0.45 λ_0 [22]. To understand the behaviour of the cross-polarization, phase center locations of the principal E- and H-plane patterns are important. It is shown in [22] that the peak cross-polarization depends on the radiation pattern difference of the two principal planes. For symmetric amplitude patterns it depends on the phase difference which in turn depends on the axial distance between the phase center locations of the two principal planes.

Introducing a quarter wavelength choke on the waveguide wall nearly equalize the beamwidths of the principle planes. The effect of a quarter wavelength choke on the cross-polarization and back lobe level was studied by Shafai et al. [22]. The improvement of back lobe level is about 10 dB, which can be generalized for most feeds using a single choke to reduce the back radiation. Increasing the number of chokes or corrugations, further improves the back lobe level and cross-polarization. Shafai et al. [22] showed that in a flange with three rectangular corrugations, the separation of the corrugated surface from waveguide open end varies the phase center location and at some specific value the E- and H-plane patterns coincide and thus minimize the feed cross-polarization.

Feeds with rectangular corrugations are normally used as a feed for reflector antennas. However, the rectangular corrugations are difficult to fabricate. Mentzer et al. [25] have shown that V-shape corrugations can also be designed to perform similar to rectangular corrugation. The intermediate geometry between the V-shape and the rectangular corrugations is the trapezoidal corrugation, which has the trapezoid angle as an additional parameter. Furthermore, the trapezoidal corrugations are more suitable for mass production technique such as casting or stamping. In [26], Kishk et al. showed that the flange has three profiled corrugations of trapezoidal shape also behave the same as rectangular case. The most interesting result is that the shape of a corrugation has a definite effect on the location of the phase center. However the peak gain factor is relatively independent of the corrugation shape and number. The gain factor and the spillover efficiency are also computed for these types of feeds. The results show that introducing chokes improves both the gain factor and the spillover efficiencies [22].

In [22] Shafai et al. have studied the effect of the distance L between the corrugation surface and the waveguide open end. Their result showed that increasing L tends to broaden the feed patterns, and the aperture angle for peak gain factor increases with L. Thus the parameter L can be used effectively to design feeds for different aperture angles and to control the feed cross-polarization without significantly affecting the reflector gain.

The focal region field of prime focus reflectors can also be realized by coaxial ring aperture fields which lead to the development of a coaxial feed by koch [27]. It consists of a coaxial waveguide surrounded by multiple coaxial rings which made the feed a flexible one, but its geometry was complicated to fabricate. The rings, however, can also

be excited by the aperture through open end of the waveguide. In this design the excitation coefficient is not high but it results in a simpler configuration. Also, the size and location of the rings with respect to the waveguide aperture can be used as parameters to control the feed radiation patterns. A feed using this approach was originally designed by Wohlleben et al. [28], where by recessing the corrugated flange behind the waveguide aperture, wide angle radiation patterns were obtained. Broadening of the radiation patterns by E-plane slots waveguide wall was later studied by Shafai [29].

In some applications, it is desirable to use reflectors with small f/D values which mean feed must therefore have wide-angle patterns with high aperture efficiency. Conventional feeds radiation patterns are tapered monotonically from 0 dB on the broadside to a value which lies between -8 and -10 dB at an angle corresponding to the reflector rim [11]. To increase the aperture efficiency, it is required to produce a uniform illumination over the parabolic aperture. Such feeds are often difficult to design and fabricate especially with low cross-polarization and high gain factors. A circular waveguide feed using multiple co-axial radiating waveguide rings was reported by Koch [27] by the possibility of generating sector shaped patterns. The feed showed a wide beamwidth with good radiation patterns. However the feed geometry was complex to be used as a simple primary feed. Scheffer [30] and Koch [27] et al. developed three simple configurations of the co-axial cavity feed and one of these feeds analysed using the geometrical theory of diffraction [31], where only the co-polar patterns were reported. In [32], Kishk used a numerical method to improve the radiation characteristics of this feed by optimizing its dimensions to achieve symmetrical radiation patterns with low cross-polarization. Neither of the above feeds incorporates chokes and their back radiations are

high. After adding a single choke it showed improvement in the back lobe level [22]. The gain factor and spillover efficiency were also improved in this case.

2.3.2 Dipole Feeds

The dipole antenna is widely used as a first category of reflector feeds, because of the simplicity of construction [33], though, it has omni-directional radiation patterns in H-plane. To illuminate the reflector efficiently, a small circular disc was used as a sub-reflector to direct the dipole radiation toward the reflector [34]. While these designs are simple and used extensively as low-cost and low-frequency feeds, the asymmetric dipole radiation in its E- and H-planes does not illuminate the reflector effectively. It is well known that the asymmetric beam pattern of the dipole feeds results in low aperture efficiency and an increase in spillover loss, when used as a feed for prime focus reflector. Therefore, a symmetric beam pattern is often required in order to be a feed for prime focus reflector. Moreover, the asymmetric radiation causes an excessive cross-polarization. Since the dipole radiation patterns are asymmetric, the resulting pattern also becomes asymmetric. To generate symmetric patterns one must use an antenna, which also have symmetric radiation patterns. This can be achieved by cone-dipole feed [34], where the dipole is in its standard form, but the disc is bent. As a second solution to dipole-pattern asymmetry, a short cylindrical section may be placed over the disc to form a cavity [34]. Here, the cavity-dominant mode controls the pattern shape and consequently, its behaviour is easier to understand.

The beam pattern of a dipole-disk antenna can be shaped by a corner reflector instead of a flat one [35]. Because of its asymmetric structure, it is hard to use. Corrugated horns [36]-[37] have equal beamwidths in E- and H-plane, and can be used as a feed for prime focus reflector. However, their geometry is complicated and hard to fabricate, and become large and heavy at low frequencies. In order to mitigate these limitations by achieving the pattern symmetry of a dipole-disk antenna, a beamforming ring (BFR) was added [38], to compress the H-plane pattern, without modifying the E-plane pattern. The BFR dipole-disk antenna was investigated and analyzed in references [39]-[40]. However the shortcoming of a BFR dipole-disk antenna is that the ring greatly increases its profile.

2.3.3 Microstrip and Backward Feeds

Microstrip antennas are becoming increasingly popular because of light weight, low profile, low cost and ease of fabrication. Progress in their design and analysis has also removed most of their earlier limitations in bandwidth and radiation characteristics. Consequently, they are also becoming acceptable candidates as reflector antennas feed. The merits of microstrip feeds depend on the type of applications. In symmetric prime focus reflector systems, the feed normally blocks the central region of the aperture and causes reductions in the aperture efficiency and gain factor. A larger feed blocks a larger portion of the reflector central region and also requires a heavier support structure. A microstrip feed is normally smaller and reduces the central blockage and its subsequent degrading effects. The early use of microstrip antennas as reflector feeds was reported in [41]. Feed optimization and the achievable reflector characteristics in gain factor and

cross-polarization however were not provided there. The use of single microstrip antennas and arrays of microstrip antennas as reflector feeds was investigated by Hall and Prior [42,43] and a numerically optimized feed was investigated by Kishk and Shafai [44]. A circular microstrip antenna is a good candidate as a feed for a symmetric reflector [45]. Its pattern shape can be controlled readily by the size and thickness of the ground plane. Symmetrical patterns are achievable with small ground planes, which reduce the blockage. However, the back radiation is high and its bandwidth is normally narrow.

A disadvantage with such microstrip feed antenna is that the support struts of the feed block the reflector aperture and thereby causes low efficiency and high sidelobes. These blockage losses can be eliminated if the feed is self supporting, being for instance a backward radiating antenna located along the symmetry axis of the reflector. This feed also makes it possible to locate the transmitter/receiver on the rear side of the reflector without the use of thin and lossy cables. The backward radiating waveguide feeds have been known since the early days of radio communication. In 1947 Cutler [46] introduced “ring focus” and “cup” feed and some years latter an improved backward-radiating feed, with equal E- and H-plane patterns was presented by Clavin [47]. A new ring focus feed was patented by Cutler [48] in 1964 that uses a corrugated surface, but was not analyzed in detail. Newham [49] has presented an improved dual polarized “splashplate” antenna and Poulton [50] has introduced an improved waveguide “cup” antenna. The shortcoming of both these designs is that the waveguide itself gives an undesirable contribution to the primary radiation, because it blocks the splash plate radiation. The disadvantage of these backward radiating feed antennas is that they are geometrically complicated and their implementation cost is high.

2.4 Summary

In this chapter the criteria for reflector feeds were discussed. Normally, for a prime focus reflector the feed criteria were - symmetrical radiation patterns, low cross polarization and low back lobe level. The beamwidth of the feed should match the reflector aperture angle, and depending on the application as a feed it could be narrow or wide. The stability of the feed parameters with frequency was very important. In most applications this should be maintained within a performance of 10% frequency bandwidth or more. The gain factor and various antenna efficiencies of the reflector system were reviewed and the concept of phase center and its determination process were discussed. A literature review of the previous work, related to the feed design, was also provided in this chapter.

Chapter 3

Slotted Circular Waveguide Feeds

3.1 Introduction

Circular waveguide feeds have been used as a primary feed for parabolic-reflector antennas for many years because of their low cost and simple construction. The radiation patterns of the feed depend on the cross-section of the waveguide. In a feed with small radius (< 0.48 λ_0) the E-plane pattern is broader than the H-plane pattern, but for large radius (> 0.48 λ_0) it is narrower than the H-plane pattern. The crossover occurs at radius equal to 0.48 λ_0 [22]. In prime focus reflectors, it is desirable to use smaller radius feeds, as the feeds normally block the central region of the aperture, causing reductions in the aperture efficiency and gain factor and raising the side lobe levels. However, in smaller radius feeds (less than 0.48 λ_0) the E- and H-plane plane patterns are not symmetric, which causes less illumination efficiency and ultimately reduces the efficiency of the antenna.

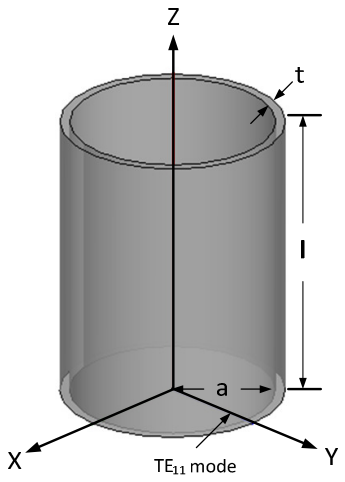

Fig. 3.1 Circular waveguide feed operating at 10 GHz; l = 60 mm, a = 10.5 mm, t = 1 mm, excitation TE_{11} mode in y-direction.

Fig. 3.1 illustrates the geometry of a circular waveguide feed that is operating at 10 GHz. The dimensions of the waveguide are: length l = 60 mm (2 λ_0), radius a = 10.5 mm (0.35 λ_0) and wall thickness t = 1 mm (0.033 λ_0). The length of the waveguide is selected as 60 mm and it has no effect on radiation patterns, with TE_{11} excitation. The thickness of the wall has effect on radiation patterns, but it is selected here as 1 mm from the fabrication point of view. The radius of the waveguide is 10.5 mm, which is 0.35 λ_0 at 10 GHz and only the dominant TE_{11} mode is propagating in the waveguide. Fig. 3.2 (a) shows the amplitude patterns of this waveguide feed at 10 GHz, where it is evident that the 10-dB beamwidths for the E- and H-plane patterns are 156^0 and 142^0 respectively, with the E-plane providing a wider beamwidth than the H-plane. The peak of cross-polarization level at 45^0 plane is -26.7 dB for the aperture angle, $\theta = 72^0$. The back lobe level is -12 dB. Fig. 3.2 (b) exhibits the phase patterns of the feed, when the co-ordinate origin is at the waveguide aperture. The E- and H-plane phase angles vary with the

reflector aperture angle. However, the phase difference between the E- and H-planes is small at higher angles.

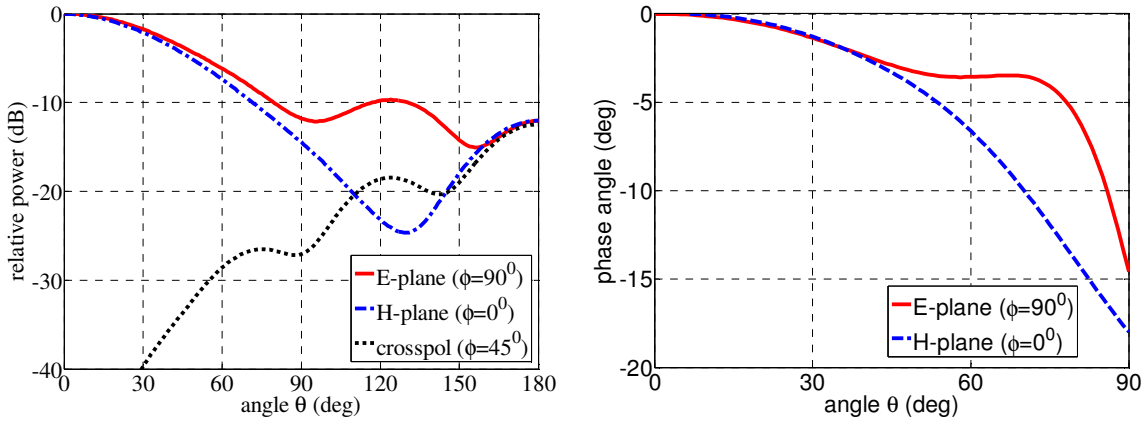

(a) **(b)**

Fig. 3.2 Radiation patterns of the circular waveguide feed, l = 60 mm, a = 10.5 mm and t = 1 mm. (a) amplitude pattern at 10 GHz, (b) phase pattern, with respect to the co-ordinate origin at waveguide face.

Therefore, it is evident that the small radius (0.35 λ_0) circular waveguide feed can be a candidate for a prime focus reflector for its small feed blockage, which ultimately improves the gain factor of the antenna. However, the E- and H-plane radiation patterns of the feed are not symmetric in the principal planes. Therefore, in the next section, these types of feeds are discussed with slots in the waveguide wall to improve the radiation patterns symmetry.

3.2 Slotted Circular Waveguide Feeds

The radiation patterns of a small diameter feed were not symmetric, with the E-plane pattern having wider beamwidth than the H-plane pattern, which was discussed in the previous section. Therefore, in this section attempt is made to equalize its E- and H-plane

patterns by slotting the circular waveguide wall. The slots are cut in the waveguide wall, in the opposite side of each other, and symmetric with respect to the X-axis. The width of the slots is perpendicular to the axis. The main advantage of using slots in the opening end of the waveguide is that they don't change the overall size of the feed. On the other hand, the field in the slots radiates, and hence changes the E- and H-plane radiation patterns. Therefore, slots acts as additional sources to control the E- and H-plane radiation patterns of the feed.

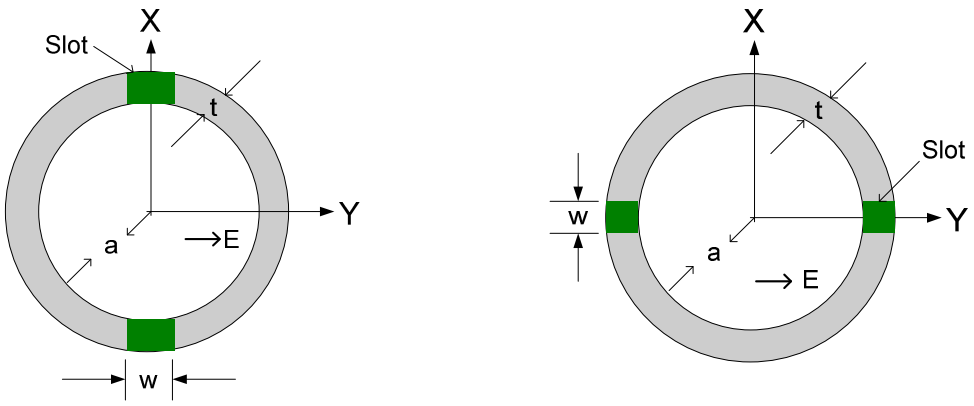

(a) **(b)**

Fig. 3.3 Two different slot positions based on the direction of Electric field distribution (Electric field is in Y-direction, YZ-plane is E-plane and XZ-plane is H-plane). (a) E-plane slots, (b) H-plane slots.

Depending on the polarization of the electric field, the slots are classified as the E-plane or H-plane slots, which are shown in Fig. 3.3. If the electric field over the aperture is polarized in the Y-direction so that the YZ-plane is the E-plane of the system, then the cut in YZ-plane is E-plane slots. On the other hand, the XZ-plane is the H-plane of the system and the cut in the XZ-plane is called the H-plane slots.

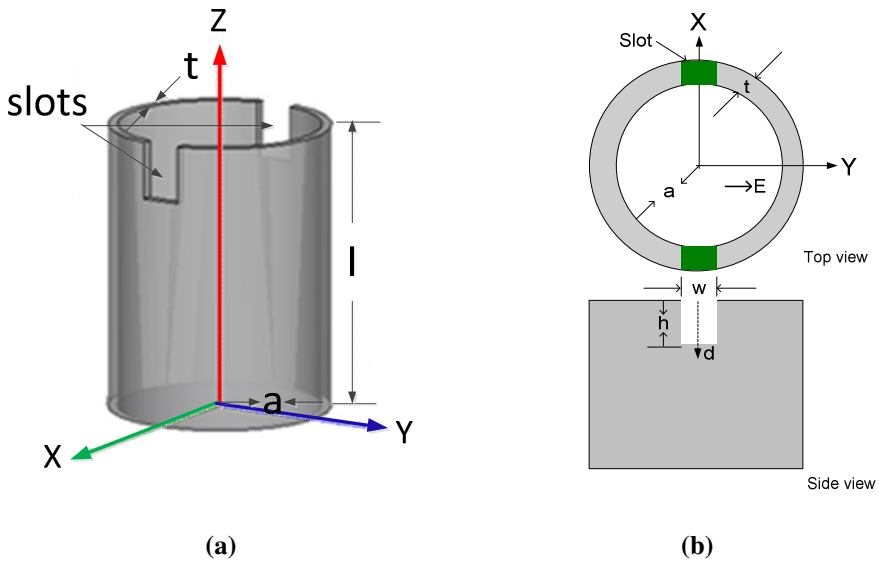

Fig. 3.4 E-plane slotted circular waveguide feed, for y-polarization; l = 60 mm, a = 10.5 mm, t = 1 mm. (a) 3-D view (b) 2-D view.

The geometry of the E-plane slotted circular waveguide feed [51] is shown in Fig. 3.4. The aperture of the antenna is parallel to the XY-plane, with the polarization of the principal TE_{11} mode in the Y-direction. Two opposite rectangular slots are in the opening face of the circular waveguide wall in the YZ-plane, or the E-plane, are transverse to the direction of the principal mode. These slots are centered and symmetric with respect to the X-axis.

The geometry of the H-plane slotted circular waveguide feed is shown in Fig. 3.5. The dimensions of the circular waveguide are same as E-plane slotted case and the two opposite rectangular slots are at the opening face of the waveguide wall in the XZ-plane or the H-plane, and are symmetric to the Y-axis.

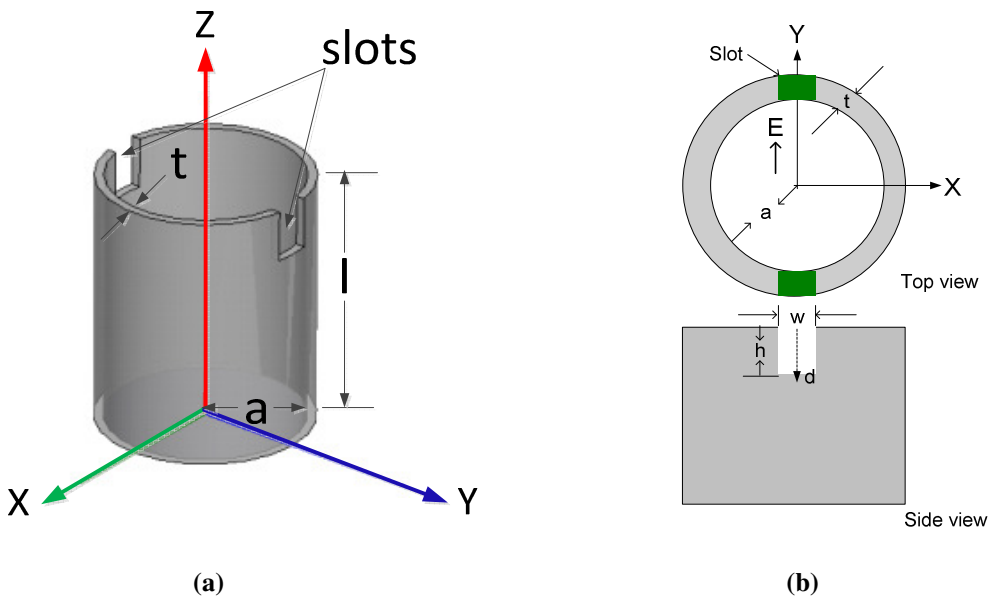

Fig. 3.5 H-plane slotted circular waveguide feed, for y-polarization; l = 60 mm a = 10.5 mm, t = 1 mm. (a) 3-D view (b) 2-D view.

3.2.1 Effects of Slots

To understand the complete behaviour of the slots, their width is varied from 2 mm to 18 mm with the variation of slots height, h from 0 mm to 8 mm. The selection of the larges range of the slots width and height is to check the complete behaviour of the slots with the waveguide. Figs. 3.6 (a) and (b) show the 10-dB beamwidths in the E- and H-planes, with the variation of slots width and height, for the E-plane slot case. It shows that for small h, the E-plane and H-plane patterns give small beamwidths, irrespective of the slots width. However, by increasing h, the E- and H-plane beamwidths become different. Therefore, for small slot height case, there are slot widths when both the E-and H-plane pattern beamwidths are equal. The sudden increase in the beamwidths is due to slight change of radiation patterns, that merges the next side lobe into the main beam.

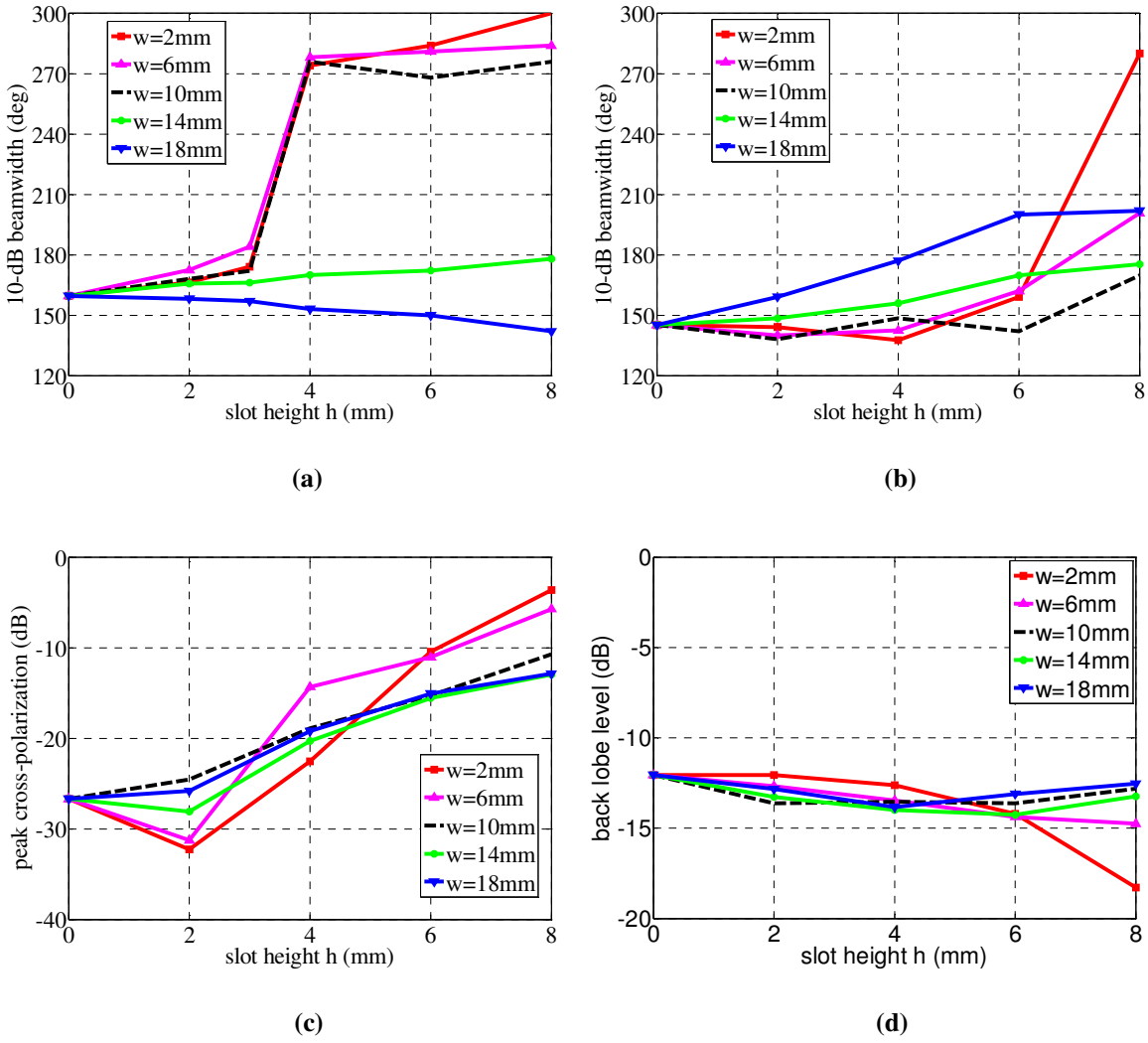

Fig. 3.6 Characteristics of the E-plane slotted circular waveguide feed varying slots width and height; l = 60 mm, a = 10.5 mm, t = 1 mm. (a) -10 dB beamwidth (E-plane), (b) -10 dB beamwidth (H-plane), (c) peak cross-polarization ($0 < \theta \leq 70^0$), (d) back lobe level.

Fig. 3.6 (c) shows the cross-polarization level at 45^0 plane, within the range of $\theta \leq 70^0$, for different slot widths and heights. It is revealed from the figure that for small slot heights, the cross-polarization level increases with slot width. The reason for increasing cross-polarization level is that, although the slots equalize the E- and H-plane radiation patterns, they increase the phase difference in the E- and H-planes and that deteriorates

the overall cross-polarization level of the feed. Fig. 3.6 (d) shows the back lobe level, which is almost independent of the slot width and height.

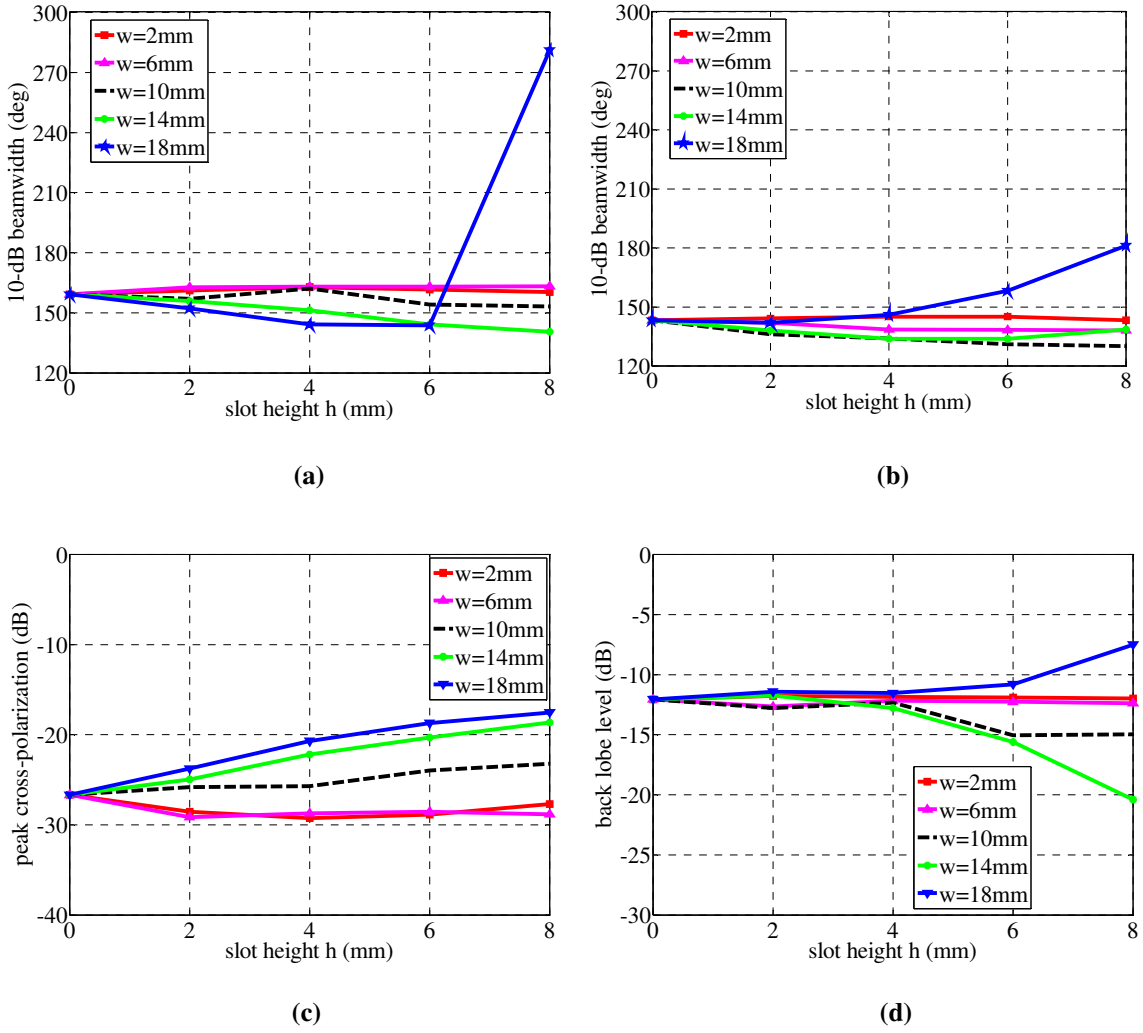

Fig. 3.7 Characteristics of the H-plane slotted circular waveguide feed varying slots width and height; l = 60 mm, a = 10.5 mm, t = 1 mm. (a) -10 dB beamwidth (E-plane), (b) -10 dB beamwidth (H-plane), (c) peak cross-polarization ($0 < \theta \leq 70^0$), (d) back lobe level.

To understand the influence of the H-plane slots on the circular waveguide radiation patterns, the slot width w and slot height h are varied, similar to the previous case. Figs. 3.7 (a) and (b) show the 10-dB beamwidths of these feeds, which indicate that, when w is

small, the E-plane pattern is broader than the H-plane pattern, for any slot height. However, when w is large (w = 18 mm), initially the E-plane beamwidth is decreasing, and then it increases quickly by increasing the slot height. Therefore, at w = 18 mm and h = 4 mm, the 10-dB beamwidths are equal in both E- and H-planes.

The cross polarization levels at 45^0 plane are shown in Fig. 3.7 (c), for different slot heights and widths. This figure shows that for small slot widths, the cross-polarization level remains almost constant, for any slot height. However, for large slot widths, the cross-polarization level increases with slot height. Fig. 3.7 (d) presents the back lobe level for the same conditions, which reveals that for small h, the back lobe level remains almost the same for all cases of w. However, when h becomes large, it increases for w = 18 mm.

3.2.2 Slotted Waveguide Feeds Design

In the previous sub-section, effects of slot width and slot height were investigated for the slotted circular waveguide feeds. The results showed that the antenna performance depends strongly on these parameters. It was found that for the E-plane slot case, the E- and H-plane beamwidths equalize, when the slot width and height are 18 mm and 2 mm respectively. For the H-plane slots, they equalize for width and height become 18 mm and 4 mm. Therefore, the feed antennas are designed using these slot parameters.

The simulated radiation amplitude and phase patterns of the E-plane slot case are shown in Figs. 3.8 (a) and (b), respectively. Fig. 3.8 (a) exhibits that the E- and H-plane radiation amplitude patterns are symmetric, up to $\theta = 88^0$, which is very good for a prime

focus reflector having f/D = 0.26. The cross-polarization level at 45^0 plane is -26 dB, which is quite reasonable for this kind of feeds. Although amplitude patterns of the E- and H plane are quite similar (Fig. 3.8 (a)) but the phase difference between the E-and H-planes is 12^0 at $\theta = 70^0$ and 23^0 at $\theta = 90^0$ (Fig. 3.8 (b)). This phase difference not only increases the cross-polarization level, but also causes different phase center locations in the E- and H-planes. It is also the reason for phase center displacement from the waveguide open end face.

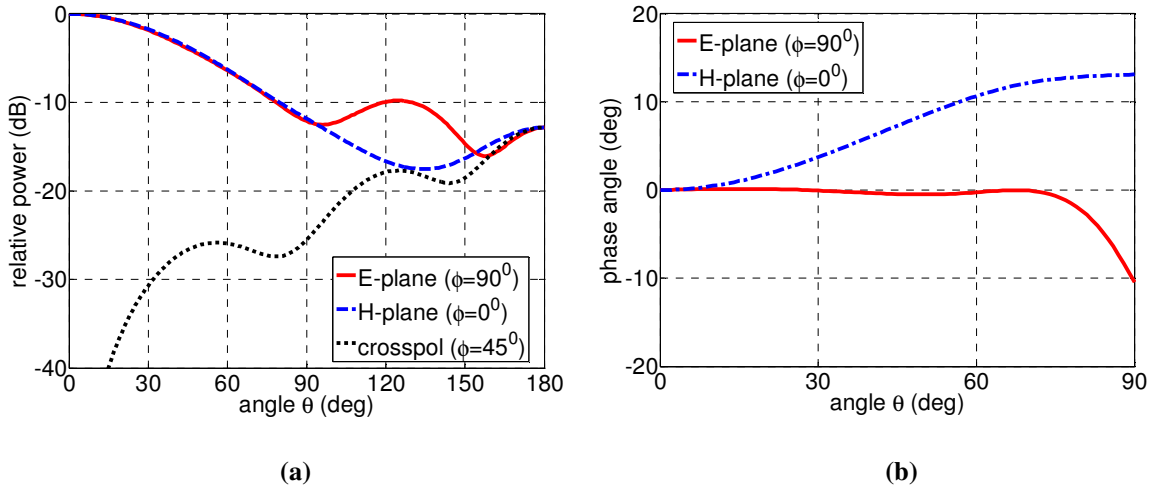

(a) **(b)**

Fig. 3.8 Radiation patterns of the E-plane slotted circular waveguide feed; l = 60mm, a = 10.5 mm, t = 1 mm, w = 18 mm and h = 2 mm. (a) amplitude pattern at 10 GHz (b) phase pattern, with respect to the co-ordinate origin at waveguide face.

Figs. 3.9 (a) and (b) show the amplitude and phase patterns of the H-plane slot case, for optimum slot parameters. The E- and H-plane patterns are symmetric up to $\theta = 84^0$, which is very good with prime focus reflectors having f/D = 0.28. The cross-polarization level at 45^0 plane is around -21 dB, which is reasonable for this kind of feeds. Although the amplitude patterns of the E- and H planes are similar, but their phase difference in the E-and H-planes is almost 28^0 at $\theta = 70^0$ and 30^0 at $\theta = 90^0$. This phase differences are

higher than those of the E-plane slot cases, causing higher cross-polarization level than the E-plane slot case.

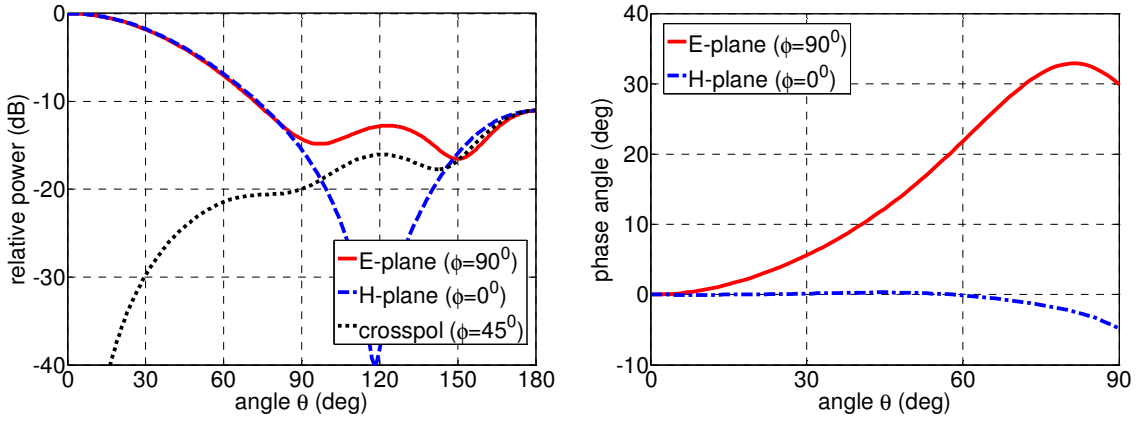

(a) **(b)**

Fig. 3.9 Radiation patterns of the H-plane slotted circular waveguide feed; l = 60mm, a = 10.5 mm, t = 1 mm, w = 18 mm and h = 4 mm. (a) amplitude pattern at 10 GHz (b) phase pattern, with respect to the co-ordinate origin at waveguide face.

Table 3.1 Radiation characteristics of circular waveguide feeds: no-slot, E-plane and H-plane slot cases; l = 60 mm, a = 10.5 mm, t = 1 mm.

	No-slot [22]	E-plane slots w = 18 mm, h = 2 mm	H-plane slots w = 18 mm, h = 4 mm
-10 dB beamwidths, (E-plane)	156	156	142
-10 dB beamwidths, (H-plane)	142	156	142
Cross-pol at 45^0, ($0< \theta \leq 90^0$)	-25 dB	-25.9 dB	-20.6 dB
Back lobe level	-12 dB	-12.9 dB	-11.1 dB

Table 3.1 summarizes the circular waveguide feed with radius 0.35 λ_0, for the no-slot [22], and the E- and H-plane slot cases. It is noticed from the table that pattern equalization is possible for both the E- and H-plane slot cases, although the beamwidths are different for each case. The -10 dB beamwidth for the E -plane slot case is 156^0, which is wider than the H-plane slot case. Therefore, it requires a reflector with larger

aperture angle, or small f/D. The cross-polarization level is lower for the E-plane slot case than the H-plane slot case, and the back lobe level is almost the same for both cases.

3.2.3 Performance of Slotted Waveguide Feeds

When an antenna is used as a feed on a prime focus reflector, its performance in terms of spillover efficiency, illumination efficiency and gain factor are the most important parameters. The other important factor for the feed is the stability of its parameters within its frequency band. In the following sub-section, the performance of the above E- and H-plane slotted circular waveguide feeds are investigated for the efficiency and frequency stability, and discussed.

3.2.3.1 Performance of Slotted Waveguide Feeds

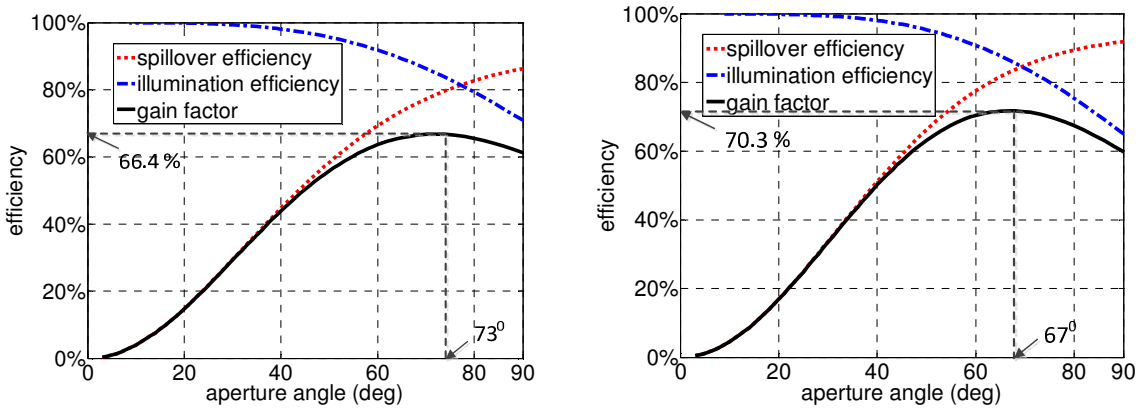

Fig. 3.10 Gain factor, spillover efficiency and illumination efficiency of the slotted circular waveguide feed; l = 60 mm, a = 10.5 mm, t = 1 mm. (a) E-plane slot (b) H-plane slot.

The performances in terms of the spillover efficiency, illumination efficiency and gain factor of slotted circular waveguide feeds are shown in Fig. 3.10, for the above two

cases, shown in Table 3.1. Fig. 3.10 (a) shows the results for the E-plane slot case, with w = 18 mm, and h = 2 mm. Fig. 3.10 (b) shows the same results for the H-plane slot case, with w = 18 mm and h = 4 mm. As expected, by increasing the aperture angle the gain factor of the feed is increasing until its reaches to its maximum point when multiplication of spillover and illumination efficiency is highest, and after that point the gain factor is decreasing again.

Table 3.2 Performance of a circular waveguide feed for no-slot, E-plane slot and H-plane slot cases at angle θ_0, where the gain factor is maximum; l = 60 mm, a = 10.5 mm, t = 1 mm.

	No-slot	E-plane slots w = 18mm, h = 2 mm	H-plane slots w = 18 mm, h = 4 mm
θ_0	68^0	73^0	67^0
η_s	77.6%	79.5%	83.1%
η_i	86.6%	84.4%	86.4%
$\boldsymbol{\eta}_g$	67.2%	66.4%	70.3%

where,

θ_0 = aperture angle at which gain factor is maximum,
η_s = spillover efficiency at θ_0,
η_i = illumination efficiency at θ_0,
$\boldsymbol{\eta}_g$ = maximum gain factor at θ_0.

Table 3.2 compares the gain factor, spillover efficiency and illumination efficiency for the no-slot case with these two cases. For the E-plane slot case, the peak gain factor occurs for the aperture angle 73^0, where the spillover and illumination efficiencies are 79.5% and 84.4% respectively. For the H-plane slot case, they are 83.1% and 86.4% respectively and occur at a smaller angle $\theta_0 = 67^0$. Therefore, both efficiencies are higher for the H-plane slot case because at -10 dB edge taper, the beamwidth is narrower than that of the E-plane slot case (see Fig. 3.8(a) and Fig. 3.9(a)). The gain factor of the E-

plane slotted circular waveguide feed is 66.4% at aperture angle 73^0, which is almost same as no-slot case. However, the gain factor for the H-plane slotted feed is 70.3% at the aperture angle $\theta_0 = 67^0$, which provides larger gain factor than the E-plane slots and the no-slot cases. Therefore, the gain factor is improved for the H-plane slot case.

3.2.3.2 Frequency Stability of Slotted Waveguide Feeds

To determine the performance of slotted waveguide feeds as a function of frequency, feeds are simulated at 10% bandwidth around the center frequency of 10 GHz. The performance data for the E-plane slotted feed which is from 9.7 GHz to 10.7 GHz is shown in Table 3.3. The data shows excellent results for the E- and H-plane -10 dB beamwidths within the 10% frequency band. The cross-polarization and back lobe levels are almost the same for all three different frequencies. The gain factor of the antenna is slightly lower in the lower limit of the frequency band.

Table 3.3 Performance of the E-plane slotted circular waveguide feed within 10% bandwidths; l = 60 mm, a = 10.5 mm, t = 1 mm, w = 18 mm, h = 2 mm.

	$0.97f_0$	f_0	$1.07f_0$
-10 dB beamwidth, (E-plane)	158^0	156^0	144^0
-10 dB beamwidth, (H-plane)	148^0	156^0	140^0
Cross-polarization level, $(0 < \theta \leq 70^0)$	-25.6 dB	-25.9 dB	-26.8 dB
Back lobe level	-14 dB	-13.2 dB	-13.4 dB
Max gain factor at $\theta = 71^0$	64.9%	66.4%	67.4%

Table 3.4 shows the performance data for the H-plane slotted feed from 9.5 GHz to 10.5 GHz. The 10 dB beamwidths of the feed for the E- and H-plane at three different

frequencies are almost the same. The cross-polarization levels at three different frequencies are -20.5 dB, -20.6 dB and -20.5 dB, respectively, and are also almost the same for three cases. The back lobe levels are also the same for all three cases. The gain factor of the feed is above 68.5%, and increases with frequency.

Table 3.4 Performance of the H-plane slotted circular waveguide feed within 10% bandwidths; l = 60 mm, a = 10.5 mm, t = 1 mm, w = 18 mm, h = 4mm.

	$0.95f_0$	f_0	$1.05f_0$
-10 dB beamwidth, (E-plane)	150	142	138
-10 dB beamwidth, (H-plane)	144	142	137
Cross-polarization level ($0 < \theta \leq 70^0$)	-20.5 dB	-20.6 dB	-20.5 dB
Back lobe level	-12 dB	-10 dB	-13.3 dB
Max gain factor at $\theta = 67^0$	68.5%	70.3%	71.1%

3.2.4 Phase Center of Slotted Waveguide Feeds

The phase centers of these slotted feeds [52] are expected to move on the Z-axis, as the configuration is symmetric about the Z-axis and radiation is in that direction. Since the phase of the radiated field components cannot be completely constant over entire θ ranges, the aim here is to find the point on the Z-axis that leads to a minimum variation in the phase of the E- and H-plane radiated fields. The phase data of the far field component is used to calculate the displacement needed on the Z-axis to minimize the phase difference in the radiated far field phase over certain θ ranges for different ϕ values. As the phase center location and reflector focal point are the same, attention is given to the θ ranges up to 70^0 or f/D = 0.36, assuming that the feed will be used on that reflector.

Fig. 3.11 compares the phase variations and phase center locations for the no-slot, E-plane slot and H-plane slot cases, verses the aperture angle. Fig. 3.11 (a) shows that the phase variation is increasing with the aperture angle and it is less with the no-slot case, than the other two cases. Since the phase variations are higher at higher aperture angles that cause the change in the phase center location which is shown in Fig. 3.11 (b). It also indicates that the cross-polarization level will be higher for the E- and H-plane slot cases with respect to the no-slot case.

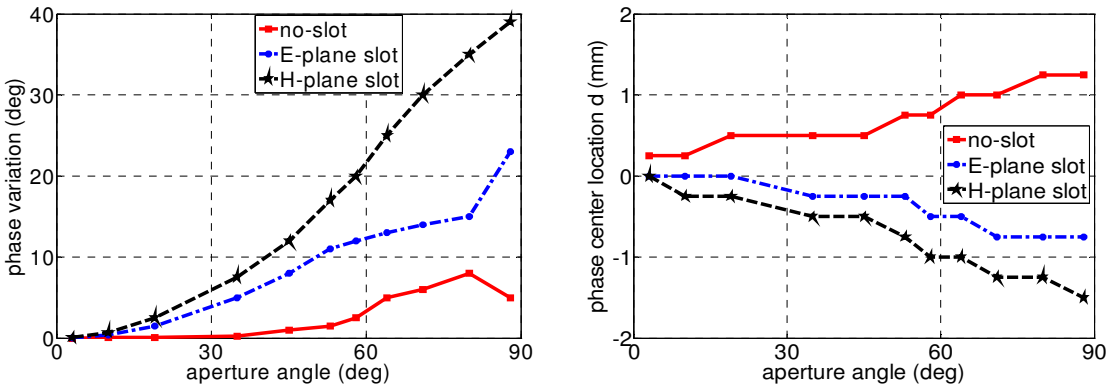

Fig. 3.11 Phase variations and phase center locations of a circular waveguide feed for three different cases; l = 60 mm, a = 10.5 mm, t = 1 mm, w = 18 mm. E-plane slot case: h = 2 mm, H-plane slot case: h = 4 mm. (a) phase variation, (b) phase center location. The phase center location is measured from the waveguide aperture.

Figs. 3.12 (a) and (b) show the phase center location d in the E-plane d_E, H-plane d_H and combined d_c locations of the E- and H-plane slotted circular waveguide feeds by varying the slot height. The negative value of d_c indicates that the combined phase center location is inside the waveguide for both cases. From the figure it is evident that for the E-plane slot case, the phase center distance d_c is approximately half of the slot height, irrespective of the height. However, for the H-plane slot case, initially d_c is half of the

slot height, and then increases with the slot height. This indicates that for larger slot heights, the phase variations of the both E- and H-plane slots are higher, and also the phase variation of the H-plane slot is higher than the E-plane slot. As phase variation is higher at larger slot heights, for both cases, the cross-polarization level is also higher for these cases.

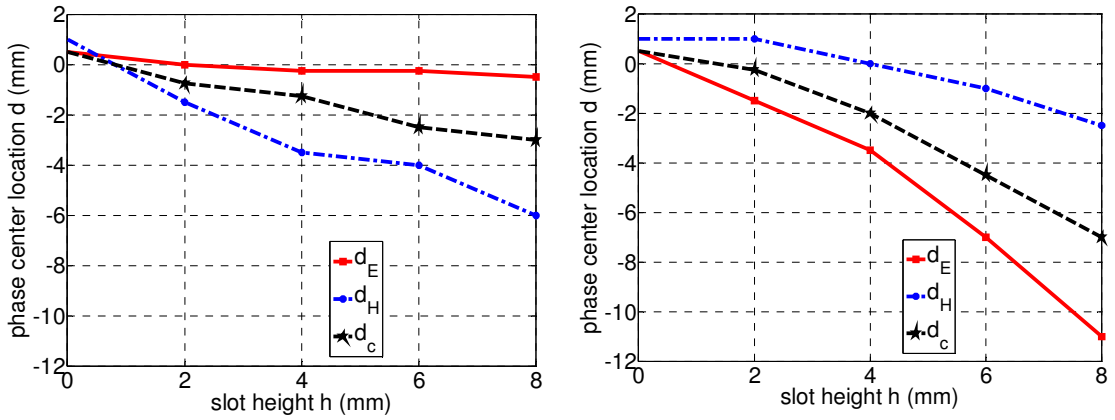

Fig. 3.12 Phase center location d of the slotted circular waveguide feeds for different slot heights at aperture angle $\theta_0 = 70^0$; l = 60 mm, a = 10.5 mm, t = 1mm, w = 18 mm. (a) E-plane slots (b) H-plane slots.

3.2.5 Experimental Verification of Slotted Feeds

In the previous sub-sections, the E- and H-plane slotted circular waveguide feeds were investigated, where slot width and height influenced the radiation patterns of the feed. It is therefore important to study experimentally the performance of a fabricated antenna, which will also be influenced by both fabrication tolerances and measurement accuracy. Thus a feed antenna was fabricated with its dimensions as: length l = 60 mm, radius a = 10.5 mm and wall thickness t = 1 mm. The fabricated feed antenna is shown in Fig. 3.13. For the simplicity of the feed fabrication, one slot size (w = 18 mm and h = 4

mm) was selected for the H-plane slot case. The antenna was fed by a rectangular waveguide, which was connected to the feed using a short rectangular-to-circular waveguide transition, having a diameter of 26 mm, which is slightly larger than the feed waveguide diameter of 21 mm. Therefore, the feed diameter was tapered slightly to 26 mm to match that of the transition.

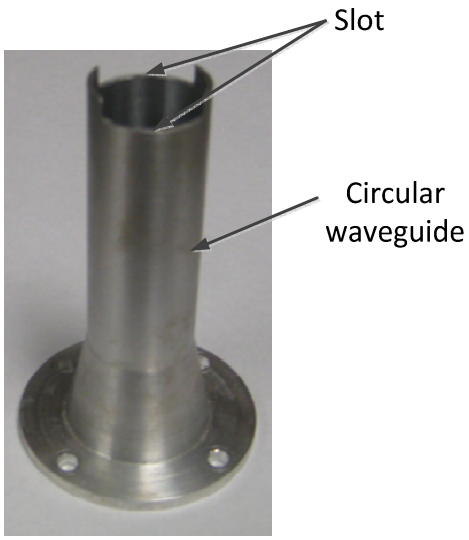

Fig. 3.13 Fabricated slotted circular waveguide feed. Feed dimensions: l= 60 mm, a = 10.5 mm, t = 1 mm, slot dimensions: w = 18 mm, h = 4 mm.

The fabricated antenna was tested in the antenna Laboratory at the University of Manitoba. The simulated and measured radiation patterns of the feed are shown in Fig. 3.14. The simulated and measured E- and H-plane radiation patterns are almost identical for this case. The measured cross-polarization level at 45^0 plane is also almost identical as the simulated cross-polarization level.

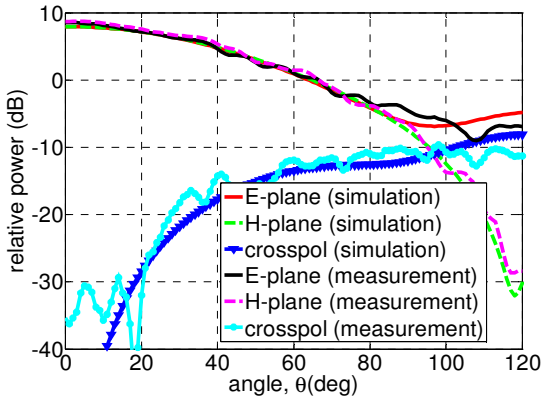

Fig. 3.14 The simulated and measured radiation patterns of the H-plane slotted circular waveguide feed of, a = 10.5 mm, t = 1 mm, w = 18 mm and h = 4 mm at 10 GHz.

3.3 Slotted Waveguide Feeds with a Choke

Slotted circular waveguide feeds presented in the previous section showed the symmetrical E- and H-plane radiation patterns. However, the beamwidths of the antenna were wide at -10 dB edge taper, which caused lower spillover efficiency and that ultimately reduced the gain factor of the antenna. The cross-polarization and back lobe levels also did not improve and therefore, gain factors remained the same. Hence, attempts have been made to decrease the beamwidths, improve the cross-polarization and back lobe levels, by retaining pattern symmetry.

We know that the back lobe level is strongly influenced by diffractions from the edges, especially from those that are perpendicular to the E-field of the aperture. The diffractions also lead to undesirable radiations in the back directions. It also affects the main lobes and the minor lobes. Therefore, attempts are made to reduce the diffractions from the edges by using chokes. The region between the open end of the waveguide and choke wall act like a shorted section of a transmission line, where by making the choke

height equal to $\lambda_0/4$, large reactive impedance is created. Thus, the current is almost zero on that region. Initially a single choke is introduced in the slotted circular waveguide feed, to improve the cross polarization and back lobe levels, along with the pattern symmetry of the E- and H-planes. The effects of multiple chokes on the feed performance are also addressed later. The above two geometries of slotted circular waveguides are discussed for this reason. The first geometry is the E-plane slotted feed and the other geometry is the H-plane slotted feed. As the slots locations are different in the two cases, their effects are different. It is therefore necessary to investigate them separately.

3.3.1 Slotted Feed Design with a Choke

The E-plane slotted circular waveguide with a single choke feed [53] is shown in Fig. 3.15. The waveguide dimension l = 60 mm, a = 10.5 mm and t = 1 mm are chosen, so that only the dominant TE_{11} mode will propagate in the structure. The aperture lies on the parallel to XY-plane and the electric field is excited in the y-direction. As before, two opposite rectangular E-plane slots, cut in the opening end of the waveguide wall are transverse to the direction of the electric field, width w, and height h.

A choke is introduced with this structure. The radius cr of the choke is from the center point to the inner side of the choke wall and the thickness of the choke wall is the same as the waveguide wall thickness. For simplicity of the explanation the choke gap g_1 is denoted as distance between the outer wall of the waveguide to the inner wall of the choke. The choke gap is selected as 1 mm to keep the overall radius of the feed as small

as possible. The height of the choke is denoted by ch, which is designed to be around quarter wavelength of the operating frequency, which is 7.5 mm at 10 GHz.

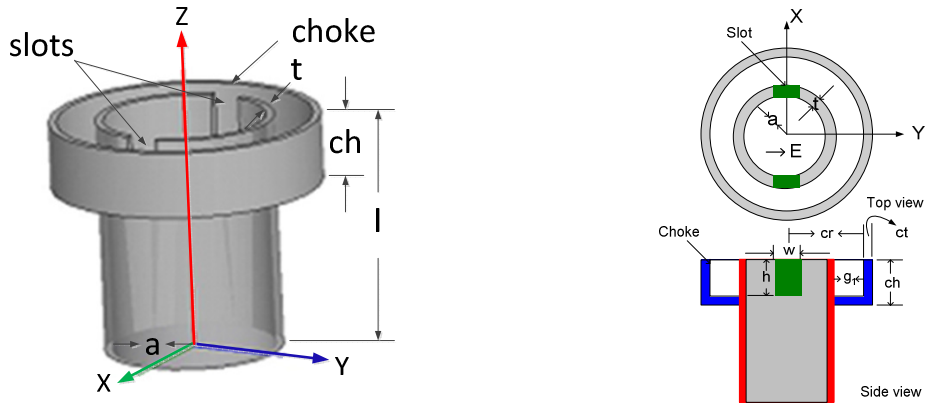

(a) (b)

Fig. 3.15 E-plane slotted circular waveguide feed with a single choke, at y-polarization; l = 60 mm, a = 10.5 mm and t = 1mm; (a) 3-D view, (b) 2-D view.

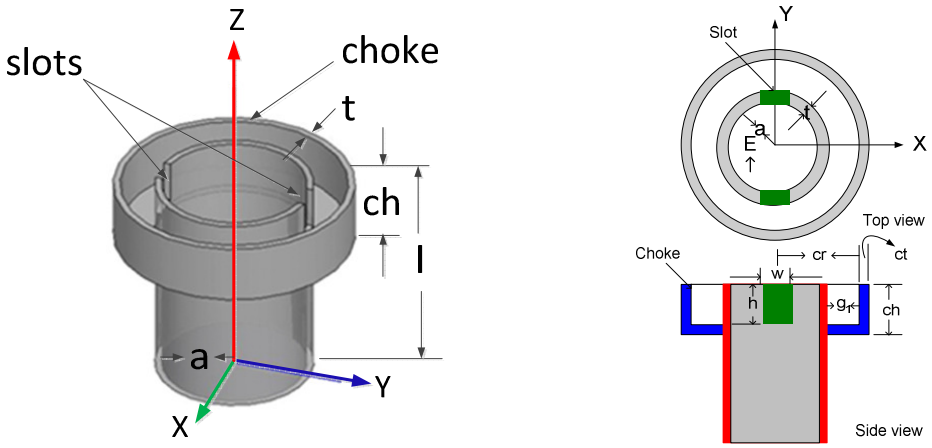

(a) (b)

Fig. 3.16 H-plane slotted circular waveguide feed with a single choke, at y-polarization; l = 60mm, a = 10.5 mm, t = 1 mm; (a) 3-D view, (b) 2-D view.

The geometry of the H-plane slotted waveguide feed with a single choke is shown in Fig. 3.16. Two opposite rectangular H-plane slots, cut in the open face of the waveguide

wall, are perpendicular to the direction of the electric field and their dimensions are denoted by width w, and height h. Like the previous case, a choke of height ch and gap g_1 is introduced with the structure.

3.3.1.1 Radiation Patterns of Slotted Feeds with a Choke

The feeds are designed and simulated, after several iterations. For the E-plane slot case, the optimized slot width and height are 2 mm and 3 mm, respectively. The amplitude patterns of the feed are shown in Fig. 3.17 (a), which shows pattern symmetry up to 80^0, which is very useful as a feed for prime focus reflector antennas. The cross-polarization and back lobe level are -33 dB and -26 dB, respectively, which are also very low. Fig. 3.17 (b) indicates the phase angle variations up to 30^0, for an aperture angle of 80^0, which indicates a phase center location outside the waveguide aperture. However, the minimum phase difference between the E- and H-plane is low that indicates low cross-polarization level, which is confirmed by Fig. 3.17 (a).

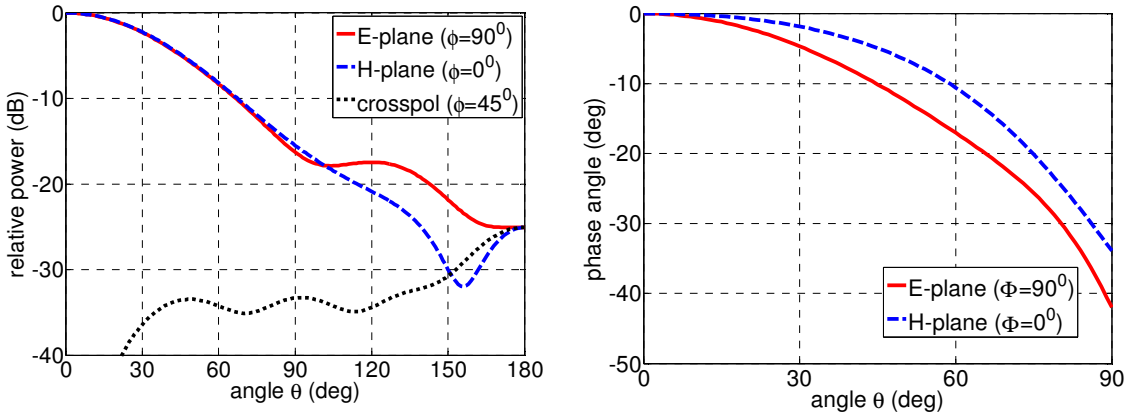

(a) **(b)**

Fig. 3.17 Radiation patterns of the E-plane slotted circular waveguide feed with a single choke; l = 60 mm, a = 10.5 mm, t = 1 mm, w = 2 mm, h = 3 mm, g_1 = 1 mm, ch = 7.5 mm. (a) amplitude patterns at 10 GHz, (b) phase patterns with respect to the co-ordinate at waveguide face.

For the H-plane slot case, slot width w and slot height h are selected as 16 mm and 4 mm, respectively, after several iterations. The radiation patterns of the feed are shown in Fig. 3.18 (a), where all antenna dimensions are also shown. The co-polar radiation patterns are symmetric up to 90^0 and that angular range is good enough for the feed of a prime focus reflector antenna. The cross-polarization at 45^0 plane and back lobe levels are -22.5 dB and -13.3 dB, respectively. Fig. 3.18 (b) shows the phase patterns of the feed when the coordinate origin at waveguide aperture, where the phase variations of the E- and H-plane increase with the aperture angle. As the phase difference between E- and H-planes is higher for a higher aperture angle, it indicates a higher cross-polarization level, which is confirmed by Fig. 3.18 (a).

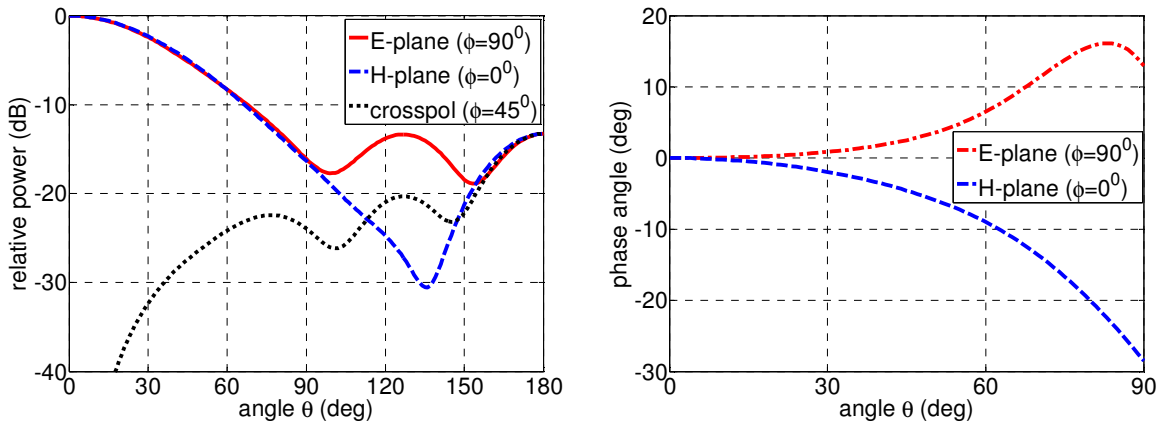

(a) **(b)**

Fig. 3.18 Radiation patterns of the H-plane slotted circular waveguide feed with a single choke; l = 60 mm, a = 10.5 mm, t = 1mm, w = 16 mm, h = 4 mm, g_1 = 1 mm, ch = 7.5 mm. (a) amplitude patterns at 10 GHz, (b) phase patterns with respect to co-ordinate at waveguide face.

Table 3.5 shows the electrical characteristics of the circular waveguide with a single choke feed, for three different cases: no-slot, E-plane slot and H-plane slot. It shows that

radiation patterns are equal in the E- and H-plane slot cases, compared to no-slot case. The beamwidths for the E- and H-plane slot cases are 135^0 and 134^0 respectively. The cross-polarization level for the E-plane is -33.5 dB compare to -22.5 dB for the H-plane slot case. Therefore, the cross-polarization level is lower for the E-plane than the H-plane slot case. This is because of the smaller phase difference between E- and H-planes, in the E-plane slot case, than the H-plane slot (Fig. 3.17 (b) and Fig. 3.18 (b)). The back lobe level for the E-plane is -26 dB, which is lower than the H-plane slot case (-13.3 dB), and again it is comparable with the no-slot case.

Table 3.5 Radiation characteristics of the slotted circular waveguide feed with a single choke for various cases; l = 60 mm, a = 10.5 mm, t = 1 mm, g_1 = 1 mm, and ch = 7.5 mm.

	No-slot with a single choke [22]	E-plane slots with a single choke (w= 2 mm, h = 3 mm)	H-plane slots with a single choke (w=16 mm, h = 4 mm)
-10 dB beamwidths, (E-plane)	128^0	135^0	134^0
-10 dB beamwidths, (H-plane)	135^0	135^0	134^0
Cross-pol at 45^0, ($0< \theta \leq 90^0$)	-32 dB	-33.5 dB	-22.5 dB
Back lobe level	-25 dB	-26 dB	-13.3 dB

3.3.2 Performance of Slotted Feeds with a Choke

The performance in terms of the spillover, and illumination efficiencies and the gain factor of the circular waveguide feed with a single choke, for three different cases: no-slot, E-plane slot and H-plane slot, are demonstrated in Table 3.6. The spillover efficiencies are 82.4%, 85.7% and 83.4%, respectively, for the no-slot, E-plane slot and H-plane slot case. It is higher for the E-plane slot case because of the low relative power beyond the aperture angle θ_0. The illumination efficiencies are around 85%, which are

almost the same for all three cases. The gain factors for no slot, E- and H-plane slot cases are 68.8%, 72.8% and 70.5% respectively. Therefore, it clearly shows that the gain factors are higher for the E- and H-plane slot case than the no slot case.

Table 3.6 Performance of the slotted circular waveguide feed with a single choke in terms of efficiency for various cases; l = 60 mm, a = 10.5 mm, t = 1 mm, g_1 = 1 mm, ch = 7.5 mm.

	No-slot with a single choke	E-plane slots with a single choke (w = 2 mm, h = 3 mm)	H-plane slots with a single choke (w = 16 mm, h = 4 mm)
θ_0	63^0	64^0	64^0
η_s	82.4%	85.7%	83.4%
η_i	84.8%	85.6%	85.5%
η_g	68.8%	72.8%	70.5%

where,

θ_0 = aperture angle at which gain factor is maximum.
η_s = spillover efficiency at θ_0.
η_i = illumination efficiency at θ_0.
η_g = maximum gain factor of the feed at θ_0.

3.3.3 Phase Center of Slotted Feeds with a Choke

The phase centers of these slotted feed with choke are expected to move on the Z-axis as before. As the phase center location and reflector focal point coincide with each other, attention is given to the θ ranges up to 90^0 or f/D = 0.25. Fig. 3.19 shows the phase center locations for the E- and H-plane slot cases. In this figure a positive d means that the phase center is in front of the waveguide aperture and negative d means the phase center is inside the waveguide. The figure shows that for the E-plane slot case, the phase center is outside the waveguide aperture, whereas for the H-plane slot case it is almost at waveguide face. This is because phase deviation of E- and H-plane with aperture angle is higher for the E-plane slot than the H-plane slot case. However, phase difference between

the two planes is small for the E-plane slot case than the H-plane slot case, which is confirmed by Fig. 3.17 (b) and Fig. 3.18 (b). Therefore, the cross-polarization level is low for the E-plane slot case.

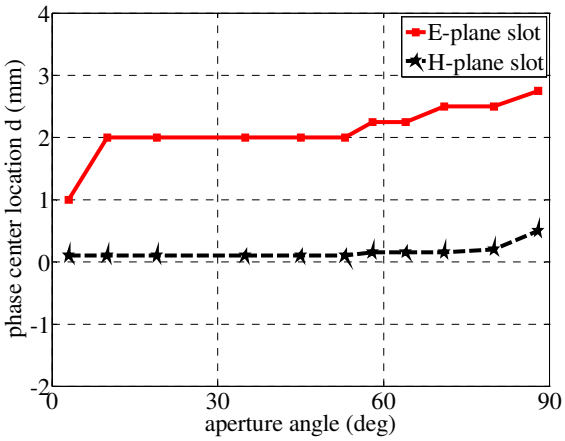

Fig. 3.19 Phase center location d of the slotted circular waveguide feed with a single choke for E- and H-plane slot cases; Feed parameters are shown in Fig. 3.17 and Fig. 3.18.

3.3.4 Experimental Verification of Feeds with a Choke

To verify the performance of the slotted feeds with choke, studied in the previous sections, one antenna was built and tested at the University of Manitoba Antenna Laboratory. The dimension of the feed was: l = 60 mm, a = 10.5 mm, t = 1 mm, g_1 = 1 mm, h = 7.5 mm, which is shown in Fig. 3.20. For the simplicity of the feed fabrication, slots with size of w = 16 mm and h = 4 mm were selected. The same feed was used for both E- and H-plane slotted cases, by changing the polarization of the field inside the waveguide. The antennas were fed by a rectangular waveguide which was connected to the feed using a short rectangular-to-circular waveguide transition, having a diameter of 26 mm, which is slightly larger than the feed waveguide diameter of 21 mm. Therefore, the feed diameter was tapered slightly to 26 mm to match that of the transition.

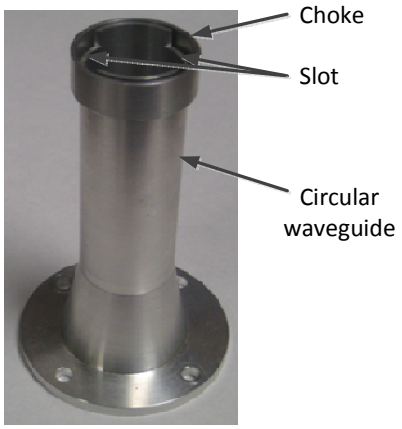

Fig. 3.20 Fabricated slotted circular waveguide feed with a single choke; l = 60 mm, a = 10.5 mm, t = 1 mm, w = 18 mm, h = 4 mm, g_1 = 1mm, h = 7.5 mm.

The simulated and measured radiation patterns of the fabricated slotted waveguide feed with choke are shown in Figs. 3.21 (a) and (b), respectively. The measured co-polar radiation patterns are almost identical to the simulated radiation pattern and symmetric up to 90^0, and that the angular range is good enough for the feed of a prime focus reflector antenna. The cross-polarization level at the 45^0 plane for simulated and measured radiation patterns is also almost the same.

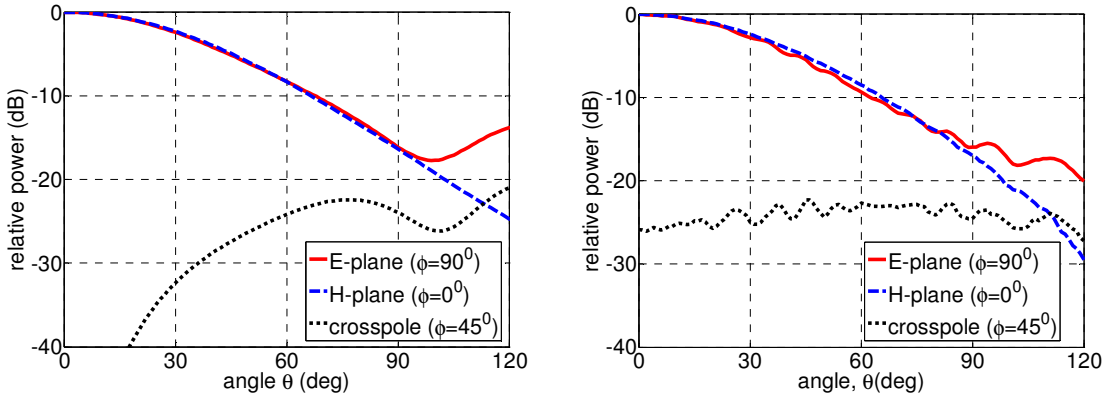

Fig. 3.21 Simulated and measured radiation patterns of the H-plane slotted circular waveguide feed with a single choke; antenna parameters are shown in Fig. 3.20. (a) simulation, (b) measurement.

3.3.5 Slotted Waveguide Feeds with Multiple Chokes

The slotted circular waveguide feeds with a single choke were investigated in the previous sub-sections, where it was found that the pattern equalization with low back lobe level was possible for these feeds. The gain factor of the feeds was also improved over those without a choke. Using the same concept describe in section 3.3.3 for reducing the cross-polarization and back lobe level, multiple chokes are added to the slotted circular waveguide feeds, to investigate the radiation characteristics and to improve their gain factors. However, adding multiple chokes increase the overall diameter of the feeds, which ultimately increase the feed blockage and reduce the gain factor. In the following sub-section, the effects of multiple chokes on the slotted waveguide feed performance are investigated, for both slotted cases.

3.3.5.1 Slotted Feed Design with Multiple Chokes

The geometry of the E-plane slotted circular waveguide feed with double chokes is shown in Fig. 3.22 (a), where all the parameters are shown in the figure caption. The gap and height of the second choke is selected after several iterations with optimization of the radiation patterns. Introducing second choke with the structure, the overall diameter of the feed is increased to 15.5 mm (0.517 λ_0), which is still small compared to the wavelength of the operating frequency.

The amplitude patterns of the feed are shown in Fig. 3.22 (b), where the E- and H-plane co-polar patterns are very symmetric up to 80^0 with very low cross-polarization. The phase pattern, shown in the Fig. 3.22 (c), illustrates that the E- and H-plane phase angle are very close to each other, though there are large phase deviations at higher

angles. This indicates that it has low cross-polarization with its phase center being outside of the waveguide face.

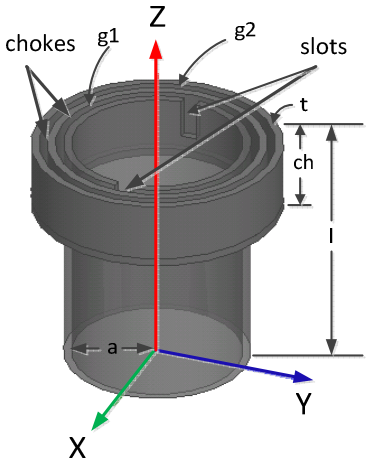

(a)

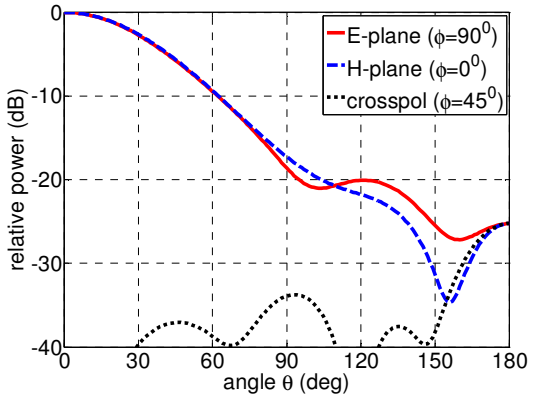

(b)

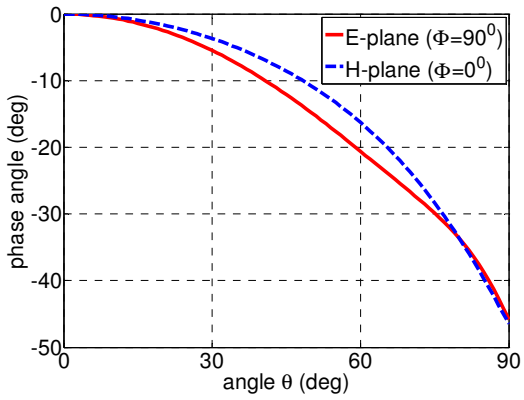

(c)

Fig. 3.22 E-plane slotted circular waveguide feed with double chokes; l = 60 mm, a = 10.5 mm, t = 1 mm, g_1 = 1 mm, g_2 = 1 mm, ch = 7.5 mm, w = 2 mm, h = 5 mm. (a) geometry, (b) amplitude pattern at 10 GHz, (c) phase pattern, with respect to the co-ordinate origin at waveguide face.

The amplitude patterns of an E-plane slotted waveguide with triple chokes are shown in Fig. 3.23 (a). All feed dimensions are the same as the previous case with the additional parameter as the third choke gap, which is 1 mm. Now the overall radius of the feed is

17.5 mm (0.583 λ_0), which is still small compared to the wavelength of the operating frequency. The amplitude patterns show that the E- and H-plane co-polar patterns are very symmetric up to 90^0 with low cross-polarization level. The advantage of using the additional choke is that the back lobe level is low compare to the previous case. The phase pattern, which is shown in Fig. 3.23 (b) shows that the E- and H-plane phase angles are very close to each other. However, there are large phase variations of the E- and H-plane with respect to the large angle. This indicates that the feed has low cross-polarization, with its phase center being the outside the waveguide face.

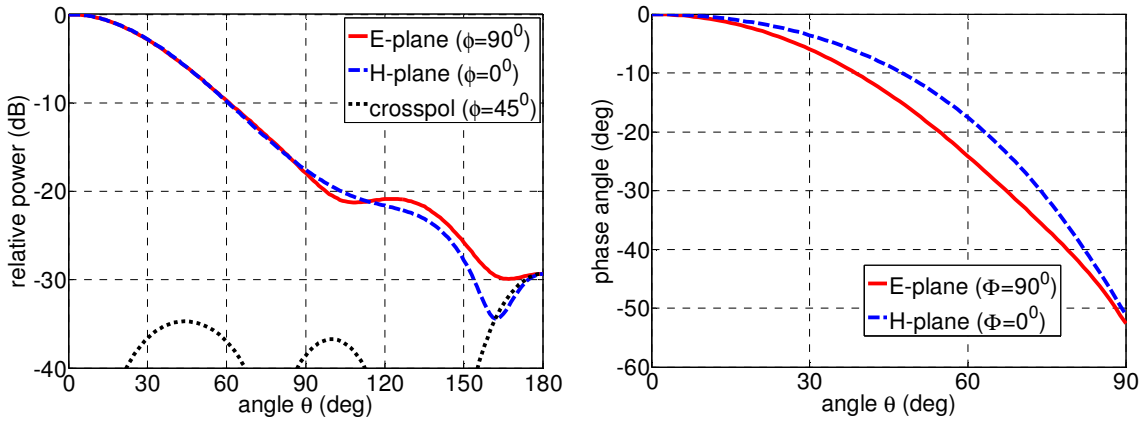

(a) **(b)**

Fig. 3.23 Radiation patterns of the E-plane slotted circular waveguide feed with triple chokes; l = 60 mm, a = 10.5 mm, t = 1 mm, g_1 = 1 mm, g_2 = 1 mm, g_3 = 1 mm, ch = 7.5 mm, w = 2 mm, h = 5 mm. (a) amplitude pattern at 10 GHz, (b) phase pattern, with respect to the co-ordinate origin at waveguide face.

The geometry of the H-plane slotted circular waveguide feed with double chokes is shown in Fig. 3.24 (a), where the antenna parameters are shown in the figure caption. Fig. 3.24 (b) shows the radiation patterns where, the E- and H-plane patterns are not symmetric, with the H-plane pattern being slightly wider than the E-plane pattern. The 10-dB beamwidth in the E- and H-plane are 124^0 and 128^0, respectively. The cross-

polarization level is very low in this case. This is because the phase patterns of the E- and H-planes are symmetric up to 70^0, which can be verified by Fig. 3.24 (c). Although the phase patterns are symmetric, there is a still phase variation of both planes with the angle, and the phase center location is outside the waveguide face. The back lobe level of the feed is -25 dB, which is also low compared to the single choke feed case.

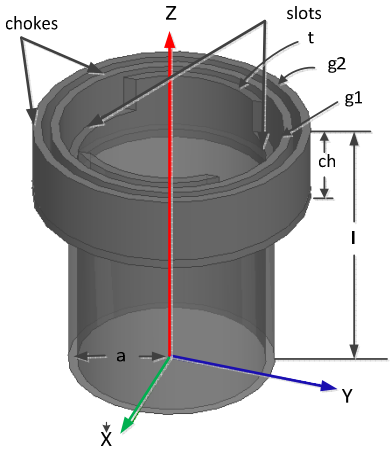

(a)

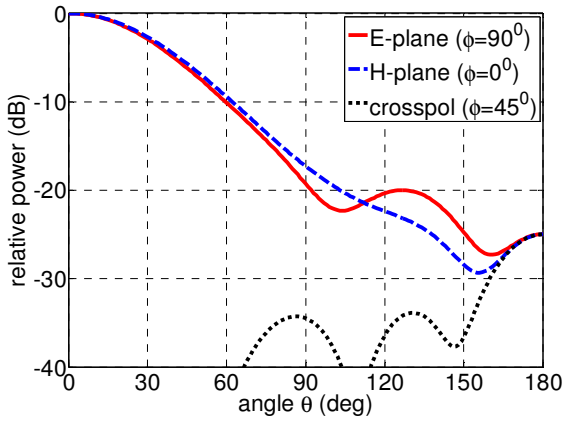

(b)

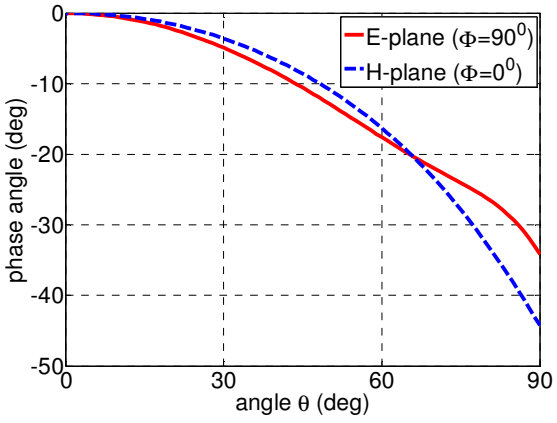

(c)

Fig. 3.24 H-plane slotted circular waveguide feed with double choke; l = 60 mm, a = 10.5 mm, t = 1 mm, g_1 = 1 mm, g_2 = 1 mm, ch = 7.5 mm, w = 16 mm, h = 4 mm. (a) geometry, (b) amplitude pattern at 10 GHz, (c) phase pattern, with respect to the co-ordinate origin at waveguide face.

3.3.5.2 Performance of Slotted Feeds with multiple chokes

The performances of the E-plane slotted circular waveguide feed with double chokes and triple chokes, and H-plane slotted circular waveguide feed with double chokes are shown in Table 3.7. The gain factor of the E-plane slotted feed with double chokes is 73.3%, and triple chokes is 72.6% and the same results for the H-plane slotted feed with double chokes is 73.3%, respectively. The results indicate that adding additional chokes decrease the beamwidth of the feed and improve the gain factor of the antenna. These results are also comparable with the feed designed by Shafai and Kishk [22]. For all cases, the gain factors of the feeds are higher than single choke case. However, two and three chokes give almost the same gain factor, although the three choke case increases the overall diameter of the feed, which causes the higher blocking effect.

Table 3.7 Performance of the feeds in terms of efficiency, waveguide radius a = 10.5 mm, wall thickness t = 1 mm, choke height ch = 7.5 mm, choke gaps g_1 = 1 mm, g_2 = 1mm, g_3 = 1mm, choke gaps are same for all cases.

	Circular waveguide feed with triple chokes, by Shafai and Kishk [22]. (feed radius 1.35 λ_0)	E-plane slotted circular waveguide feed with double chokes (feed radius 0.517 λ_0)	E-plane slotted circular waveguide feed with triple chokes (feed radius 0.583 λ_0)	H-plane slotted circular waveguide feed with double chokes (feed radius 0.517 λ_0)
θ_0	64^0	59^0	59^0	59^0
η_s	-	86.0%	85.5%	85.8%
η_i	-	86.0%	85.8%	86.0%
η_g	74.9%	73.3%	72.6%	73.3%

Where,

θ_0 = aperture angle at which gain factor is maximum.
η_s = spillover efficiency at θ_0.
η_i = illumination efficiency at θ_0.
η_g = gain factor of the feed at θ_0.

3.3.5.3 Phase Center of Slotted Feeds with Multiple Chokes

Fig. 3.25 shows the phase center location of slotted circular waveguide feeds with multiple chokes, for the E- and H-plane slot cases. For all cases, the phase center locations are outside the waveguide aperture and are further away from the waveguide face with larger aperture angles. This indicates the phase variations of the feed. However, the phase difference between E- and H-planes is small for all cases (Fig. 3.22 (c) or Fig. 3.23 (b)), indicating that the cross-polarization levels are small compared to single choke case.

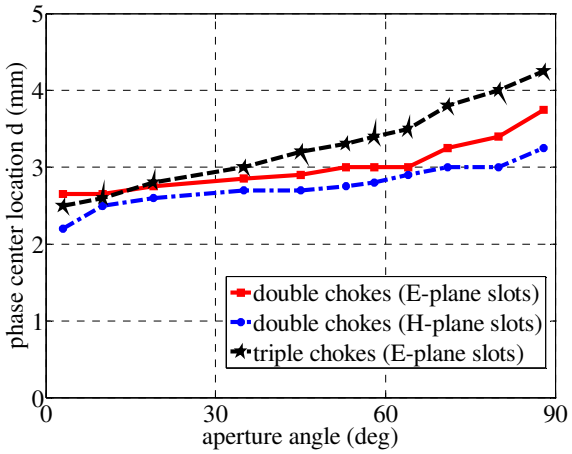

Fig. 3.25 Phase center location d of slotted circular waveguide feeds with double and triple chokes for three different cases.

3.4 Slotted Waveguide Feeds with a Cavity

Deep reflectors, which have small f/D values, or wide aperture angles, fail to provide high aperture efficiencies if the feed radiation patterns are tapered monotonically from broadside. To increase the aperture efficiency, the feed must produce uniform illumination over the parabolic aperture. Such feeds are often difficult to design as they

seldom give high gain factors, with low cross-polarizations. A circular waveguide feed with cavity have shown a good performance for the deep reflectors. This feed is composed of open ended coaxial cavity of length $\lambda_0/2$, where the current is high, with a circular waveguide acting as the inner conductor. The coaxial cavity is excited by the fields of the circular waveguide and excitation modes are decided by the cavity inner and outer diameters. Thus, the coaxial cavity acts as a non-resonance secondary source. The presence of slots in the circular waveguide opening face effects the field distribution of the waveguide. Therefore, the slots have effects on the overall feed structures.

The cavity with slotted circular waveguide increases the overall diameter of the feed, which ultimately increase the feed blockage. Therefore, this effect should be considered in designing the feed. In the following sub-section, we will discuss slotted circular waveguide feed with cavity for E- and H-plane slot cases.

3.4.1 Slotted Feed Design with a Cavity

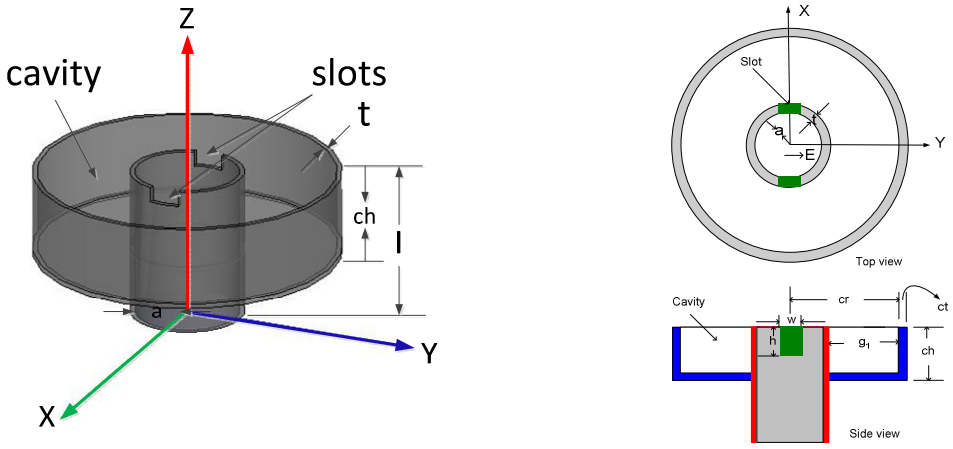

(a) **(b)**

Fig. 3.26 E-plane slotted circular waveguide feed with a single cavity, y-polarization; l = 60 mm, a = 10.5 mm, t = 1 mm, w = 16 mm, h = 1 mm, g_1 = 18.5 mm, ch = 17 mm; (a) 3-D view, (b) 2-D view.

The geometry of the E-plane slotted circular waveguide feed with a single cavity is shown in Fig. 3.26, where l = 60 mm, a = 10.5 mm, t = 1 mm, as before. The feed antenna is operating at fr = 10 GHz and its diameter confirms that only the dominant TE_{11} mode will propagate in the structure. A cavity is introduced with this structure. The radius, cr of the cavity is from the center point to the inner side of the cavity wall, and the wall thickness of the cavity is same as the waveguide wall thickness. For simplicity of the explanation, cavity gap is denoted as g_1, distance between the outer wall of the waveguide to the inner wall of the cavity. As the cavity gap increases, it increases the overall radius which will block the reflected wave from the reflector. The depth of the cavity is denoted by ch, which is initially designed around half wavelength of the operating frequency. The thickness of the cavity wall ct is the same as the thickness of the circular waveguide wall.

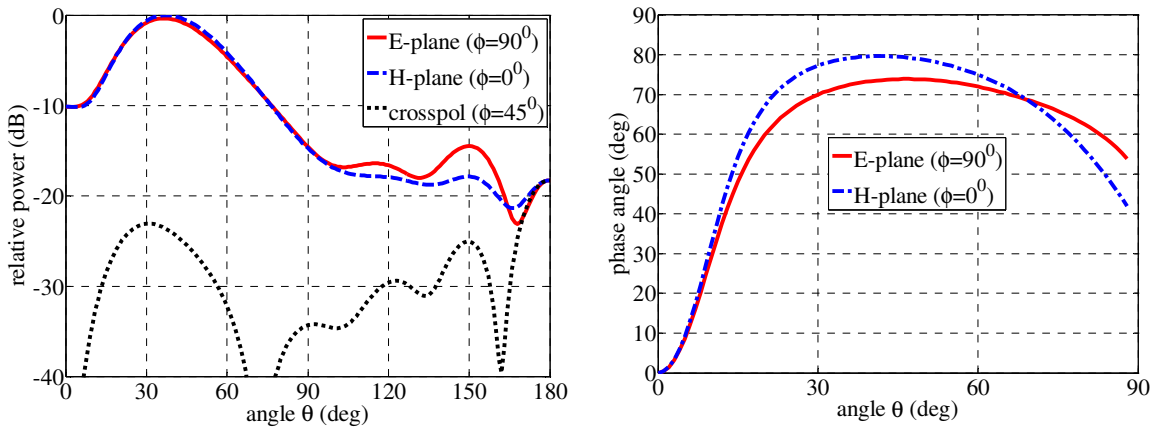

Fig. 3.27 Radiation patterns of the E-plane slotted circular waveguide feed with a single cavity. All parameters are shown in Fig. 3.26. (a) amplitude pattern at 10 GHz, (b) phase pattern, with respect to the co-ordinate origin at waveguide face.

For optimization of the feed parameters, the distance between waveguide wall and cavity gap g_1 is selected as 18.5 mm and the cavity depth ch is selected as 17 mm, after several iterations by changing the cavity gap and cavity depth. The simulated amplitude patterns of the feed are shown in Fig. 3.27 (a), with its parameters as shown in the Fig. 3.26. The radiated field can be divided into three types. One from the E-plane slotted circular waveguide, the second from the co-axial cavity, and the third from the diffracted fields due to the edges of the coaxial outer conductor. These three waves form a sector shape radiation patterns, which shows excellent pattern symmetry in the E- and H-plane. At boresight the value is -10 dB and it gradually increases with the angle, with the peak gain is at 37^0. The beamwidth at -10 dB taper of the feed is high compared to the previous cases and that causes higher gain factor of the antenna. The cross-polarization level of the antenna is low, which is reduced to -23.1 dB. Fig. 3.27 (b) shows the phase patterns of the antenna, which shows excellent phase pattern symmetry for the E- and H-planes. As the phase patterns are almost identical, the cross-polarization level is low for this case. The phase center locations for the E- and H-plane are close to each other. As Fig. 3.27 (b) shows there are phase variations in both E- and H-planes as a function of the aperture angle, and therefore the phase center is not located on the waveguide aperture.

The geometry of the H-plane slotted circular waveguide feed with a single cavity is shown in Fig. 3.28, with its parameters as shown in the figure. The aperture is parallel to the XY-plane, and the electric field is excited in the Y-direction. Two H-plane slots are placed in the waveguide open end to change the field distribution of the waveguide. The cavity gap g_1 is selected as 18.5 mm and the depth of the cavity is selected as 18 mm after several simulations by changing the cavity gap and cavity depth.

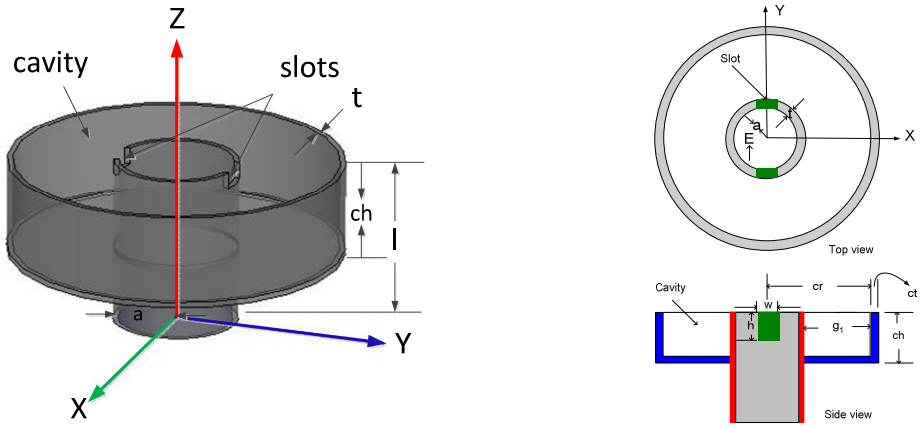

(a) **(b)**

Fig. 3.28 H- plane slotted circular waveguide feed with a single cavity, y-polarization; l = 60 mm, a = 10.5 mm, t = 1 mm, w = 16 mm, h = 1 mm, g_1 = 18.5 mm, ch = 17 mm; (a) 3-D view, (b) 2-D view.

The amplitude patterns of the feed at 10 GHz are shown in Fig. 3.29 (a), with its parameters given in the Fig. 3.28. At broadside, the value is around -12 dB and it gradually increases with the angle θ up to the peak gain of 38^0 and then gradually decreases with the angle θ. Therefore, the beamwidths at -10 dB taper of this feed are wider and that causes a higher gain factor of the antenna. The cross-polarization level of the antenna is very low, which is around -27 dB. Fig. 3.29 (b) shows the phase patterns of the antenna. The H-plane phase is higher than the E-plane phase up to the angle of 55^0 and then the E-plane phase is higher than the H-plane phase. Again as the phase of the E- and H-plane changes with the angle, it causes phase center displacement of the feed from the waveguide face.

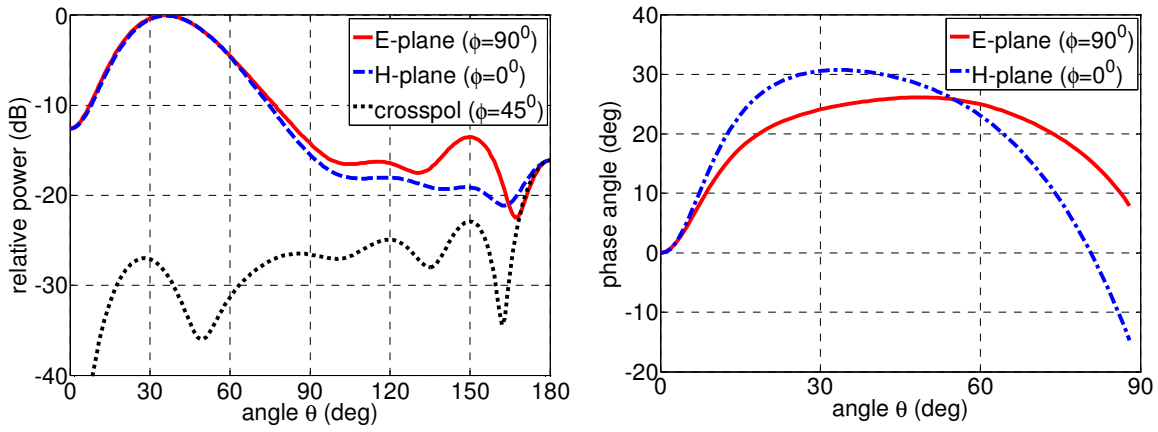

(a) **(b)**

Fig. 3.29 Radiation patterns of the H-plane slotted circular waveguide feed with a single cavity. All parameters are shown in Fig. 3.28. (a) amplitude pattern at 10 GHz, (b) phase pattern, with respect to the co-ordinate origin at waveguide face.

Table 3.8 summarize the circular waveguide feed with a single cavity for no-slot [31], E-plane slot and H-plane slot cases. From the table it is observed that the pattern equalization is possible for the E- and H-plane slot cases. However, the -10 dB beamwidths are higher for the E- and H-plane slot cases, compared to no-slot case. The cross-polarization level is lower for the E and H-plane slot cases than the no-slot case.

Table 3.8 Radiation characteristics of the slotted circular waveguide feed with a single cavity; l = 60 mm, a = 10.5 mm, t = 1 mm.

	E-plane slotted case (g_1 = 18.5 mm, ch = 17 mm, w=16 mm, h = 1mm)	H-plane slotted case (g_1 = 18.5 mm, ch = 18 mm. w=16 mm, h = 1mm)	No-slot case [31] (a=11.9 mm, g_1 = 20.6 mm, ch = 14.1 mm)
-10 dB beamwdith, (E-plane)	152^0	152^0	142^0
-10 dB beamwdith, (H-plane)	152^0	150^0	144^0
Cross-pol at 45^0, ($0< \theta \leq 90^0$)	-23.1	-27	-16.9
Back lobe level	-18.3	-16.2	-24.1

3.4.2 Performance of Slotted Feeds with a Cavity

The performance in terms of gain factor of a circular waveguide feed with a cavity for three different cases: no-slots, E-plane slots and H-plane slots are listed at Table 3.9. The feed dimensions are shown in Fig. 3.26 for the E-plane slot and Fig. 3.28 for the H-plane slot case. The gain factor for the E-plane, H-plane and no-slot case are 77.6%, 78.5%, and 81.4% respectively. Usually, the phase efficiency and the cross-polarization efficiency are not dominant in the gain factor calculation in a sense that their efficiency is high. However, the phase efficiency is accountable for the gain factor, when there are large phase errors in the feed. In the E-plane slotted feed case, the spillover and illumination efficiencies are higher than H-plane slot case. However, the phase efficiency is 96.5% at $\theta_0 = 68^0$. Therefore, the overall gain factor of the antenna is 77.6% at that angle. For the H-plane slotted case the phase efficiency is 99.6% and in that case the gain factor is 78.5%. Therefore, the overall gain factor of the feed for the H-plane slot case is higher than that of the E-plane slot case.

Table 3.9 Performance of the slotted circular waveguide feed with a single cavity, in terms of efficiency; l = 60 mm, a = 10.5 mm, t = 1 mm.

	E-plane slotted case	H-plane slotted case	No-slot case [31]
θ_0	68^0	67^0	60^0
η_s	88.1%	86.9%	89.9%
η_i	91.3%	90.7%	90.5%
η_g	77.6%	78.5%	81.4%

Where,

θ_0 = aperture angle at which gain factor is maximum
η_s = spillover efficiency at θ_0.
η_i = illumination efficiency at θ_0.
η_g = gain factor of the feed at θ_0.

3.4.3 Phase Center of Slotted Feeds with a Cavity

The phase center locations of these feeds are again expected to be on the Z-axis. In these feeds the phase variations with the angle θ are very high as shown in Fig. 3.27 (b) and Fig. 3.29 (b) and therefore, it is hard to find a unique phase center location. Again due to these large phase variations, the phase efficiency of these feeds is low and it is should be counted in the gain factor calculation. The phase center location of these feeds is calculated by selecting the location with the highest phase efficiency. The result shows that for the E-plane slot case, the phase efficiency is highest (96.5%), when the phase center location is 3 mm inside the waveguide and at that point the gain factor of the antenna is 77.6%. For the H-plane slot case, the phase efficiency is highest (99.6%), when phase center location is 1 mm inside the waveguide and at that point the gain factor of the antenna is 78.5%.

3.4.4 Experimental Verification of Feeds with a Cavity

To confirm the simulation studies, the slotted circular waveguide feed with a cavity was fabricated and tested at University of Manitoba antenna laboratory. Fig. 3.30 shows the feed with the dimension of the circular waveguide: l = 60 mm, a = 10.5 mm and t = 1 mm, the cavity was: g_1 = 18.5 mm, ch = 17 mm, and slots: w = 18 mm and h = 1 mm selected. By changing the polarization within the slotted waveguide, the E- and H-plane cases were selected. The feed was again fed by a rectangular to circular waveguide transition, which was connected through a feed line. The dimension of the transition was

higher than slotted waveguide. Therefore, the feed diameter was tapered and slightly increased to 26 mm to match with that of the transition.

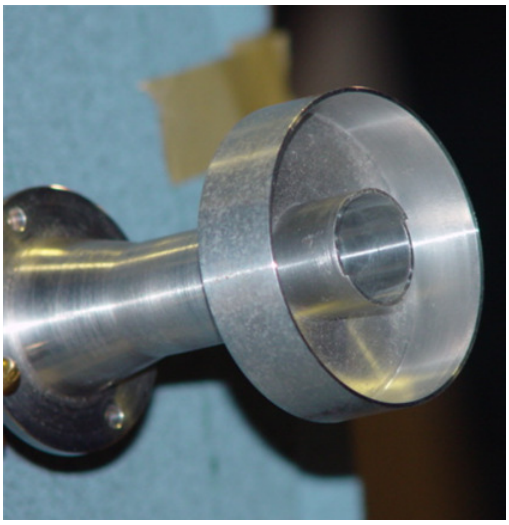

Fig. 3.30 Fabricated slotted circular waveguide feed with a single cavity; l = 60 mm, a = 10.5 mm, t = 1 mm, w = 18 mm, h = 1 mm, g_1 = 18.5 mm, ch = 17 mm.

The fabricated antenna was tested in the antenna Laboratory at the University of Manitoba for both cases. The simulated and measured radiation patterns of the E-plane slotted circular waveguide feed are shown in Fig. 3.31. The H-plane pattern is slightly higher than the E-plane pattern. This is because of the selected slot dimensions for the E-plane slot case. The measured cross-polarization level is slightly lower than the simulated cross-polarization level. However, they are very close to each other.

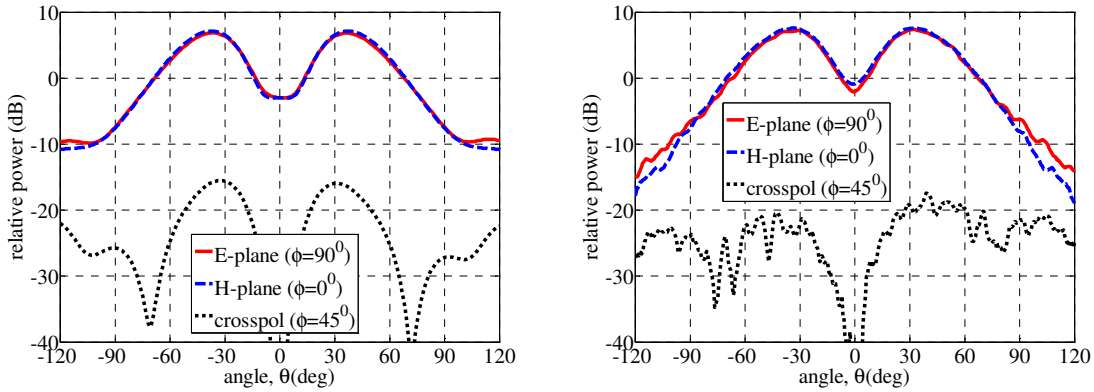

Fig. 3.31 Radiation patterns of the E-plane slotted circular waveguide with a single cavity feed of radius a = 10.5 mm, wall thickness t = 1 mm, slots width w = 16 mm and slots height h = 1 mm, cavity gap g1 = 18.5 mm, cavity depth ch = 17 mm at 10 GHz; (a) simulation, (b) measurement.

3.4.5 Slotted Feeds with a Cavity and $\lambda_0/4$ Choke

The slotted circular waveguide feed with a single cavity has a high back lobe level. A quarter wavelength choke can be used with the cavity to reduce the back lobe level. Usually cavity height of the feed is higher than $\lambda_0/4$ of the operating frequency. Therefore, if a quarter wavelength choke is incorporated with the cavity, it will act as a quarter wavelength transmission line. It reduces the unwanted current in the outer region of the cavity and improves the back lobe level of the feed.

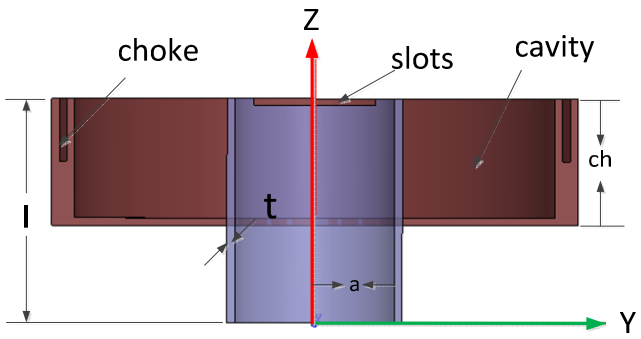

(a)

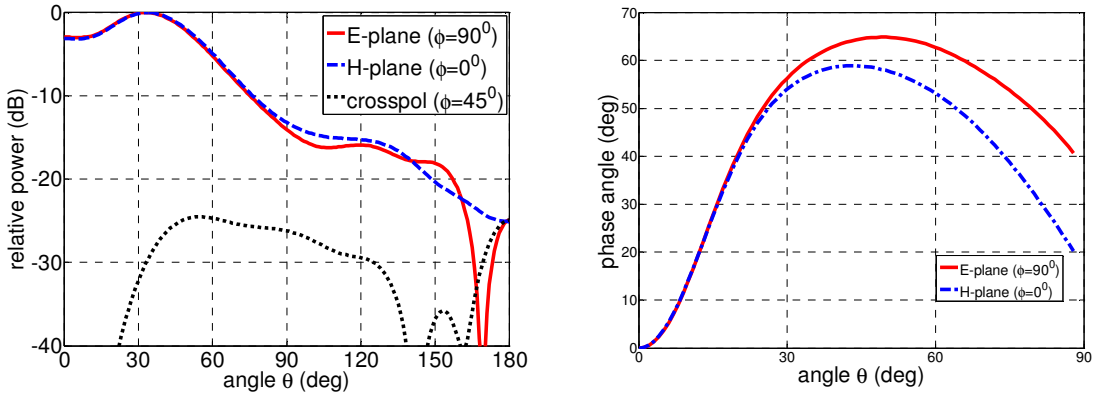

(b) (c)

Fig. 3.32 E-plane slotted circular waveguide with a single cavity with $\lambda_0/4$ choke feed; l = 60 mm, a = 10.5 mm, t = 1 mm, w = 16 mm, h = 1 mm, g_1 = 18.5 mm, ch = 16 mm, choke height 7.5 mm, thickness 1 mm. (a) geometry, (b) amplitude pattern at 10 GHz, (c) phase pattern, with respect to the origin at waveguide face.

Fig. 3.32 (a) shows the geometry of the feed, where choke height is 7.5 mm ($\lambda_0/4$). The thickness of the cavity wall is now 3 mm so that it can incorporate the slotted choke. All other parameters are the same as the previous case. The amplitude patterns are shown in the Fig. 3.32 (b), which shows good symmetrical patterns with a reasonable cross-polarization. However, a significant improvement has been found in the back lobe level. Fig. 3.32 (c) shows the phase pattern of the feed. At 70^0, the phase difference between the E- and H-plane is almost 12^0, which causes the phase center displacement from the waveguide face.

The H-plane slotted circular waveguide feed with a single cavity has also high back lobe level. To reduce the back lobe level, a quarter wavelength choke is introduced with this structure, which is shown in Fig. 3.33 (a). All parameters are the same as the previous case. The amplitude patterns of the feed are shown in Fig. 3.33 (b), which shows good symmetrical patterns with a reasonable cross-polarization. A significant

improvement is found in the back lobe level, which is -23 dB, and lower than the single cavity case. Fig. 3.33 (c) shows the phase patterns of the feed. At 70^0 the phase difference between E- and H-plane is almost 22^0, and that is the reason for the higher cross-polarization level. It should be mentioned that the phase difference is higher for the H-plane slot case than that of the E-plane slot case, and that causes higher cross-polarization level of the former.

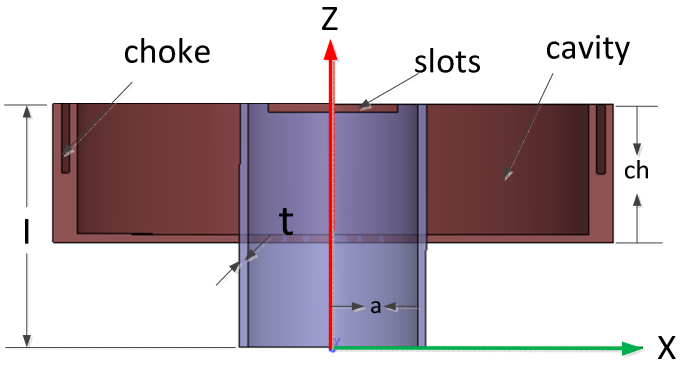

(a)

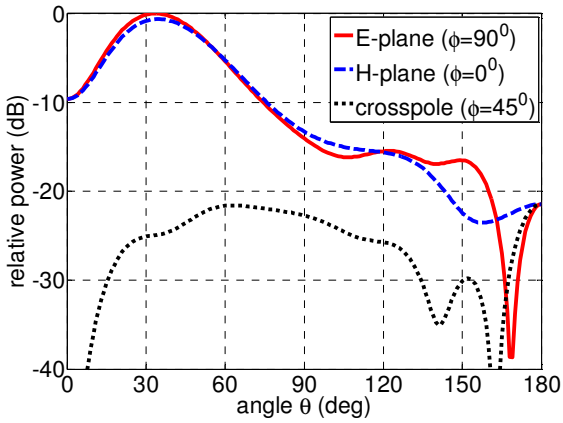

(b)

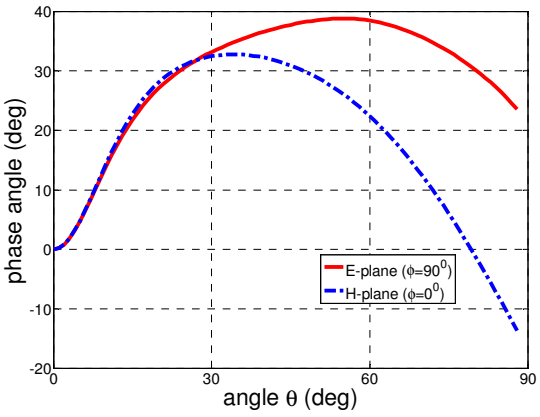

(c)

Fig. 3.33 H-plane slotted circular waveguide with a single cavity with $\lambda_0/4$ choke feed l = 60 mm, a = 10.5 mm, t = 1 mm, w = 16 mm, h = 1 mm, g_1 = 18.5 mm, ch = 16 mm, choke height 7.5 mm, thickness 1 mm. (a) geometry, (b) amplitude pattern at 10 GHz, (c) phase pattern, with respect to the co-ordinate geometry at waveguide face.

3.5 Summary

The circular waveguide used as a feed for prime focus reflector antenna, for its low cost and simple fabrication techniques. However, waveguide feeds, with smaller radii around 0.35 λ_0, had unequal E-and H-plane radiation patterns with the E-plane providing a wider beamwidth than the H-plane. Introducing slots in the waveguide open end wall equalized the E- and H-plane radiation patterns. Therefore, the design of the feed with symmetric radiation patterns and having smaller waveguide radius was possible. For the E-plane slot case the best possible results were found, when slot width was 18 mm and slot height was 2 mm and for the H-plane slot case slot width was 18 mm and slot height was 4 mm. The gain factors of the feeds for the two cases were evaluated and the overall efficiencies were found 66.4% and 70.3%, respectively, for the E- and H-plane slot cases. The performance of the feed antennas, in terms of frequency was also studied for these two cases, and it showed that the feeds had stabled performance within a 10% frequency band. The phase center locations of both feeds were also studied. It was found that their phase center locations were varied with the slot dimensions.

Slotted circular waveguides with a single choke was presented, which improved the gain factor of the feed up to 72.8%. Slots in the waveguide wall equalized the E- and H-plane radiation patterns, while the choke reduced its cross-polarization and back lobe level. It also reduced the beamwidths of the antenna. As a result, the illumination efficiency was improved, which improved the gain factor of the antenna. To further investigate the gain factor, the slotted circular waveguide with multiple chokes were designed and simulated. The results showed that the feed with multiple chokes further

improved the radiation characteristics, as well as the gain factor of the antenna. The frequency stability of the feeds and its performance were also studied. The comparisons were shown in different tabular format. The phase center locations of the feeds were also discussed in this chapter. It was found that the phase center locations for the E- and H-plane slotted circular waveguides with choke were outside the waveguide face.

Slotted circular waveguides with a cavity were also presented in this chapter. It equalized the E- and H-plane radiation patterns with broader beamwidths. The back lobe level of the feed was high. To improve the back lobe level, slotted circular waveguides with a choke in the cavity wall was designed and simulated. It showed good radiation characteristics with improved back lobe level. All feeds were fabricated and measured in the University of Manitoba antenna laboratory. The measured radiation patterns were matched with the simulation results.

Slotted circular waveguide feed presented in this chapter was simple and easy to fabricate and showed good radiation patterns, improved cross-polarization and back lobe level. Therefore, it is used as a feed for prime focus reflectors. However, it needs struts support to mount it on a reflector. Moreover, it is hard to integrate it with other microwave devices. Microstrip dipole feeds with backward radiation have the attractive features of low profile, light weight, easy of fabrication, simple mount, and easy of integrate with other circuitry. In the following chapter, we will introduce microstrip dipole feeds and investigate some of their properties.

Chapter 4

Microstrip Dipole Feeds

4.1 Introduction

Dipole antennas are used in various applications such as phased array or feeds for the reflectors. Compared to the straight wire dipole antennas, microstrip dipole antennas have additional advantage is being planner structure, and light weight. These antennas are generally economical to produce because of their adaptability with integrated circuits fabrication techniques [54]. Therefore, attempts have been made to design microstrip dipole antennas for reflector feed.

Most existing micorstrip dipole antennas are based on the popular printed dipole design proposed in [55]. In this design, the dipole arms are connected to microstrip lines through integrated balun which is fed by a 50Ω single-ended microstrip line. It is known that dipole antennas need balanced feeding. This feeding can be achieved by using parallel dual-line transmission lines. However, microstrip lines that are used in RF & microwave circuits are unbalanced type. Therefore, balun is required to convert a single microstirp line to dual-transmission lines.

Microstrip dipole with directors is also used in some applications, where it acts as traditional Yagi-Uda case. One of these designs is presented in [56], where the driver and director are printed dipoles placed on one side of the substrate with a high dielectric permittivity and the dipole-reflector is a truncated ground plane placed on the other side of the substrate. The driver is fed by the odd-mode current of a coplanar strip line (CPS). The CPS line is connected to the microstrop line through a transition balun. This feeding mechanism is geometrically complex and requires a relatively complicated balun that not only increase the size of the structure, but also degrades the radiation performance of the antenna. Alternative methods of feeding such antennas is presented in [57]-[58]-[59], where one of the dipole arms is printed on one side of substrate and connected to one of the parallel microstrip line. The other dipole arm is placed on the other side of the substrate, which is connected to the truncated ground plane by the other parallel strip mcirostrip line. Therefore, the feeding mechanism is a simple parallel microstrip feed line which simplifies the complex feeding network. Although these antennas are simple to design, they provide patterns with forward radiation and therefore need conventional strut supports, as a prime focus reflector feed.

4.2 Backward Microstrip Dipole Feeds

In this section a new microstrip dipole feed is designed and studied. It is a microstrip dipole antenna with a dipole-reflector in front of the dipole arms to provide backward radiation, thereby eliminating the need for strut supports. In addition, the printed dipole has inherently small physical cross section, limited only by its substrate thickness. The

antenna design is similar to a traditional Yagi-Uda antenna [57]-[60], except the main beam is directed back along the feed transmission line axis. In the design process, a truncated/tapered ground plane act similar to a director element and the dipole-reflector which is placed in front of the dipole arms act as a reflector. The feeding mechanism is a simple parallel strip feed line, where one of the dipole arms is placed on one side of the substrate which is connected to one of the parallel microstrip line. The other dipole arm which is placed on the other side of the substrate is connected to the truncated ground plane by the second mcirostrip line. The antenna configuration and design are presented and studied in the following sections.

4.2.1 Design of the Backward Microstrip Dipole Feed

The schematic and parameters of the proposed antenna are shown in Fig. 4.1 [43]. The antenna is operating at fr = 3 GHz and is printed on a substrate of length L = 60 mm, width W = 60 mm, dielectric constant $\varepsilon_r = 2.5$, loss tangent (tan δ) = 0.002 and thickness t = 1.58 mm with metallization on both sides. The two arms of the dipole antenna act as a driver element which is fed from a microstrip through a two parallel strips transmission line. The arms of the dipole are located at the end the transmission line, placed on each face of the substrate in a complementary manner, which creates 180^0 phase difference between the arms, providing the correct feed to the antenna. To start with the design, the length of the dipole needs to estimate, which must be about 0.5 λ_0, where λ_0 is the wavelength in the medium [60]. In microstrip line case, the effective relative permittivity is calculated from [61].

$$\varepsilon_{eff} = \frac{\varepsilon_r + 1}{2} + \frac{\varepsilon_r - 1}{2} \frac{1}{\sqrt{1 + 12t/\mathrm{w}}}$$

where, ε_r is the relative permittivity of the substrate, t is its thickness and w is the metallization width. In the present case the effective permittivity will be smaller, since dipole is not printed over a ground plane. Nevertheless, we start with the above effective relative permittivity. Therefore, at 3 GHz operating frequency and ε_r = 2.5, the driver length, L_{DRI} (from one side of the first arm to other side of the second arm) becomes 0.35 λ_0. After some iteration process, the drive length is found to be 0.4 λ_0. The width of the dipole arm, W_{DRI} is chosen approximately to be one-tenth of a wavelength based on iteration process to achieve good radiation patterns and impedance bandwidth. The dipole length and width are reciprocal that means if the width gets wider, the length becomes shorter and if width is narrower, then the length will be longer.

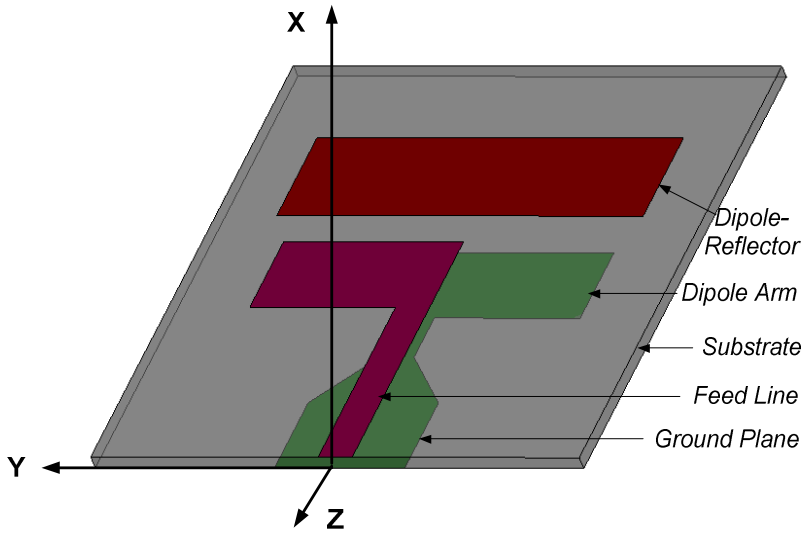

(a)

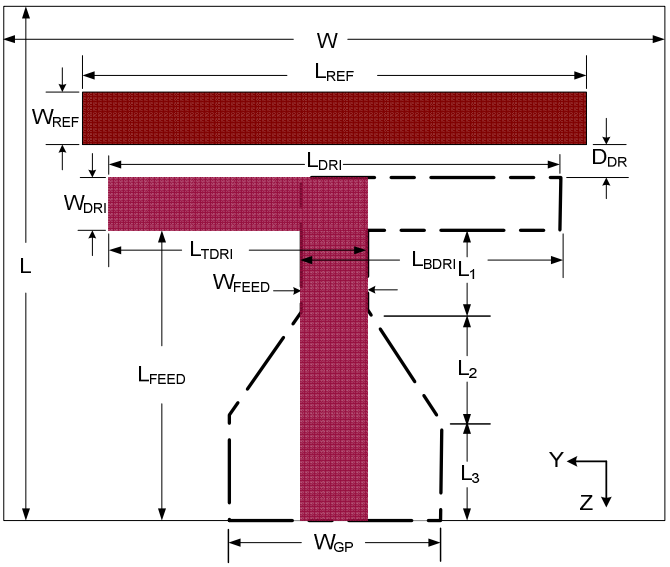

(b)

Fig. 4.1 Geometry and coordinate system of a microstrip dipole feed. The dipole-reflector, one of the dipole arms and feed line is one side of the substrate. Another dipole arm and partial ground plane are connected by a feed line and are other side of the substrate; (a) 3-D view (b) top view.

The metallization on the bottom plane is a truncated ground plane, and behaves like a director element for the antenna. It is called a "truncated ground plane" because its width W_{GP}, perpendicular to the microstrip feed transmission line, is reduced to less than 4 times the width of the microstrip line. The length of the ground plane can be set to any value as long as it matches with 50 Ω line.

The dipole-reflector is placed parasitically on the upper face of the substrate opposite to the ground plane. The main goal of designing the dipole-reflector is to direct the radiation backward, toward the microstrip feed line. Its length L_{REF} is set slightly larger than the driver length, L_{DRI} similar to Yagi antenna case. As driver length L_{DRI} is 0.4 $\lambda_{0,}$ the dipole-reflector length L_{REF} is selected as 0.45 $\lambda_{0.}$ The dipole-reflector width W_{REF} is chosen approximately to be one-tenth of a wavelength based on iteration process to

achieve good radiation patterns and impedance bandwidth. The separation between the driver element and dipole-reflector element is set approximately to one twentieth of the wavelength. This selection is based on the coupling nature between the dipole-reflector and the driver element. The major role of the dipole-reflector is played by the first element, and very little in the performance of a Yagi antenna is gained if more than one (at the most two) elements are used as dipole-reflectors.

Table 4.1 Design parameters of the microstrip dipole feed antenna shown in Fig. 4.1.

Antenna parameters	Values
Substrate Width , W	60 mm
Substrate Length, L	60 mm
Substrate Thickness, t	1.58 mm
Substrate Dielectric	ε_r= 2.5, tan δ= 0.002
Microstrip Feedline Width, W_{FEED}	4.2 mm
Microstrip Feedline Length, L_{FEED}	23 mm
Ground Plane Length, $L_2 + L_3$	10 mm + 7 mm
Ground Plane Width, W_{GP}	16 mm
Ground Plane to Driver Distance, L_1	6 mm
Dipole Width, W_{DRI}	10 mm
Dipole Length, L_{TDRI} or L_{BDRI}	22.1 mm
Driver Length, L_{DRI}	40 mm
Dipole-Reflector Length, L_{REF}	45 mm
Dipole-Reflector Width, W_{REF}	12 mm
Driver to Dipole-Reflector Distance, D_{DR}	4 mm

The feeding structure consists of a microstrip line on one side of the substrate and a truncated ground plane on the other side, both connecting to two arms of a parallel strip

transmission line L_1 that feeds the dipole, as shown in Fig. 4.1. Based on the substrate thickness of 1.58 and relative permittivity 2.5, the width of the microstrip line is set to be 4.2 mm, for the characteristics impedance of 50 Ω over a ground plane. The length of the microstrip line including transmission line is set to 0.23 λ_0. The length of the microstrip line should be selected to give an input/impedance of 50 Ω, to match that of feeding microstrip line.

Using this simplified feeding structure, the length of the feed transmission line and consequently, the feed losses are reduced. Although, the length should be carefully selected as it affects the radiation patterns of the feed antenna.

4.2.2 Simulation Study of the Microstrip Dipole Feed

Based on the above discussion, the feed antenna is simulated by a finite element method based on 3-D full wave simulator, Ansoft HFSS ver. 14 [62]. The design parameters of the feed antenna given in Table 4.1 were selected after several simulations.

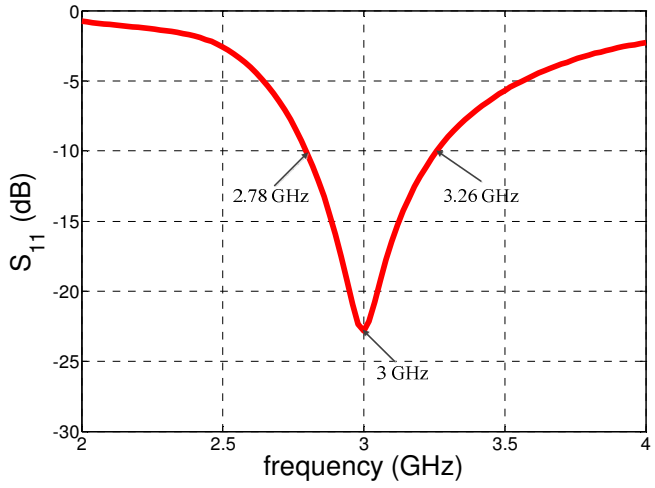

Fig. 4.2 Simulated S_{11} of the microstrip dipole feed shown in Fig. 4.1.

The simulated S_{11} of the antenna is shown in Fig. 4.2. The antenna is matched at 3 GHz frequency range and the -10 dB S_{11} bandwidth is from 2.78 GHz to 3.26 GHz, which means impedance bandwidth of the antenna is 15.9%.

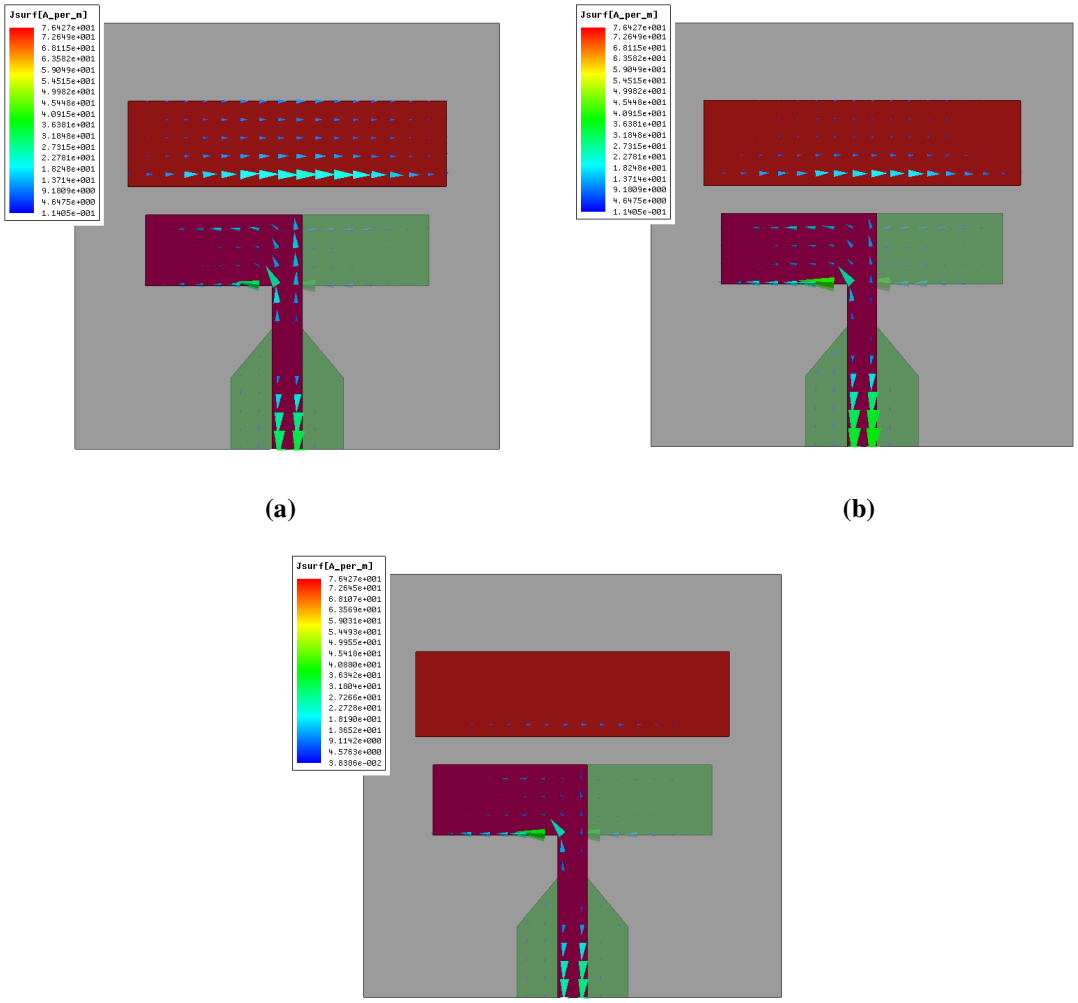

Fig. 4.3 Simulated surface current distribution of the microstrip dipole feed shown in Fig. 4.1 at different frequencies; (a) 2.8 GHz, (b) 3.0 GHz, (c) 3.3 GHz.

To confirm the backward radiation mechanism, which requires higher gain in the backward ($\theta = 0^0$) than forward direction ($\theta = 180^0$), the simulated surface current distributions are illustrated in Fig. 4.3. The surface currents on the dipole arms and

dipole-reflector are in opposite directions at all three different frequencies, and as in Yagi antennas their phase relationship results in the peak radiation away from the dipole-reflector.

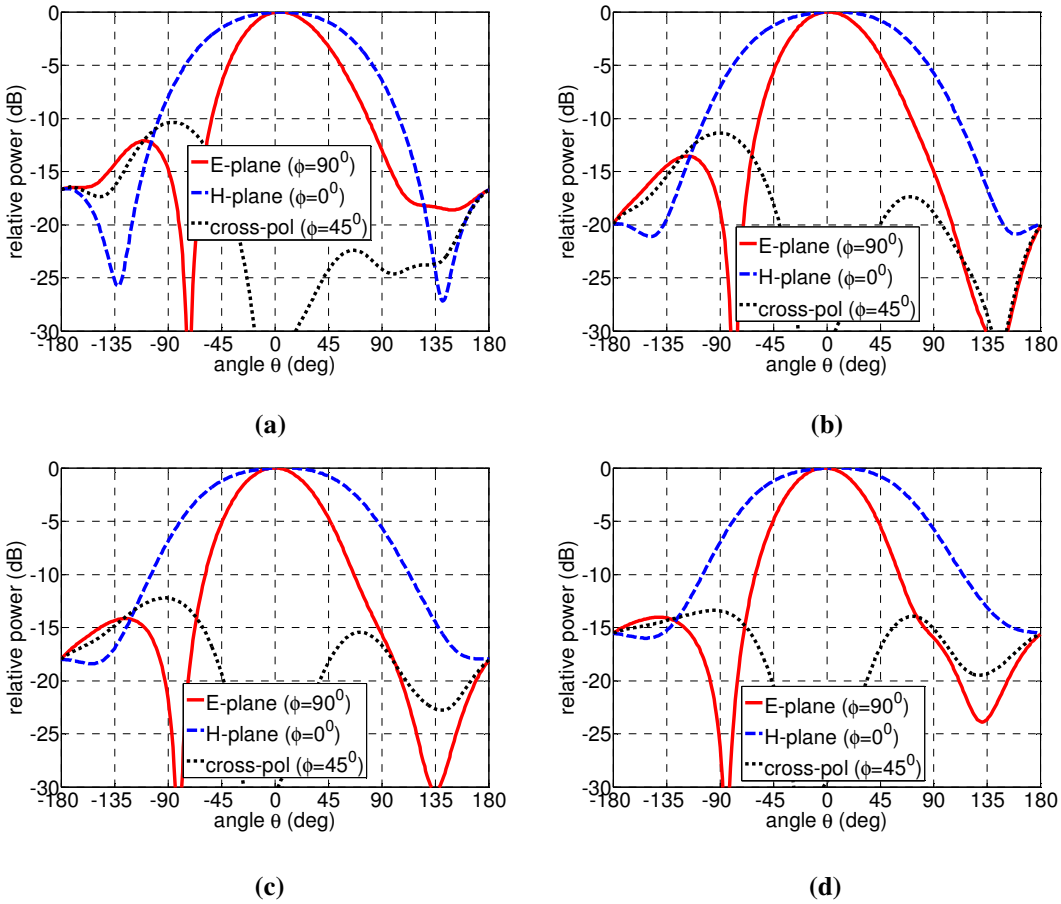

Fig. 4.4 Simulated radiation patterns of the microstrip dipole feed shown in Fig. 4.1 at different frequencies; (a) 2.8 GHz, (b) 3.0 GHz, (c) 3.15 GHz and (d) 3.3 GHz.

The simulated radiation patterns of the feed antennas are shown in Fig. 4.4 for four different frequencies. The antenna is radiating in the backward direction with the H-plane pattern being wider than the E-plane pattern for all frequencies. The -10 dB beamwidth in the H-plane is almost the same for all cases. In the E-plane, at lower frequencies the beamwidth is not symmetric with respect to the radiation axis. As the frequency

increases, the beamwidths become more symmetric. As a result, the cross-polarization levels are improved at higher frequencies and at 3.3 GHz it is -14 dB compare to -11 dB at 2.8 GHz. The back lobe level of the antenna is -20 dB at 3 GHz, which is the lowest than other frequencies.

The main beam especially at the E-plane is not symmetric with respect to the Z-axis. This could be a sign that the edges of the ground plane are radiating. A symmetric nature of main beam could be found by changing the dipole arm lengths, which is discussed later.

4.2.3 Effects of Various Parameters

In order to understand the influence of the input parameters on its impedance bandwidth and radiation patterns, a detailed parametric study is carried out using the finite element method based on 3-D full wave simulator, Ansoft HFSS ver. 14. There are several parameters of the feed antenna which affect its impedance bandwidth and radiation patterns. However, very few important parameters are selected for the study.

4.2.3.1 Effects of the Dipole Arms

In printed dipole antenna, the dipole arm length is determined by the operating frequency of the antenna. The driver length which is the total length of the two dipole arms from one end to another is set to 40 mm at 3 GHz, after some iteration. Since it is determined by the operating frequency, the effect of varying driver length L_{DRI}, on its S_{11} is shown in Fig. 4.5. With an increase in the driver length from 35 mm to 45 mm, the center frequency is shifted from 3.5 GHz to 2.5 GHz. Therefore, the main design

parameter of the antenna is its driver length. The radiation patterns of the antenna for different lengths are almost the same at resonance frequency and therefore omitted from the study.

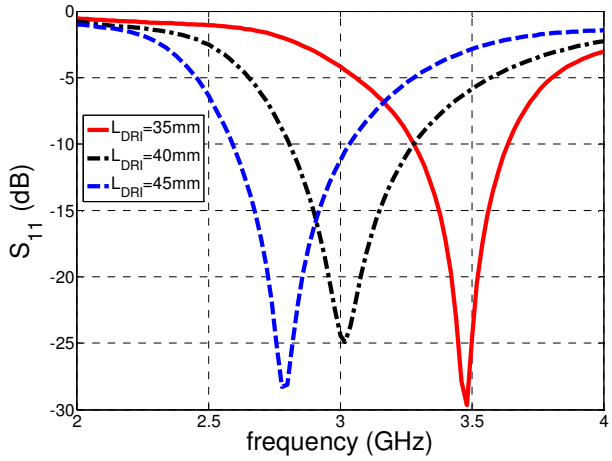

Fig. 4.5 Simulated S_{11} of the microstrip dipole feed shown in Fig. 4.1 with different driver length L_{DRI}; antenna parameters are given in Table 4.1.

The size variation of the dipole arm width has an effect on the impedance matching. Fig. 4.6 (a) shows the effect of the dipole arm width on S_{11}. The resonant frequency of the antenna moves to a lower frequency, with the increase of the width, and S_{11} is high when the width is too small (4 mm) or too large (16 mm). Therefore, the antenna is well matched at its corresponding width of 8 mm. This can be explained using the plotted Smith chart in Fig. 4.6 (b), corresponding to the input impedance of the antenna. At small width, the frequency loop is large about the center of the Smith chart, which indicates the antenna is far from 50 Ω. By increasing the width, the loop size is reduced but it moves away from the center. At larger widths, the locus lies below the real axis. As the loop goes further from the center point of the Smith chart, the antenna impedance become

more reactive and is not well matched. Therefore, a good result is found when the size is 8 mm. The radiation patterns of the antenna for different widths are almost same at resonance frequency and therefore omitted from the study.

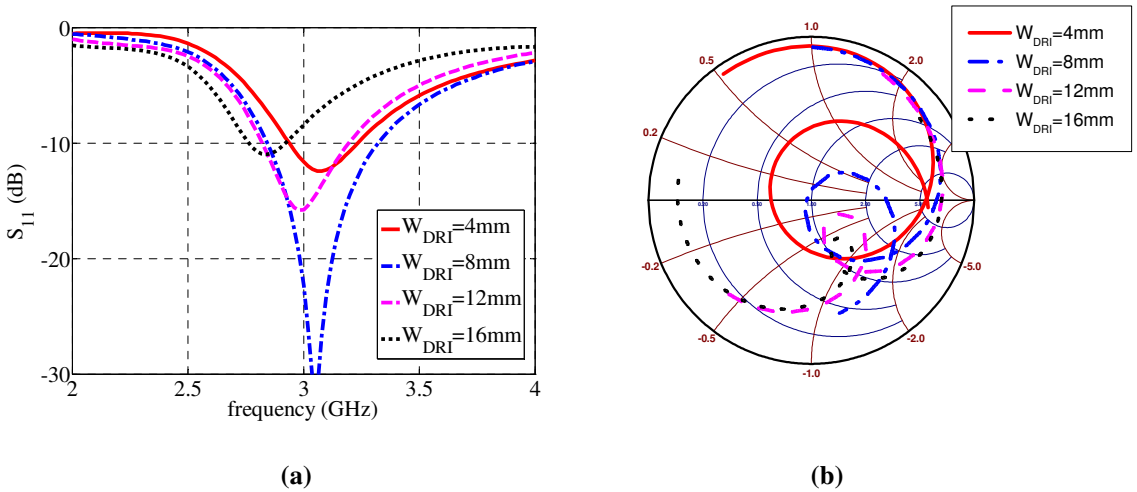

(a) **(b)**

Fig. 4.6 Simulated S_{11} and Smith chart of the microstrip dipole feed shown in Fig. 4.1 with different driver width W_{DRI}; antenna parameters are shown in Table 4.1.(a) S_{11} (b) Smith chart.

4.2.3.2 Effects of the Dipole-Reflector

The length of the dipole-reflector is slightly larger than the length of the driver element. In order to examine the effects of varying the dipole-reflector length on various antenna parameters, several simulations have been conducted. The radiation patterns of the antenna are almost the same except the back lobe level which is slightly different, as shown in Figs. 4.7 (a) and (b). For both planes, the back lobe level is less for small length (42 mm), compared to the larger ones. Therefore, the best result in terms of the back lobe level is found when the reflector length is slightly larger than the driver length. The S_{11} of the antenna is almost the same for different dipole-reflector lengths. Therefore, they are omitted from the study.

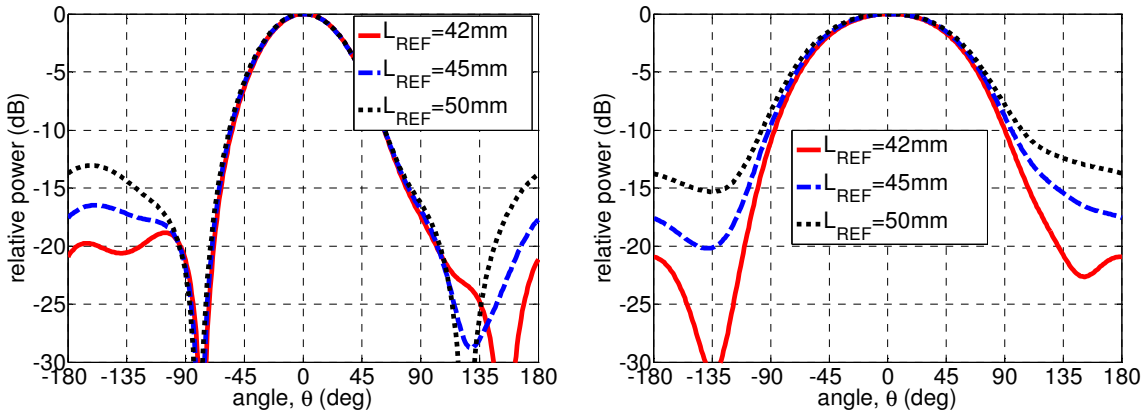

Fig. 4.7 Simulated radiation patterns of the microstirp dipole feed at 3 GHz shown in Fig. 4.1 with different reflector length L_{REF}; antenna parameters are mentioned in Table 4.1. (a) E-plane pattern, (b) H-plane pattern.

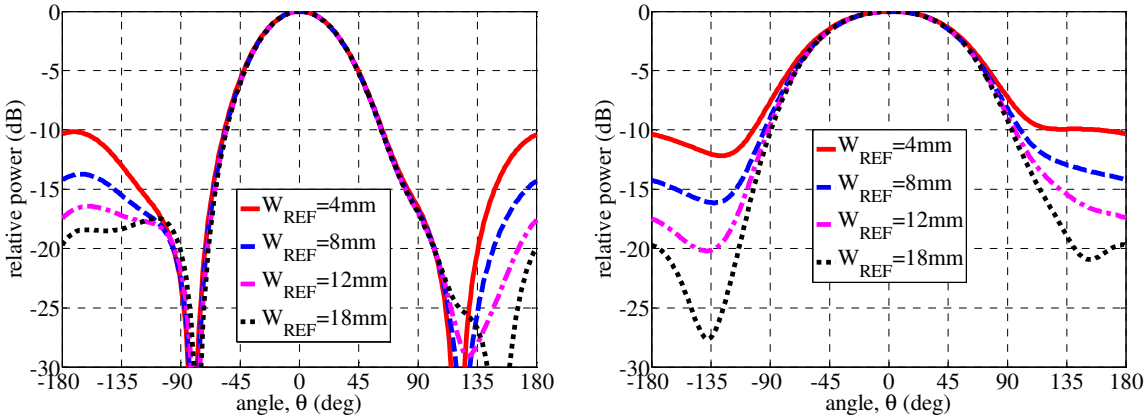

Fig. 4.8 Simulated radiation patterns of the micostrip dipole feed at 3 GHz shown in Fig. 4.1 with different reflector width W_{REF}; antenna parameters are shown in Table 4.1. (a) E-plane pattern, (b) H-plane pattern.

In order to examine the effects of varying the dipole-reflector width on various output parameters, it is varied from 4 mm to 18 mm. The input impedance of the antenna is not affected with the different dipole-reflector width and therefore is omitted from further studies. The radiation patterns of the antenna for different width are almost the same,

except the back lobe level, which is slightly different, as shown in Figs. 4.8 (a) and (b). For both E- and H-plane patterns, the back lobe level is decreased when the width is increased. Therefore, to get a higher front to back ratio, we can increase the width of the dipole-reflector without deteriorating the impedance matching of the antenna.

4.2.3.3 Effect of the Gap between Dipole Arms and Dipole-Reflector

The gap between dipole arms and the dipole-reflector is also important for this type of antennas, as it affects the impedance matching. Fig. 4.9 (a) shows the effect of the gap between the driver (dipole arms) and dipole-reflector, on its S_{11}. When the gap is small, the antenna is matched at -10 dB point. If the gap is increased, matching of the antenna is decreased and at one stage, when the gap is too large, the central frequency shifts slightly to a lower frequency, with a higher S_{11}. Fig. 4.9 (b) shows the Smith chart corresponding to the input impedance of the antenna. When gap is small the frequency loop is just passed the center point of the Smith chart, indicating a good match with 50 Ω. With the increase of the gaps the loops becomes small but away from the center point of the Smith chart. This indicates that the reactive portion of the input impedance is large and thus shows poor matching. Therefore, if we reduce the reactive portion of the input impedance, the loop will encircle the center point of the Smith chart and will be matched with 50 Ω. The radiation patterns of the feed for this case are omitted, as they show little effects with the gap.

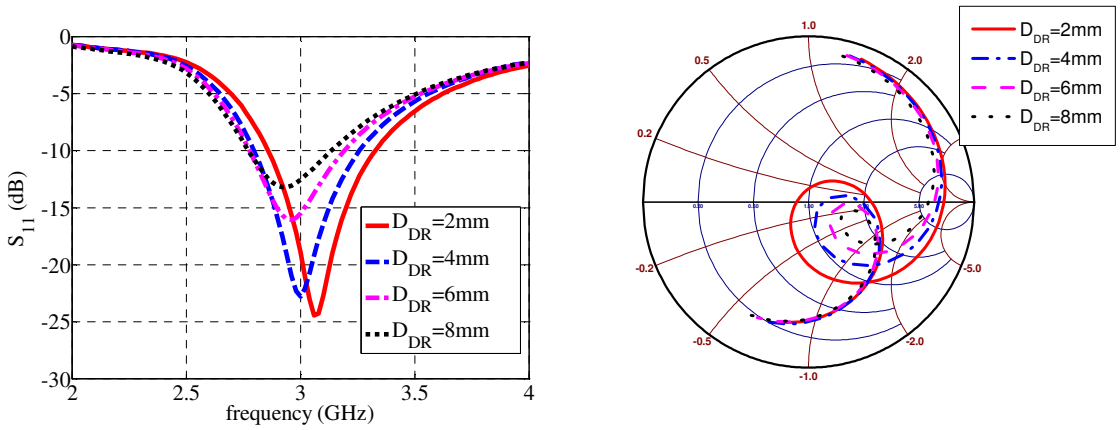

(a) **(b)**

Fig. 4.9 Simulated S_{11} and Smith chart of the microstrip dipole feed shown in Fig. 4.1 with different driver and dipole-reflector distance D_{DR}; antenna parameters are mentioned in Table 4.1. (a) S_{11}, (b) Smith chart.

4.2.3.4 Effect of the Transmission Line

The length of the transmission line is set as 23 mm after several iteration processes. The reason for selecting this transmission length is that if the length is too small, it will reduce the distance between ground plane and dipole arms. If the ground plane is too close to the radiating element it diffracts the field, causing asymmetrical radiation pattern. On the other hand, if the length is too large, then the transmission line will radiate more energy, which ultimately affects the radiation patterns and it will also increase the back lobe level of the antenna. If the length is too long, side lobe will appear and that is undesirable as a feed antenna. Therefore, the length of the transmission line should be set somewhere between these two regions. Figs. 4.10 (a) and (b) show the E- and H-plane radiation patterns for four different cases. These figures show that the back lobe level is lower for smaller transmission line length and it increases with the increase of the length. On the other hand, if the length is larger, then the pattern symmetry is achieved in the E-

plane. In the H-plane case, the pattern symmetry is independent of the transmission line length. The transmission line length also affects the side lobe level of the radiation patterns. If the length is large, the side lobe level in the H-plane pattern appears. Therefore, it is necessary to select appropriate length of the transmission line so that it will fulfills all the necessary requirements of the feed antenna. The S_{11} of this case is omitted as it has little effect on antenna matching.

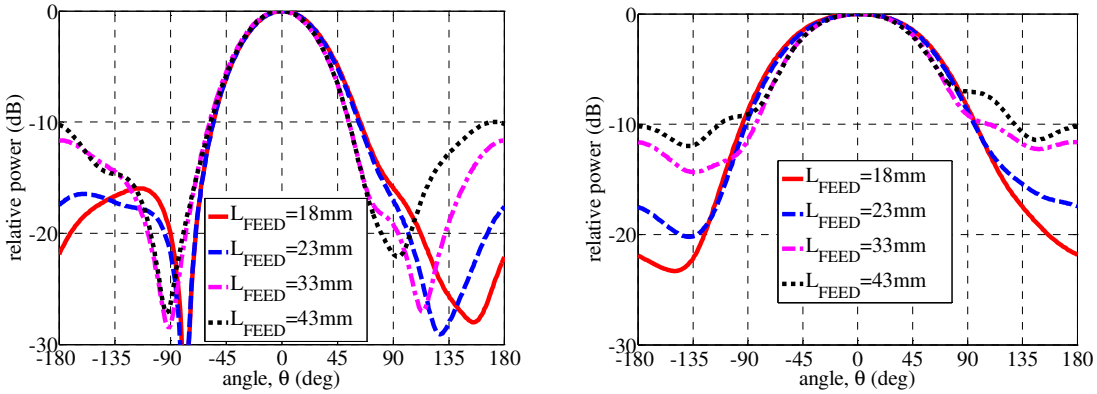

Fig. 4.10 Simulated radiation patterns of the micostrip dipole feed at 3 GHz shown in Fig. 4.1 with different transmission line length L_{FEED}; antenna parameters are shown in Table 4.1. (a) E-plane pattern, (b) H-plane pattern.

4.2.3.5 Effect of the Ground Plane

In this antenna design process, the ground plane is located on one side of the substrate and acts like a director element, similar to Yagi-Uda antenna case. The length of the ground plane is smaller than the length of the transmission line. The width of the ground plane is smaller than the driver element and is selected by the iteration process. The ground plane has a tapered shape on one side, because of its smooth transition to the transmission line. Fig. 4.11 (a) shows the effect of the ground plane, on its S_{11}. The figure

shows that a lower S_{11} is achievable when the ground plane is much smaller than the driver element, which is also verified by the Smith chart in Fig. 4.11 (b). When the ground plane width is large, the frequency loop is at the center of the Smith chart with a large loop. That indicates a poor matching to 50 Ω around 3 GHz. However, if we decrease the width, the loop becomes smaller with a slight shift from the center of the Smith chart. This indicates that feed matches with 50 Ω at the center frequency.

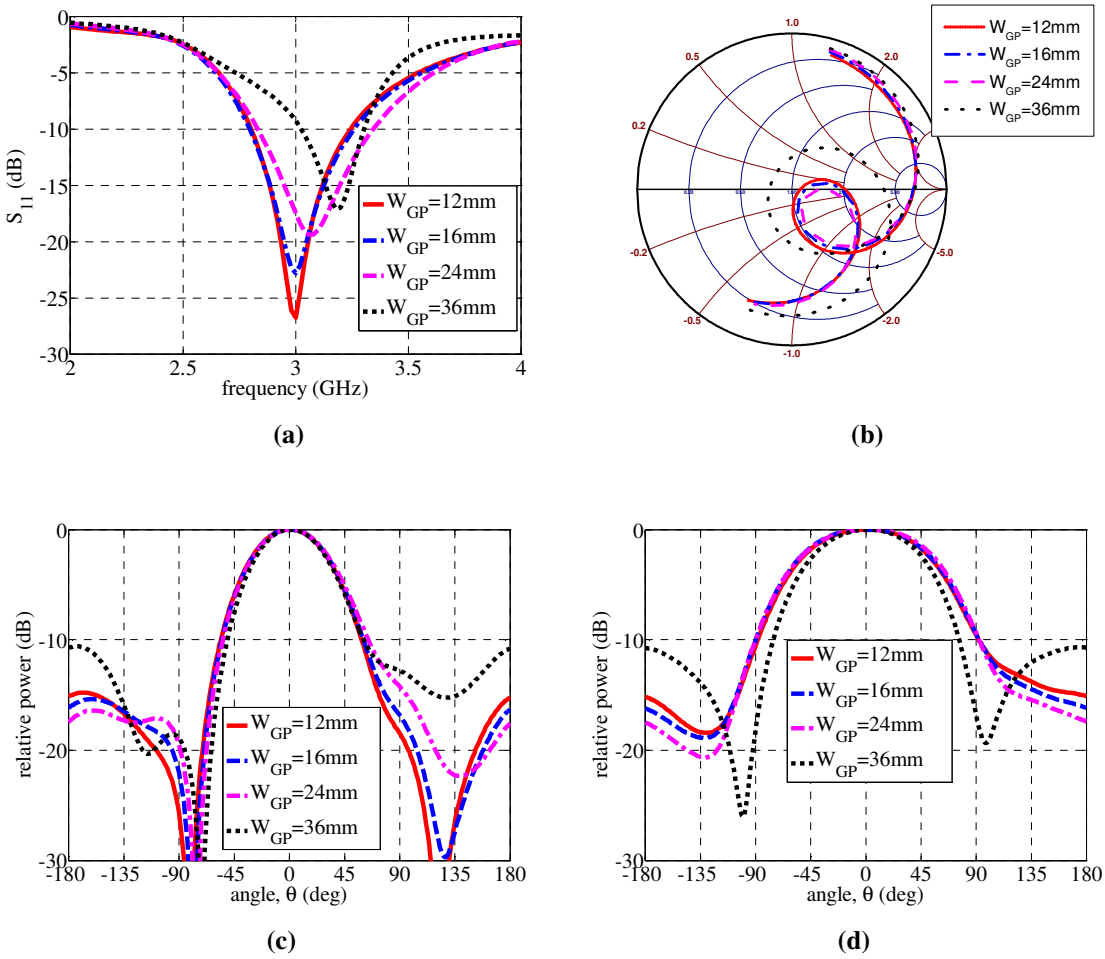

Fig. 4.11 Effect of varying the ground plane width W_{GP} of the microstrip dipole feed shown in Table 4.1; antenna parameters are shown in Table 4.1. (a) S_{11}, (b) Smith chart, (c) E-plane pattern, (d) H-plane pattern.

The radiation patterns of the antenna for this case are shown in Figs. 4.11 (c) and (d) at the center frequency of 3 GHz. At the E-plane, pattern symmetry is possible when the width of the ground plane is 12 mm compared to 36 mm. The H-plane patterns remain the same for most of the cases. Therefore, it is better to keep the width of the ground plane, 3 to 4 times that of the feed line.

4.2.4 Phase Center of the Microstrip Dipole Feed

In prime focus reflector antennas, the feed is located at the focal point and the phase center of the feed coincides with that point. Therefore, it is necessary to know precisely the phase center of the feed antenna. In the printed dipole antenna radiations are in the z-direction with an end-fire radiation characteristics. Therefore, the phase center locations of these types of antennas are on the Z-axis.

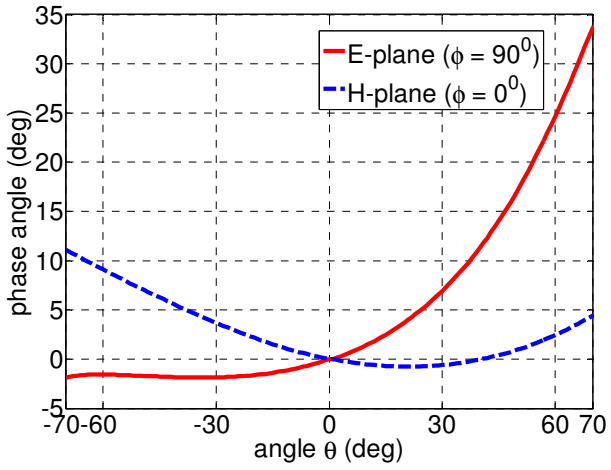

Fig. 4.12 Phase variations of the microtrip dipole feed shown in Fig. 4.1 with angle θ = 70⁰, when the co-ordinate origin is 27 mm from the co-axial feed point.

In order to determine the phase center location, we need to know the phase variations of the feed antenna, which is shown in Fig. 4.12 with aperture angle of 70^0, when the co-ordinate origin is 27 mm from the co-axial feed point. The phase variations for the E- and H-planes are different and not symmetric with respect to the axis. Hence, the phase center locations for the E- and H-planes are different for each plane. Furthermore, the E- and H-plane phases are not constant with aperture angle that means the phase center locations are not at the initial point. Therefore, the combined phase center location, which is calculated based on the optimum phase variations of the E- and H-plane, is also outside the initial point.

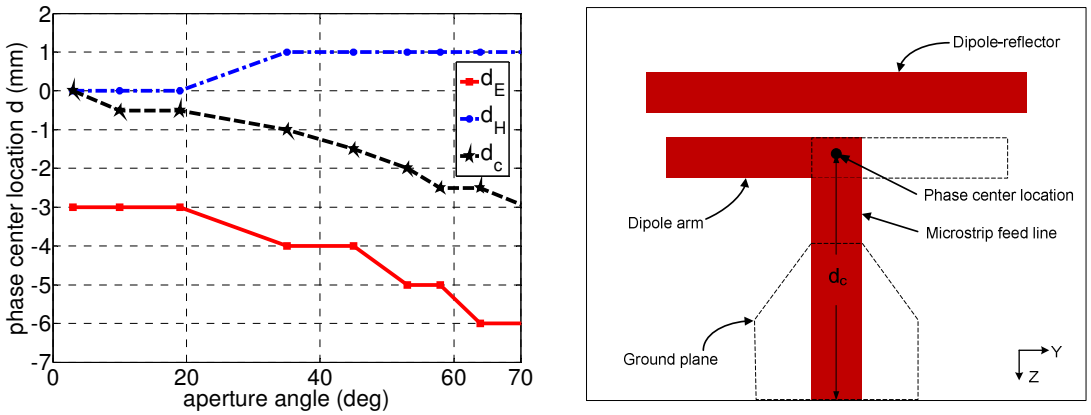

(a) **(b)**

Fig. 4.13 Phase center location of the microstrip dipole feed shown in Fig. 4.1 with minimum phase variations. Original location d = 0 is at 27 mm from the co-axial feed point. (a) with aperture angle, (b) phase center location in the geometry.

Fig. 4.13 (a) shows the E-plane, the H-plane and the combined phase center locations of the feed antenna, which are indicated as d_E, d_H and d_C, respectively. In this figure, d = 0 indicates the phase center location is 27 mm away from the feed point (Fig. 4.13 (b)). A positive d means that the phase center is toward the dipole-reflector, and negative d

indicates that it is toward the feed point. The d_E varies with aperture angle and at 0^0 aperture angle, it is -6 mm away from d = 0 and at higher aperture angle, it is toward the feed point. However, d_H is 1 mm away from d = 0 and almost constant with aperture angle. The d_c is -3 mm away from d = 0, at 70^0 aperture angle.

4.2.5 Performance of the Microstrip Dipole Feed

To evaluate the performance of the microstrip dipole feed with reflectors, the data on the gain factor, the spillover & the illumination efficiency must be known. These data are calculated for the center frequency at 3 GHz and shown in Fig. 4.14. The figure shows that when the aperture angle varies from 0^0 to 90^0, the spillover efficiency increases and the illumination efficiency decreases as expected. The maximum gain factor of 69.2% is found, when the aperture angle is 78^0 and the overall gain factor varies from 0 to 69.2 percent, which is reasonable for a reflector feed.

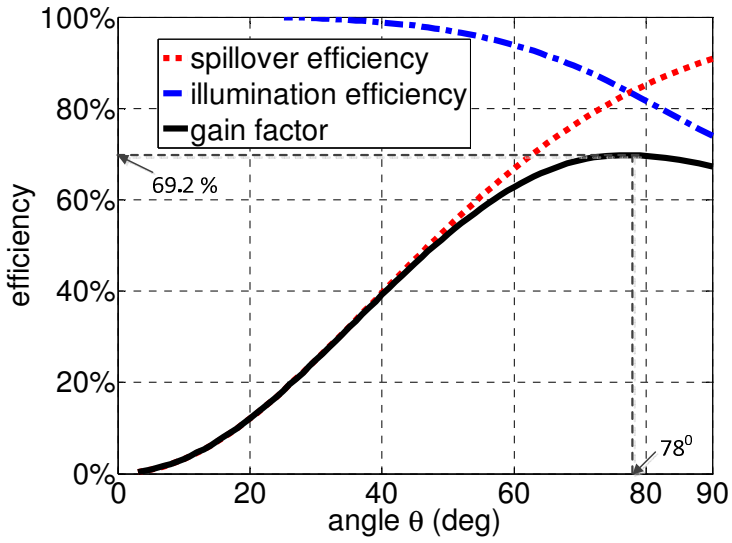

Fig. 4.14 Spillover efficiency, illumination efficiency and gain factor of the microstrp dipole feed shown in Fig. 4.1; all parameters are listed in Table 4.1.

The performance of the feed with two other frequencies is also investigated. Table 4.2 summaries the gain factor, the spillover, and the illumination efficiencies for three different frequencies at 2.8 GHz, 3 GHz and 3.15 GHz, respectively. The gain factors of these three different frequencies are found 73%, 69.2% and 65.7%, respectively, which gradually decreases with increasing frequency. Therefore, the feed parameters are very stable with frequency, in terms of the gain factor. The phase center location d_c for these frequencies are 22 mm, 23 mm and 23 mm, respectively, from the feed point toward the z-axis (Fig. 4.13(b)), which confirms the phase center stability of the feed.

Table 4.2 Performance of the microstrip dipole feed for three different frequencies; all parameters are shown in Table 4.1.

Frequency	2.8 GHz	3.0 GHz	3.15 GHz
θ_0	80^0	78^0	78^0
η_s	86.9 %	85.3 %	82.4 %
η_i	86.0 %	85.5 %	86.0 %
η_g	73.0 %	69.2 %	65.7 %
d_c	22 mm	23 mm	23 mm

where,

θ_0 = aperture angle at which gain factor is maximum,
η_s = maximum spillover efficiency at θ_0,
η_i = maximum illumination efficiency at θ_0,
η_g = maximum gain factor at θ_0,
d_c = phase center location from co-axial feed point toward z-axis

4.2.6 Experimental Verification of the Dipole Feed

To validate the design of the simulated feed antenna, one antenna was fabricated on an Arlon Diclad substrate with a thickness of 1.58 mm, dielectric constant of 2.5, loss

tangent (tan δ) of 0.002, and an area of 60 × 60 mm^2 with the parameters shown in Table 4.1. The fabricated feed antenna is shown in Fig. 4.15.

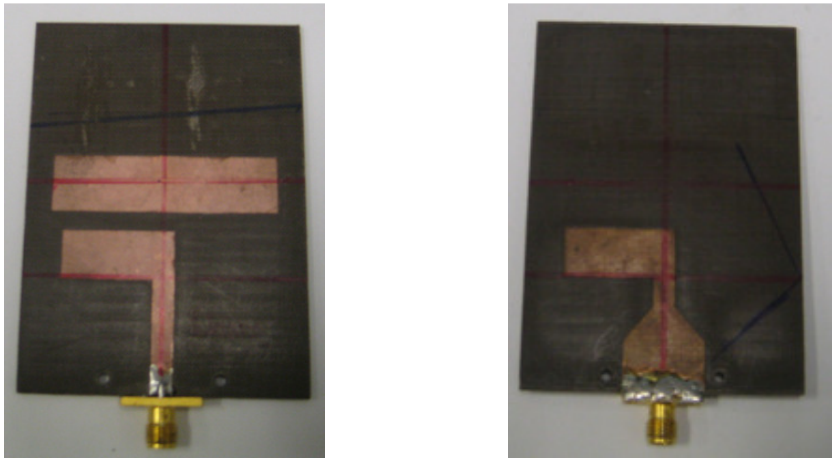

(a) Top view (b) Bottom view

Fig. 4.15 The fabricated microstrip dipole feed. Antenna parameters are given in Table 4.1.

4.2.6.1 Measurement Results for Dipole Feed

Fig. 4.16 shows the HFSS simulated S_{11} of the antenna in solid line, the measured S_{11} is in dot line. From the figure it is observed that for HFSS simulated -10dB S_{11} bandwidth is from 2.78 GHz to 3.26 GHz, which means the impedance bandwidth is 15.9%. The measured -10 dB S_{11} bandwidth is from 2.81 GHz to 3.27 GHz, which means the impedance bandwidth is 15.1%. Therefore, for all cases S_{11} is very close to each other which show a very good matching at 3 GHz range and that validate the design of the antenna.

The measured results for the E- and H-plane radiation patterns of the feed have not been included because of the back radiation properties of the feed. With this feed, the supporting rod that mounts it on a parabolic reflector is illuminated by the feed, causing

scattering. In this study the supporting rod was a semi-flexible cable with an SMA connector, as described later in the experimental study. Simulation studies were also done with this support structure connected to the feed, and compared with those of the feed alone. The difference between the two was found to be negligibly small, and did not affect the reflector antenna performance noticeably, and omitted here for brevity.

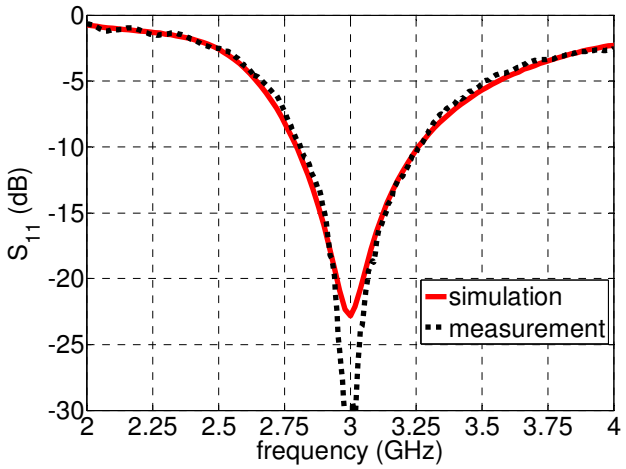

Fig. 4.16 Simulated and measured S_{11} of the microstrip dipole feed. Antenna parameters are mentioned in Table 4.1.

4.2.6.2 Feed Performance with Reflector

The performance of the feed on a parabolic reflector antenna is investigated following the established methods in [33] and [63]. The results for the gain factor, i.e. the overall efficiency, of the reflector are shown in Fig. 4.17, which excludes all the losses. It indicates a peak efficiency of 78% with a reflector having an aperture angle of 67.5^0, corresponding to an f/D of 0.375. This should be compared with 82% efficiency of theoretical feeds, as discussed in [33]. Fig. 4.17 also shows that the feed efficiency drops to 65%, for a deeper reflector with f/D = 0.25, or the aperture angle of 90^0.

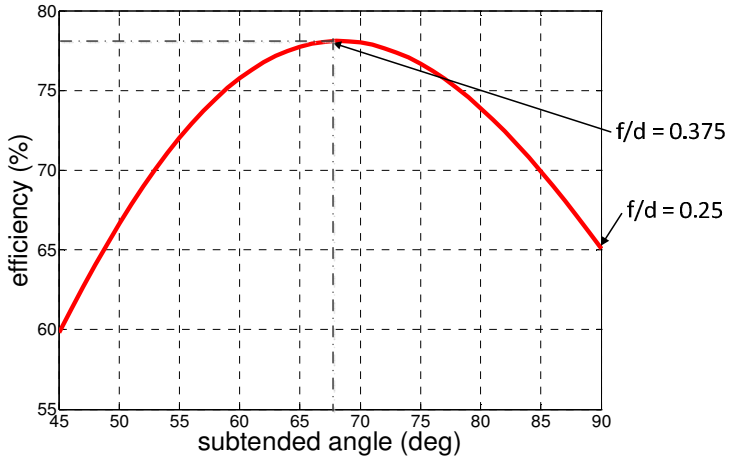

Fig. 4.17 Computed feed efficiency of a symmetrical parabolic reflector as a function of its subtended angle. The efficiency is calculated using the feed radiation patterns at 3.06 GHz.

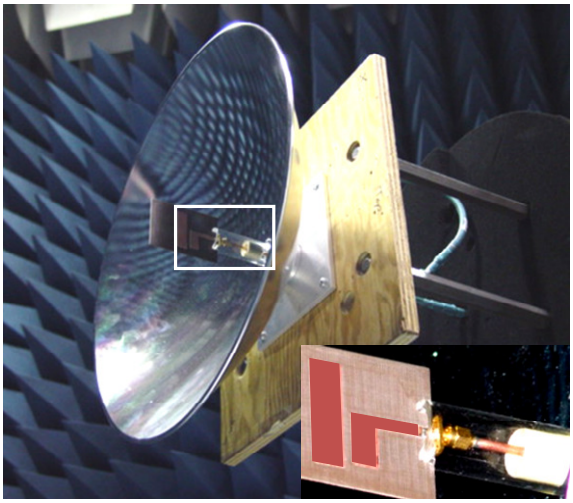

Fig. 4.18 The microstrip fed printed dipole on a 45 cm reflector with a focal length of 11.25 cm. The feed is connected to a semi rigid coaxial cable RG 402 and is mounted centrally on the reflector by foam.

In the antenna laboratory a small 45 cm parabolic reflector was available, which had an f/D of 0.25. Its focal length was 11.25 cm, which is slightly larger than one wavelength at 3 GHz. The dipole feed was connected to an RG 402 semi rigid cable with

an outer diameter of 3.6 mm, and mounted on the reflector through a central hole on the parabolic reflector without any strut support, as shown in Fig. 4.18.

The measured gain pattern of the reflector is shown in Fig. 4.19 from 2.7 GHz to 3.3 GHz. It shows that the gain is constantly increasing with frequency and then drops down, although it has small variation with frequency. This may be due to the reflector-feed resonance with frequency. Therefore, we draw a best fit line, which shows the gain is monotonically increasing with the frequency.

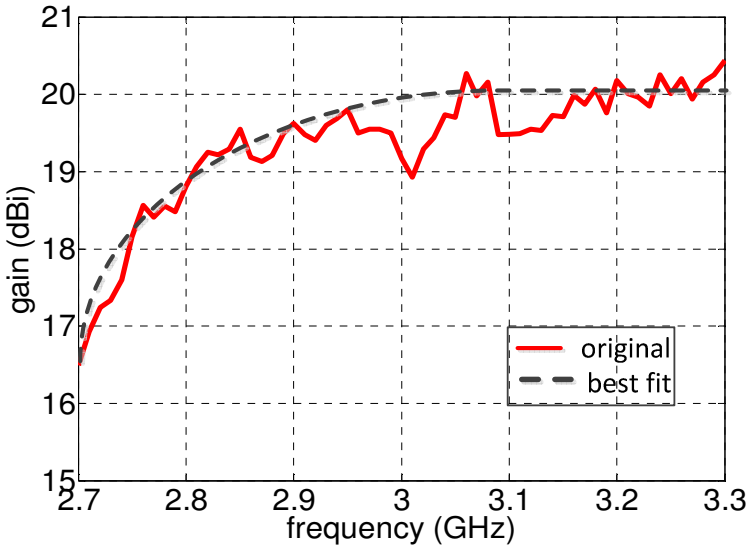

Fig. 4.19 Measured gain variation with frequency of a 45 cm reflector antenna with the microstrip dipole feed.

The measured radiation patterns of the reflector are shown in Fig. 4.20, indicating a gain of 20.2 dBi at 3.06 GHz, which includes the feed mismatch and external feed line losses. This corresponds to an overall efficiency of 50.3%.

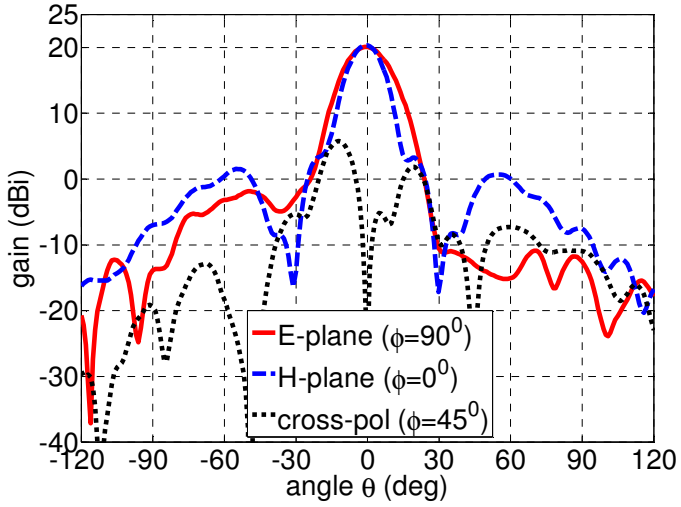

Fig. 4.20 Measured radiation patterns of the reflector at 3.06 GHz. Reflector diameter and focal lengths are 45 mm, and 11.25 cm respectively. Feed parameters are listed in Table 4.1.

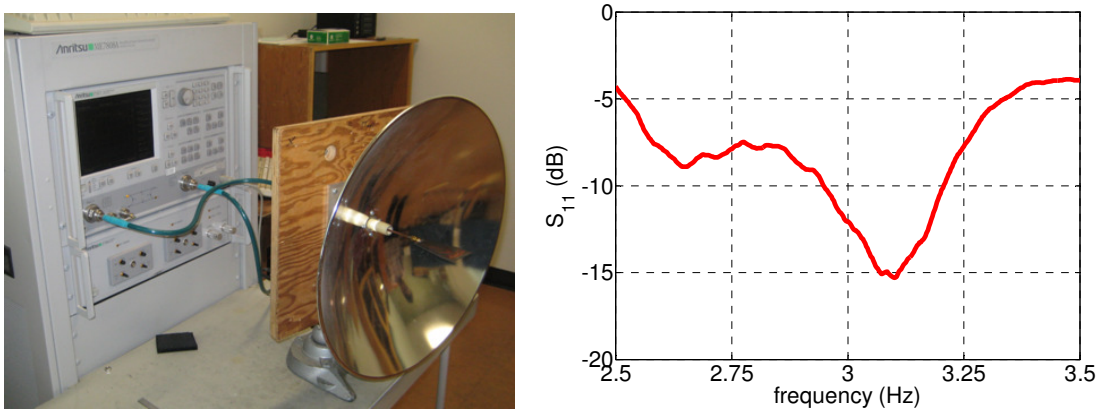

(a) S_{11} Measurement setup **(b) S_{11}**

Fig. 4.21 The measured S_{11} of the dipole feed when mounted on the reflector; (a) measurement setup, (b) S_{11}.

To calculate the mismatch loss, the S_{11} of the feed antenna was also measured with the 45 cm reflector antenna and the measurement setup is shown in Fig. 4.21 (a). In the measurement, the feed phase center is located at the focal point of the reflector. Fig. 4.21 (b) shows the measured S_{11} of the feed antenna with the reflector. From the figure it is

observed that -10 dB S_{11} bandwidth is from 2.94 GHz to 3.21 GHz. At 3.06 GHz S_{11} is -14 dB, which corresponds to 0.20 dB mismatch loss.

Excluding the losses the actual reflector gain increases to 20.4 dBi, which corresponds to an efficiency of 55%, at the feed input after the SMA connector. Thus, compared to Fig. 4.17, the measured efficiency is lower than the calculated efficiency of 65%, by about 10%. This difference can be attributed to a few factors, inherent in the feed and measurement. The microstrip feed has metallization and dielectric losses, which were calculated to be about 0.3 dB. The feed line also radiates the cross-polarized field, which is not included in the measured gain. In addition, the reflector focal length of 1.125 λ_0 is too small at 3.06 GHz. Thus the reflector is at the near field distance of the feed, causing some phase errors. Table 4.3 shows the analysis of the reflector gain, and magnitude of various losses.

Table 4.3 Gain, losses and efficiency of the microstrip dipole feed with the 45 cm reflector at three different frequencies.

	2.82 GHz	3.06 GHz	3.2 GHz
Measured Gain	19.2 dBi	20.2 dBi	20.1 dBi
Mismatch Loss	0.65 dB	0.20 dB	0.45 dB
Coaxial Cable Loss	0.15 dB	0.20 dB	0.25 dB
Gain at Feed Input	20.0 dBi	20.4 dBi	20.8 dBi
Antenna Efficiency	57%	55%	53%

Finally, it should be noted that we have verified the feed performance on a deep dish with an f/D of 0.25, which from Fig. 4.17 gives a theoretical efficiency of 65%. To improve the efficiency we either need a reflector with f/D of 0.375, which from Fig. 4.17

gives a higher efficiency of 78%. Or, use an appropriate reflector with an elliptical aperture shape.

4.3 Improvement of the Dipole Feed Performance

The microstrip dipole feeds discussed in the previous sections suffer narrow impedance bandwidth. In addition, the antenna suffers pattern asymmetry in the principal planes. Therefore, performance improvements are necessary for these two cases. They are achieved by adjusting its parameters as discussed below.

4.3.1 Broadening Impedance Bandwidth

The microstrip antennas suffer usually narrow impedance bandwidth and therefore, their applications in many systems are impeded by this bandwidth [64]**.** Therefore, it is necessary to improve the impedance bandwidth of the antennas. Generally the bandwidth of the antenna can be increased by lowering the Q factor. This can be achieved by some of the techniques like electrically thick elements [65], stacked multipatch, multilayer elements [66]**,** multiple-resonator elements [67]-[68], which already addressed in the literature. All of these techniques improve the bandwidth, although they also increase complexity and/or enlarged the size of the radiating structure, or disturb the radiation patterns, thus creating new problems. Therefore, the simplest techniques that is used for broadening impedance bandwidth without disturbing the radiation patterns is to use the impedance matching at the feed point of the antennas [69]. In the following paragraph we discuss this technique to improve the impedance bandwidth of the antennas.

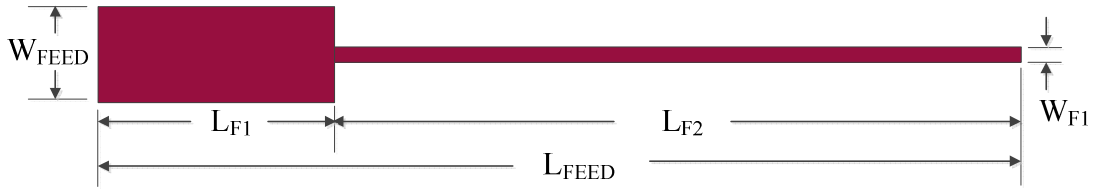

Fig. 4.22 Modified microstrip feed line for broadening impedance bandwidth; W_{FEED} = 4.2 mm, W_{F1} = 1 mm, L_{FEED} = 53 mm, L_{F1} = 10 mm, L_{F2} = 33 mm.

The impedance bandwidth of the original antenna was about 15.9%. To improve its impedance bandwidth, the microstrip feed line was carefully modified so that its impedance is matched with the dipole arms. Fig. 4.22 shows the layout of the modified microstrip feed line. In the original dipole design, one side of the microstrip feed line was connected to the SMA connector of the coaxial cable, whose characteristics impedance was 50 Ω. The other side of the microstrip feed line was connected to the dipole arms whose characteristics impedance was higher than 50 Ω. In the modified design, the width and length of the microstrip line were modified so that its impedance matched that of the dipole arms. In the original design, the entire width of the microstrip line W_{FEED} was set at 4.2 mm, based on the characteristic impedance of 50 Ω. In this modified design, the microstrip line has two parts. The first part, which is connected to the SMA connector of the co-axial cable, has a length L_{FI} and width W_{FEED} of 10 mm and 4.2 mm, respectively, for the characteristics impedance of 50 Ω. The second part, which is connected to the dipole arms has a length L_{F2} and width W_{FI} of 33 mm and 1 mm, respectively, and acts as an impedance transformer to match the characteristic impedance to that of the dipole arms. The width of the transmission line, which is connected between the ground plane and other dipole arm is also modified and set to 1 mm.

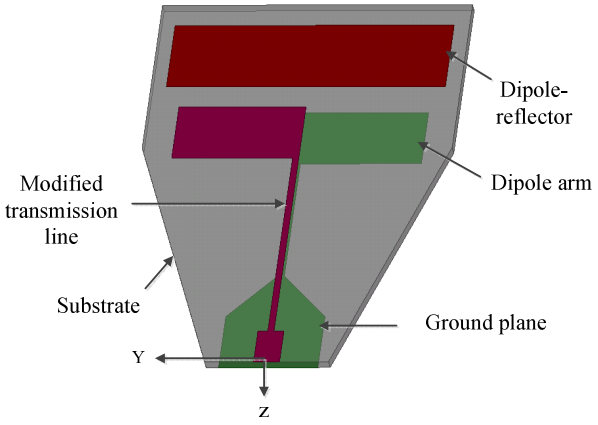

(a)

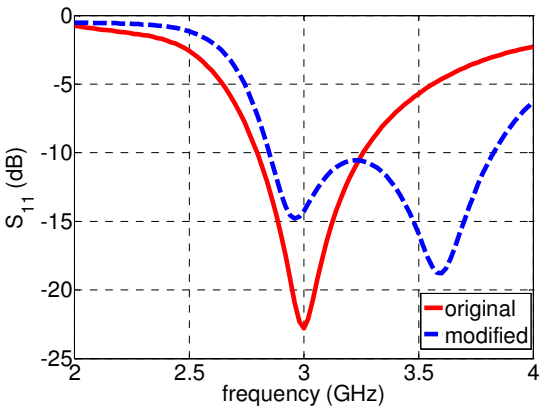

(b)

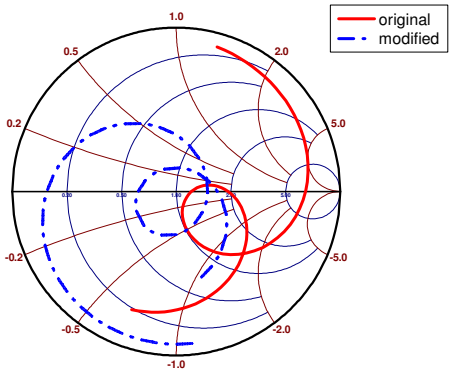

(c)

Fig. 4.23 Broadband microstrip dipole feed with modified feed line. All parameters are shown in Table 4.1 except dipole arm length L_{TDRI} = L_{BDRI} = 20.5 mm and feed line is shown in Fig. 4.22. (a) geometry, (b) S_{11}, (c) Smith chart.

The antenna geometry is shown in Fig. 4.23 (a) and simulated by Ansoft HFSS ver. 14 [70]. All parameters except the substrate size of the feed antenna are the same as shown in Table 4.1. As the feed line L_{FEED} is increased to 53 mm, the substrate size is also changed and the dimensions are now 50 mm by 70 mm. The substrate is cut and tapered in the direction of radiation. It is observed that shaping the substrate has no effect on the radiation and input impedance of the antenna. Fig. 4.23 (b) compares the simulated

S_{11} of the antenna for two different cases. For the modified feed line case, the -10 dB S_{11} bandwidth is from 2.85 to 3.82 GHz, which is 29.1% impedance bandwidth compared to 15.9%, in the original feed line case. Therefore, it is 13.2% higher than the previous case. Fig. 4.23 (c) shows the Smith chart corresponding to the input impedance of the two cases. For the modified feed line case, the matching section has moved the impedance loop to the centre of Smith chart, so the entire loop is within a constant $S_{11} \leq$ -10 dB, indicating a broadband S_{11}. The E- and H-plane radiation patterns are unchanged with the modified feed line and therefore are omitted for brevity.

4.3.1.1 Broadband Dipole Feed Evaluation

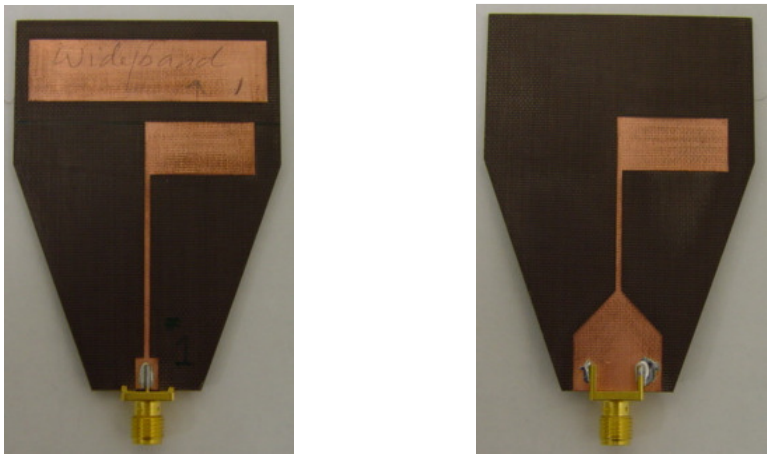

(a) **(b)**

Fig. 4.24 The fabricated broadband microstrip dipole feed. All parameters are mentioned in Table 4.1 and figure 4.23; (a) top view, (b) bottom view.

The broadband microstrip fed printed dipole antenna was also fabricated in the laboratory on an Arlon Diclad substrate with a thickness of 1.58 mm, dielectric constant of 2.5, (tan δ) of 0.002, and an area of 50 × 70 mm^2. All the parameters were selected

based on Table 4.1 and Fig. 4.24. The top and bottom view of the fabricated feed antenna are shown in Fig. 4.24 (a) and (b) respectively.

Fig. 4.25 shows the simulated and measured S_{11} of the modified feed antenna. The figure shows that simulated -10 dB S_{11} bandwidth is from 2.85 to 3.82 GHz and measured -10 dB S_{11} bandwidth is from 2.9 to 3.8 GHz. The measured S_{11} is slightly lower than the simulated S_{11}, however they almost match with each other. The measured results for the E- and H-plane radiation patterns of the feed are not included, because of the back radiation properties of the feed.

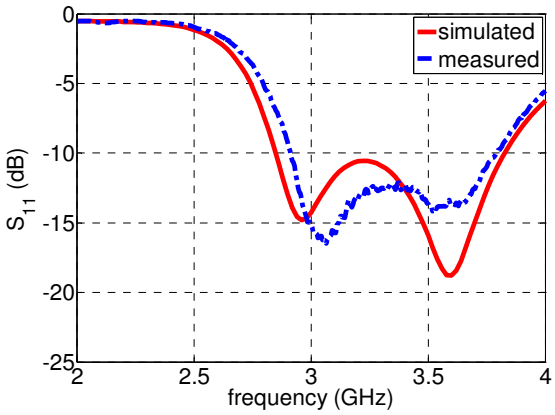

Fig. 4.25 Simulated and measured S_{11} of the broadband microstrip dipole feed.

4.3.1.2 Measurement of the Broadband Feed with Reflector

The new feed antenna was also measured with the 45 cm reflector of f/D = 0.25, available in the laboratory. The measurement setup was the same as described in 4.2.6.2. The gain patterns of the feed antenna are shown in the Fig. 4.26, where the solid line shows the original gain and the dashed line shows the best fit case. The gain is increasing

with frequency like the previous case and at 3.08 GHz the gain of the antenna is 20.1 dBi, which is almost the same as the original feed antenna case.

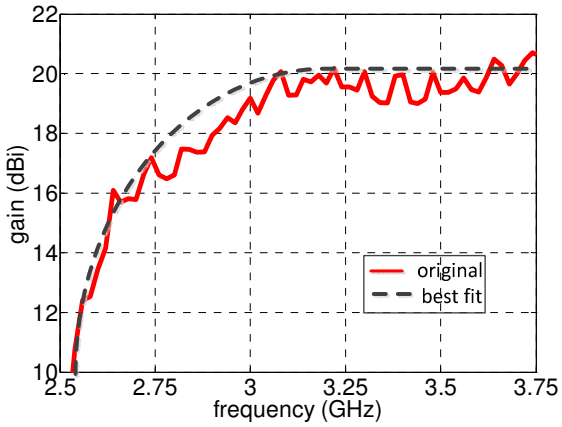

Fig. 4.26 Measured gain of the 45 cm reflector with the broadband microstrip dipole feed, at different frequencies.

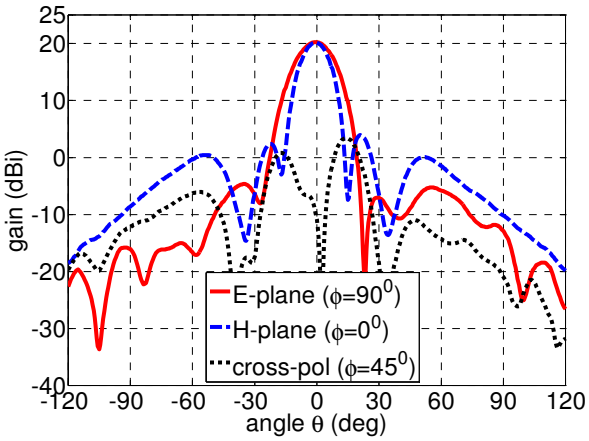

Fig. 4.27 Measured radiation pattern at 3.08 GHz of the 45 cm reflector with the broadband microstrip dipole feed.

The radiation pattern of the reflector with this feed is shown in Fig. 4.27 at 3.08 GHz which includes the feed mismatch and external feed line losses. To calculate the mismatch loss, the feed antenna is also measured with the 45 cm reflector antenna. Fig. 4.28 shows the measured S_{11} of the reflector, where the impedance bandwidth is from 2.8

GHz to 3.47 GHz. At 3.08 GHz S_{11} is -16 dB which corresponds to 0.11 dB mismatch loss. The co-axial cable loss is 0.2 dB, which is the same as previous cases. The total gain at input is 20.4 dB at 3.08 GHz. Therefore, the efficiency of the antenna including the mismatch and co-axial cable loss is 53%.

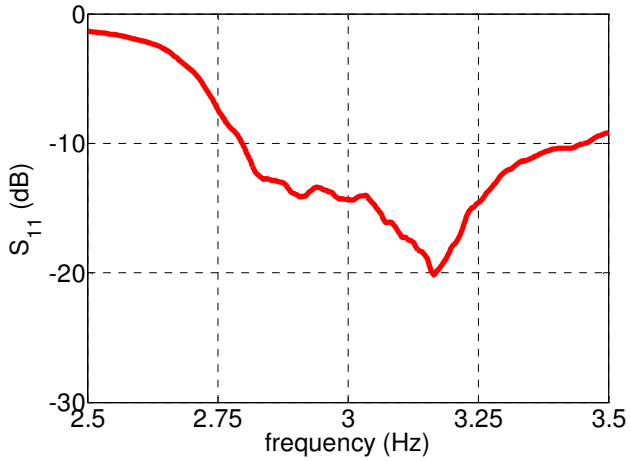

Fig. 4.28 Measured S_{11} of the broadband microstrip dipole feed on the 45 cm reflector.

4.3.2 Improving Dipole Pattern Symmetry

The original antenna geometry was symmetric about the x-z plane, which should give symmetrical E-plane radiation patterns. However with the presence of the transmission line, the co-polarization patterns of the antenna are not symmetric at the principal planes, which also cause higher cross-polarizations at the 45^0 plane. To improve the E-plane pattern symmetry for co-polarization, the lengths of the dipole arms are made unequal, but keeping the director length L_{DRI} the same. Using this technique, a good pattern symmetry is found for co-polarization patterns, which also improves the cross-polarization level at 45^0 plane. This technique is a useful solution, and does not change the overall structure of the antenna.

Fig. 4.29 (a) shows the left and right dipole arms, with unequal lengths, connected through the microstrip line. The width of the dipole arms is the same as the original case. With the change of the dipole arm lengths, now the symmetry about the XZ-plane is slightly changed and the center point of the dipole-reflector is also adjusted accordingly. The radiation patterns of the modified antenna at 3 GHz are shown in Fig. 4.29 (b). As shown in the figure, the E- and H-plane co-polar patterns are more symmetrical compared to the original case. The cross-polarization level is also lower than the original case and it is -15.6 dB at 45^0 plane, which is about -2.4 dB improvement from the original case. The S_{11} is unchanged with this case and therefore omitted for brevity.

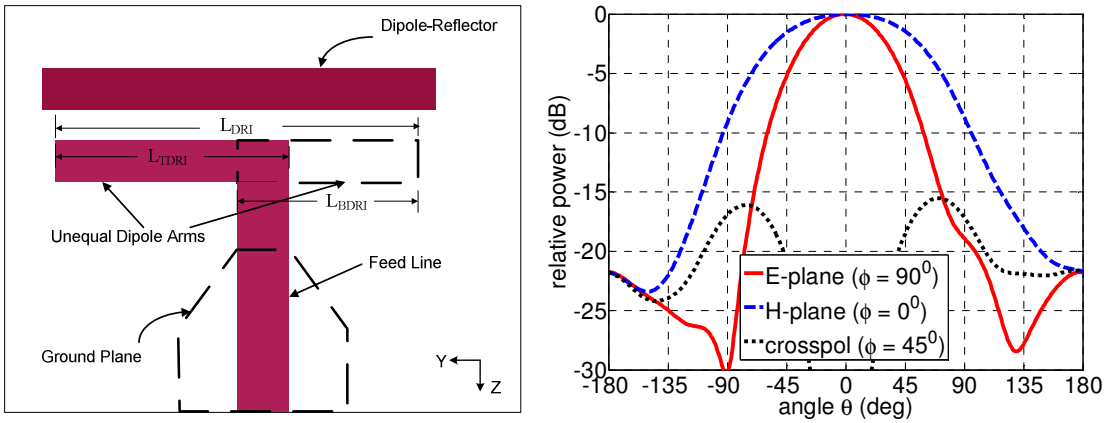

(a) **(b)**

Fig. 4.29 Unequal arm micorstrip dipole feed. Antenna parameters are mentioned in Table 4.1, except L_{TDRI} = 24.6 mm and L_{BDRI} = 19.6 mm; (a) geometry, (b) radiation pattern at 3 GHz.

4.4 Effects of Substrate Parameters on Dipole Feed

So far in the design process, the substrate thickness t and the substrate dielectric constant ε_r were kept constant. However, they are important in the design process as the

dipole arm length and feed line width are dependent on them. In the following sub-section we briefly explain the effects of these two parameters.

4.4.1 Effects of the Substrate Thickness

The substrate thickness is an important parameter in designing the dipole feed antenna. The feed line width is changed with the change of the substrate thickness. For the same dielectric constant of 2.5, at thicknesses t = 0.64 mm, 1.58 mm and 3 mm, the transmission line widths are 1.82 mm, 4.2 mm and 8.51 mm, respectively.

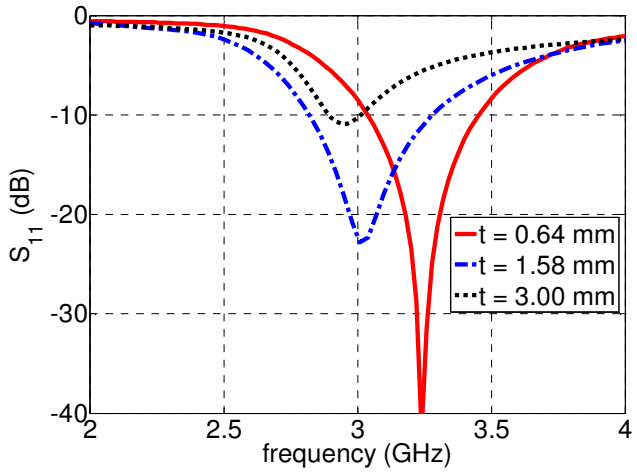

Fig. 4.30 Simulated S_{11} of the microstrip dipole feed shown in Fig. 4.1 with different substrate thickness t; other antenna parameters are listed in Table 4.1.

Fig. 4.30 shows the S_{11} of the antenna for these three different substrate thicknesses. At t = 0.64 mm, 1.58 mm and 3 mm, the operating frequencies are 3.3 GHz, 3 GHz and 2.8 GHz respectively. Therefore, the substrate thickness not only changes the width of the feed line, but it also changes the operating frequency of the antenna. From the figure, it is observed that for a higher substrate thickness, the operating frequency is lower. That means for the same operating frequency, the dipole arms is short at high substrate

thickness. Thus the overall antenna size becomes small at large substrate thicknesses. The radiation patterns are omitted in this study, because they are not changed much by changing the substrate height.

4.4.2 Effects of the Dielectric Constant

The Substrate dielectric constant is another important parameter in designing the feed antenna. The feed line width changes with the change of the dielectric constant. For the same substrate thickness of 1.58 mm, the dielectric constants of ε_r = 2.5, 6.15 and 10.2, the line widths are 4.2 mm, 1.56 mm and 1.41 mm, respectively. Fig. 4.31 shows the S_{11} of the antenna for these three different dielectric constants. When ε_r =10.2, 6.15, and 2.5, the operating frequencies are 2.1 GHz, 2.5 GHz and 3 GHz, respectively. Therefore, the substrate dielectric constant not only changes the width of the feed line, it also changes the operating frequency of the antenna. From the figure, it is observed that for higher dielectric constant, the operating frequency is lower. That means for the same operating frequency, when ε_r is high the dipole arms are short. Thus the overall antenna size becomes small at high ε_r. The radiation patterns are omitted in this study for brevity as they remain almost the same.

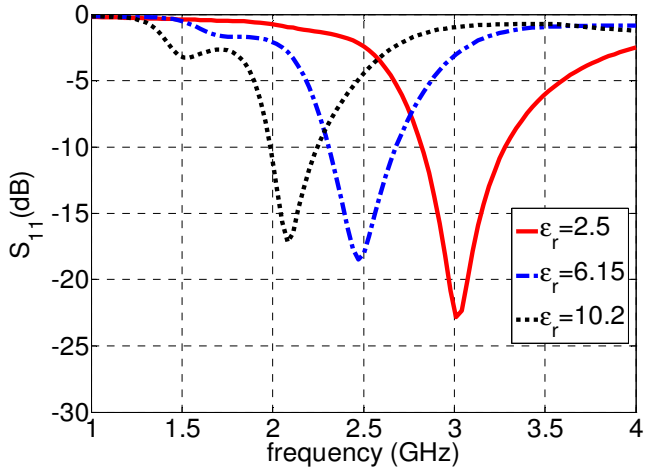

Fig. 4.31 Simulated S_{11} of the microstrip dipole feed mentioned in Fig. 4.1 with different dielectric constant ε_r; other antenna parameters are listed in Table 4.1.

4.5 Size Reduction of the Microstrip Dipole Feed

The size reduction of a feed antenna is important for the performance improvement of the reflector. It is especially true for prime focus reflectors where the feed is located at the focal point, which increases the reflector blockage, reduces the gain, and increases the side lobe level. Many methods have been used to miniaturize the antennas. One of the easiest ways to reduce the wavelength and thus the physical size of the feed antenna is to use the high dielectric constant substrates, which was shown in the previous section. It reduces the effective wavelength which in turn, shortens the dipole arm length. However, the high dielectric constants have the drawbacks of exciting the surface waves, causing a narrow bandwidth and low radiation efficiency [71]-[72]. The bandwidth can be improved by increasing the thickness of the substrate at the expense of increased surface-wave loss, but it contradicts with the philosophy of the antenna miniaturization.

The other technique that is used for antenna miniaturization without deteriorating the bandwidth is to use the magneto-dielectric materials [73] or artificial left-handed meta-materials [74]. Although, these techniques are used for antenna miniaturization, they are expensive to implement.

Another antenna miniaturization technique is to modify the geometry and shape to increase the electrical length. One of its examples is to insert slots into the patches and these slots force the surface currents to meander, thus artificially increasing the antenna's electrical length and reduce the size of the antenna. By meandering the path of the currents, so that the electrical length increases, is another example of antenna miniaturization [75]. These techniques are very simple to implement but often are frequency sensitive. Thus, the antenna bandwidth of these miniaturized antennas becomes less than that of the standard antenna. However, the advantage of these techniques is that they are very easy to implement.

In this section, we simulate and design miniaturized dipole feed antennas by modifying the antenna geometry using two different techniques. In the first method, slits are placed in the dipole arms to enhance the electrical length and reduce the physical length of the dipole arms and accordingly reduce the size of the overall feed antenna. The second method is to change the shape of the dipole arms and extend the length of the arm vertically on its edge. It reduces the dipole arms horizontally and increases the electrical length and hence reduces the size of the antenna. Finally, we will further reduce the size of the antenna by combining these two techniques.

4.5.1 Loading Slits on the Dipole Arms

A simple technique of the size reduction of a microstrip dipole antenna is to load slits on the dipole arms. Initially a single slit is placed in the dipole arm of the antenna for this purpose. The size and position of the slit is important as it determines the input impedance and also the shape of the radiation patterns. Fig. 4.32 shows the dimension and position of the slit in the dipole arms. The slit width $S1_w$ and depth $S1_d$ are 1 mm and 8 mm respectively and it is g_1 = 4 mm away from the edge of the dipole arm. As a single slit is used in the dipole arms, its length L_{TDRI} and L_{BDRI} is reduced. The position and selection of the slit is based on the optimization of the parameters.

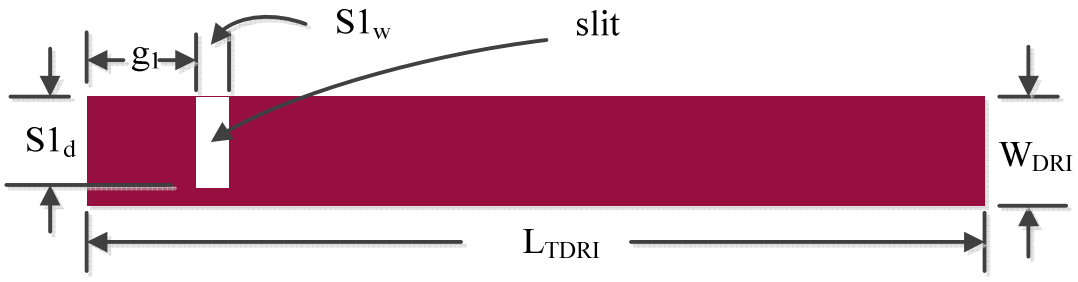

Fig. 4.32 Single slit in the dipole arm; L_{TDRI} = L_{BDRI} = 17.5 mm, W_{DRI} = 10 mm, $S1_W$ = 1 mm, $S1_d$ = 8 mm, g_1 = 4 mm.

Fig. 4.33 (a) shows the 3-D view of the antenna. All other parameters, except the dipole arms and transmission line are shown in Table 4.1. The dipole arms are designed based on Fig. 4.32. The transmission line width is modified to improve the input impedance of the antenna, which is explained in section 4.3.1. The shape of the dipole-reflector is slightly changed with vertical extension on each side to improve the radiation characteristics of the feed. The length and width of the extensions are 2 mm and 2 mm, respectively. As the length of the dipole arms are shortened by the introduction of the slit,

the length of the dipole-reflector is also shortened accordingly and selected as 40 mm. The original dipole-reflector length was 45 mm. Thus, 11.1% size reduction is achieved with this technique.

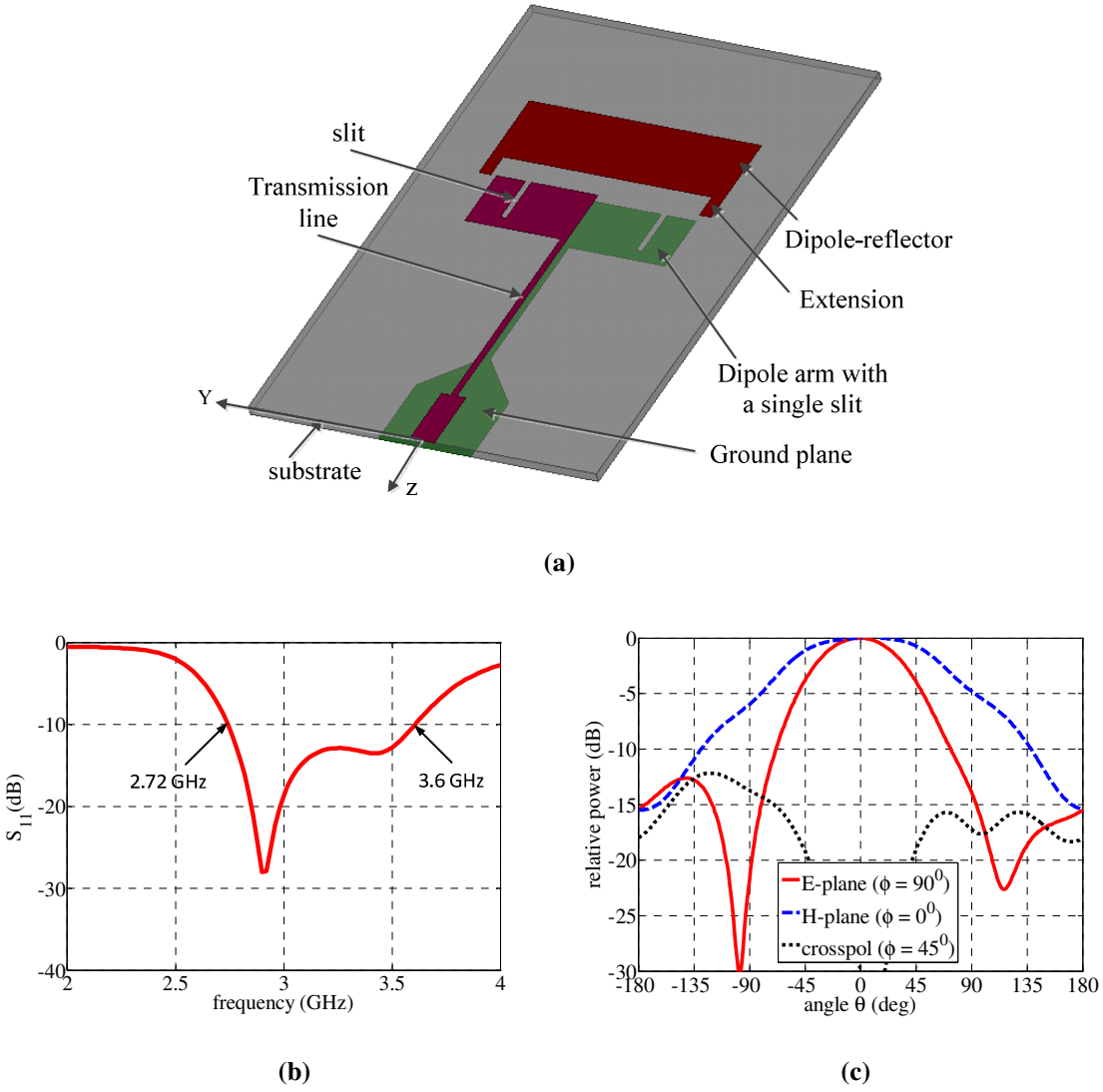

Fig. 4.33 The microstrip dipole feed with a single pair of slits at dipole arms. All parameters are shown in Table 4.1 except dipole arms which are shown in Fig. 4.32; (a) geometry, (b) S_{11}, (c) radiation patterns at 3 GHz.

The S_{11} of the antenna is shown in Fig. 4.33 (b). This figure shows that for the reduced dipole length the antenna is resonance at 3 GHz and its -10 dB S_{11} bandwidth is

from 2.72 GHz to 3.6 GHz. The simulated radiation patterns of the antenna at 3 GHz are shown in Fig. 4.33 (c). The E- and H-plane radiation patterns show excellent radiation characteristics with the H-plane pattern being broader than the E-plane pattern. The cross-polarization at 45^0 plane and back lobe level are -13 dB and -15 dB, respectively.

The overall length of the antenna can be further reduced by introduction of additional slits in the dipole arms. The number and position of the slits depend on the input impedance and radiation characteristics of the antenna. It may be mentioned that the more the slits in the dipole arms, the more the size reduction. However, the radiation efficiency of an antenna drops with the miniaturization of the antenna. Therefore, it is necessary to calculate the radiation efficiency of the miniaturized feed antenna for different pair of slits. The radiation efficiencies of the miniaturized dipole feed antennas for different pair of slits is shown in Table 4.4. The radiation efficiency of the original feed antenna is 95.02%, whereas, for a single, two, three and four pair of slits cases, the efficiency reduces to 94.66%, 94.43%, 93.90% and 92.62%, respectively. Therefore, it decreases with increasing the pair of slits. However, for all cases the radiation efficiency is higher than 90%, which is excellent for a feed antenna.

Table 4.4 Effect of size reduction on the radiation efficiency of miniaturized microtrip dipole feed with different pair of slits in the dipole arms.

	Driver length $L_{DRI,}$ mm	Dipole-reflector length L_{REF}, mm	Radiation efficiency %
Original	40 mm	45 mm	95.02%
Single pair slits	36 mm	40 mm	94.66%
Double pair slits	32 mm	38 mm	94.43%
Triple pair slits	29 mm	36 mm	93.90%
Fourth pair slits	26 mm	34 mm	92.62%

4.5.2 Changing Shapes of the Dipole Arms

Another method for the size reduction of the microstrip dipole feed is to change the shape of the dipole arms. For the microstrip dipole antenna, the dipole arm length is slightly less than quarter wavelength. However, the dipole length can be shortened by extending arm vertically in two sides so that it looks like a T-shape, from the side. By chaning the dipole arms in two sides, the current distribution within the dipole arms is changed so that, the electrical length is increased and thus the size reduction is achieved.

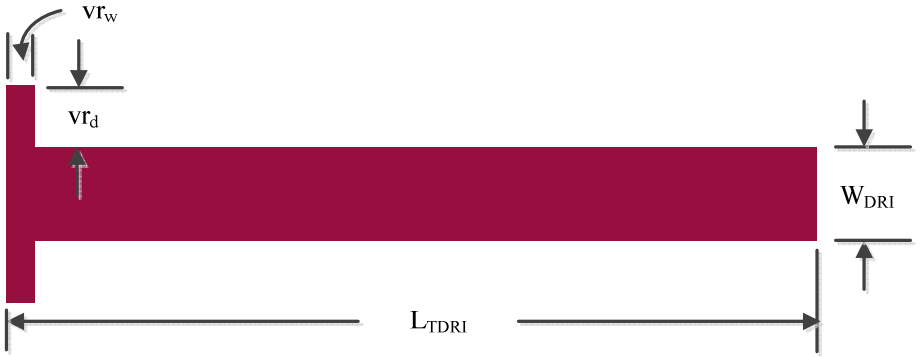

Fig. 4.34 The dipole arm with transverse extension; L_{TDRI} = L_{BDRI} = 17.5 mm, W_{DRI} = 10 mm, vr_d = 4 mm, v_{rw} = 1 mm.

Fig. 4.34 shows the design of a dipole arms with vertical extension at its far end. The figure shows that the width of the vertical extension vr_w is 1 mm and extended depth vr_d is 4 mm and the overall length of the dipole arm L_{TDRI} = L_{BDRI} is 17.5 mm, which is 3 mm shorter than the original dipole arm length of 20.5 mm.

Fig. 4.35 (a) shows the top view of the antenna by changing the dipole arms. The dipole-reflector length L_{REF} is also changed accordingly and it is selected now 40 mm. The original dipole-reflector length was 45 mm. Thus, 11.1% size reduction is achieved with this technique. The shape of the dipole-reflector is slightly changed with vertical

extension on each side to improve the radiation characteristics of the feed. The length and width of the extension are 2 mm by 2 mm, respectively. The transmission line width is also changed to increase the input impedance bandwidth of the antenna.

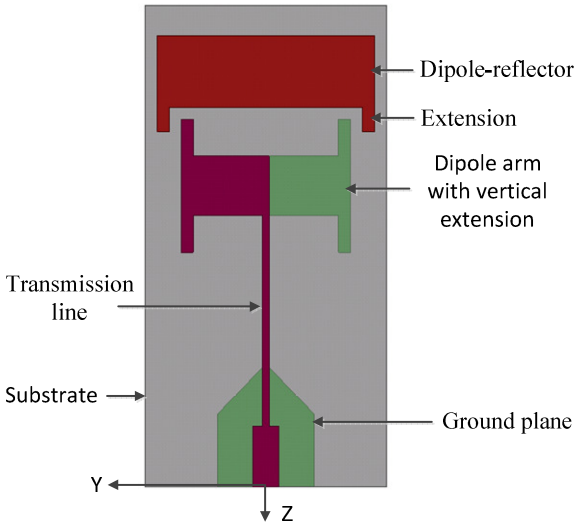

(a)

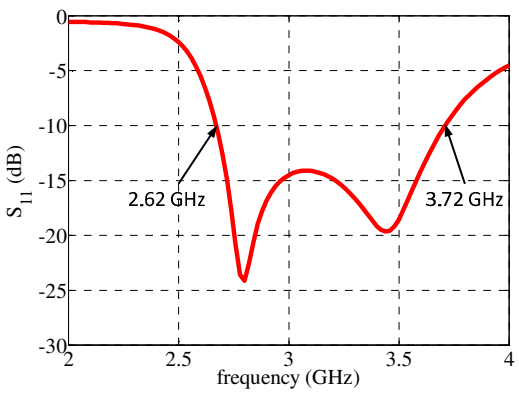

(b)

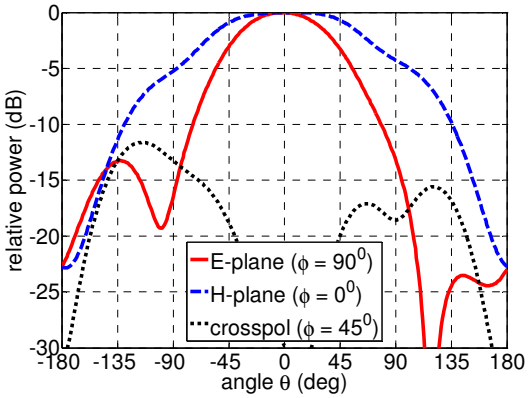

(c)

Fig. 4.35 The microstrip dipole feed with horizontal T-shape dipole arm. All parameters are shown in Table 4.1 except the dipole arms which are shown Fig. 4.34. (a) geometry, (b) S_{11}, (c) radiation pattern at 3 GHz.

Fig. 4.35 (b) shows the S_{11} of the antenna in this case. The -10 dB S_{11} bandwidth is from 2.62 GHz to 3.72 GHz and the antenna is well matched at 3 GHz frequency range.

Fig. 4.35 (c) shows the radiation pattern of the antenna at 3 GHz. The E- and H-plane radiation patterns show good radiation characteristics with the H-plane pattern being wider than the E-plane pattern. The cross-polarization level at 45^0 is -12 dB, and is not symmetric with respect to the axis. The back lobe level of the feed is -23 dB, which is better than the previous case.

4.5.3 Loading Slits on the Shaped Dipole Arms

By combining the above two methods, further size reduction is possible for the microstrip dipole feed antenna [76]. For this reason, double pair of slits is loaded in the horizontal T-shaped dipole arms. The selection of double pair of slits is based on optimum radiation efficiency, as we know that radiation efficiency of the antenna is reduced with the size reduction.

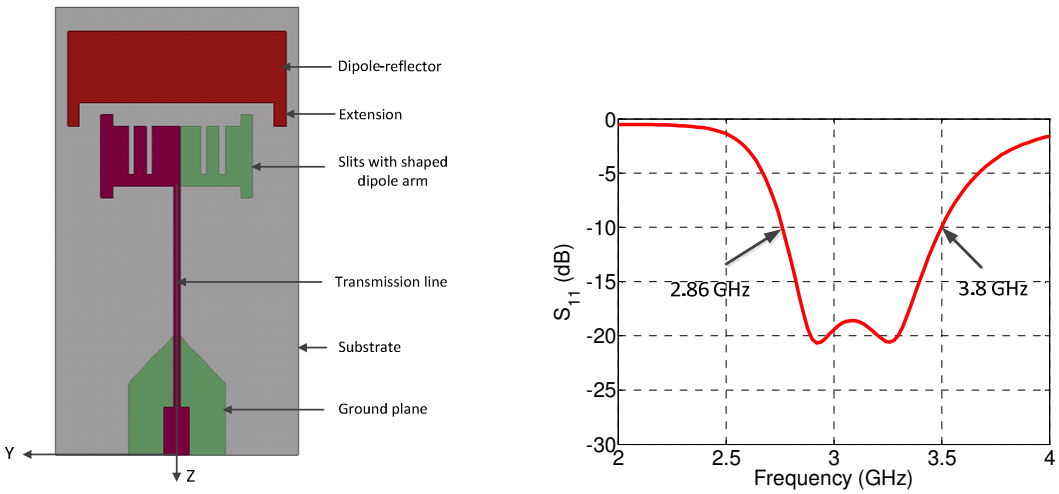

(a) **(b)**

Fig. 4.36 The miniaturized microstrip dipole feed with horizontal T-shape dipole arms with slits. All parameters are shown in Table 4.1 except the dipole arms; (a) geometry, (b) S_{11}.

The width and depth of the slits are 1 mm and 8 mm, respectively and they are located 9 mm and 4 mm away from the feed line, which is shown in the figure 4.36. The position of the slits is important as it changes the input impedance characteristics and also the radiation patterns of the antenna. Introducing slits in the horizontal T shaped dipole arms, changes the current distribution on the surface of the arms, which is forced to follow a meander route. Thus, the electrical length of the antenna is increased while its physical length is decreased. Therefore, at 3 GHz resonance frequency, the driver length L_{DRI} is reduced to 26 mm. As the dipole arms length is reduced, the dipole-reflector length L_{REF} is also reduced, which is 36 mm. The original dipole-reflector length was 45 mm. Thus, 20% size reduction is achieved with this technique. The transmission line width is modified to improve the input impedance of the antenna, which is explained in section 4.3.1. All other parameters are same as the original antenna case (Table 4.1). The S_{11} of the feed antenna are shown in Fig. 4.36 (b). It is noted that the S_{11} at -10 dB point is from 2.86 GHz to 3.8 GHz that means the impedance bandwidth is 28.2%.

The simulated radiation patterns of the proposed antenna for four different frequencies are illustrated in Fig. 4.37. The H-plane radiation patterns are almost the same for all cases. The E-plane patterns are more symmetrical at higher frequencies than the lower frequencies. The cross-polarization level increases but the back lobe level decreases with frequency. Altogether the feed shows good radiation characteristics in the frequency band.

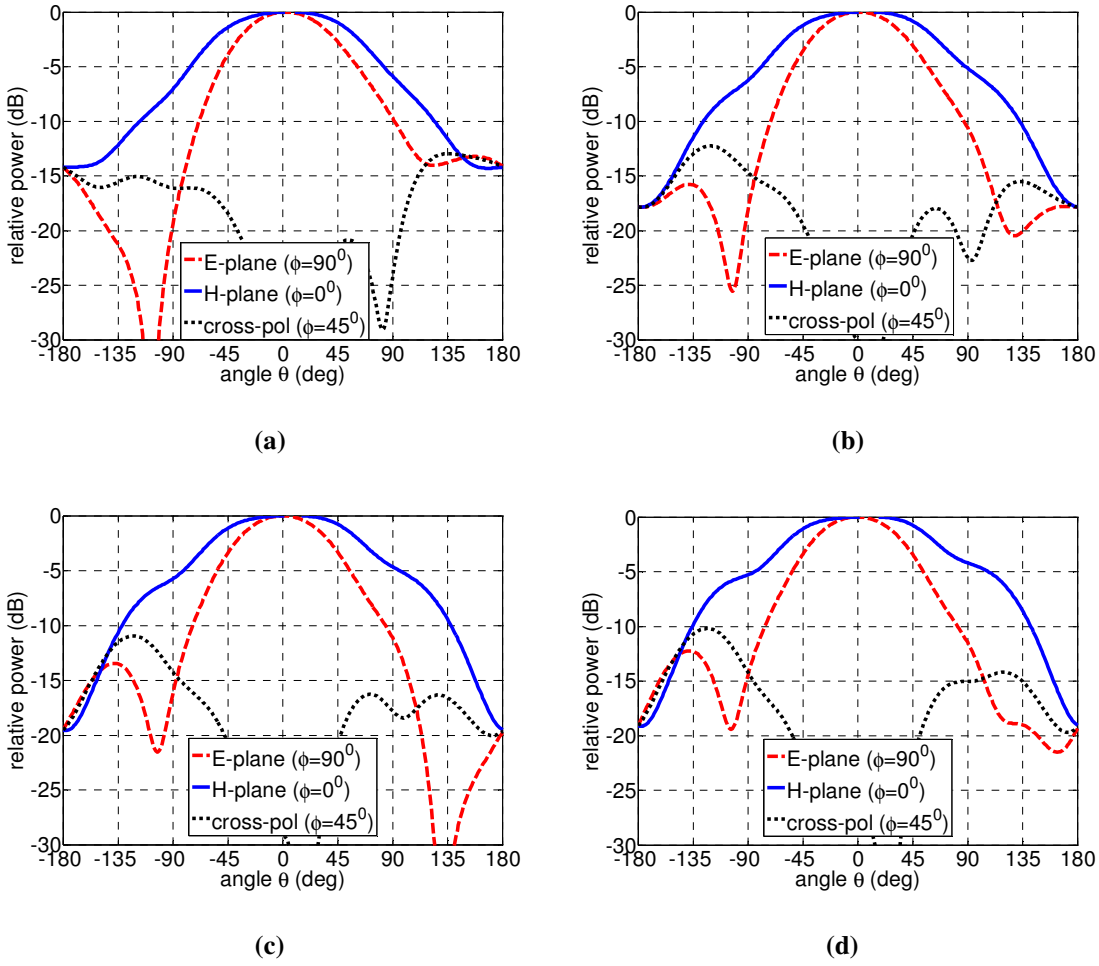

Fig. 4.37 Radiation patterns of the miniaturized micostrip dipole antenna shown in Fig. 4.36 at different frequencies; (a) 2.85 GHz, (b) 3 GHz, (c) 3.15 GHz, (d) 3.3 GHz.

4.5.4 Experimental Verification of Miniaturized Feed

The miniaturized microstrip dipole feed antenna was fabricated in the laboratory on an Arlon Diclad substrate with a thickness of 1.58 mm, dielectric constant of 2.5, loss tangent (tan δ) of 0.002, and an area of 40 × 60 mm^2. All its parameters were selected based on Table 4.1 and previous discussions. Fig. 4.38 shows the top and bottom view of the fabricated antenna.

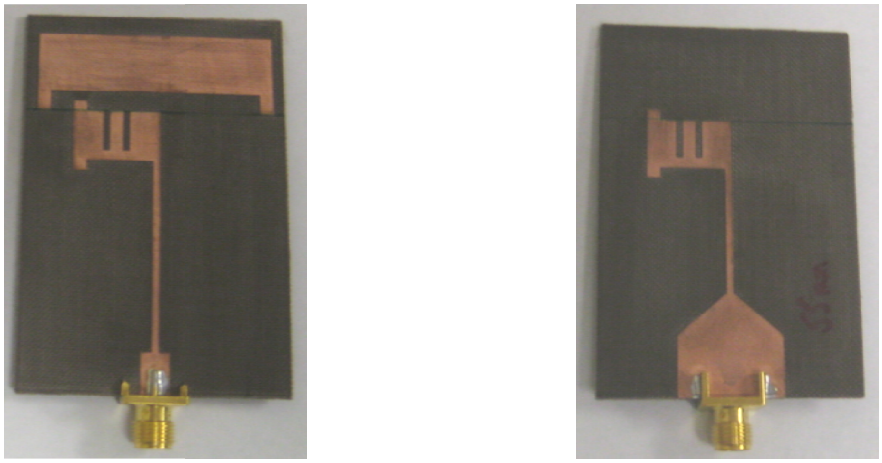

(a) (b)

Fig. 4.38 The fabricated miniaturized microstrip dipole feed. All antenna parameters are selected base on section 4.5.3. (a) top view, (b) bottom view.

The simulated and measured S_{11} of the miniaturized feed antenna are shown in Fig. 4.39. The results show that the measured -10 dB S_{11} bandwidth is from 2.7 GHz to 3.75 GHz, which is matched with the simulation results and this validates the design of the antenna. The measured results for the E- and H-plane radiation patterns of the feed have not been included because of the back radiation properties of the feed.

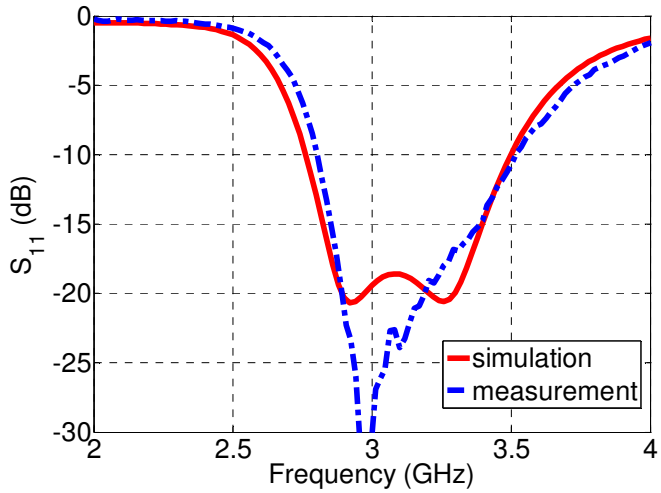

Fig. 4.39 Simulated and measured S_{11} of the miniaturized microstrip dipole feed.

4.5.4.1 Miniaturized Dipole Feed Measurement with Reflector

The miniaturized feed antenna was also measured with the 45 cm reflector with f/D = 0.25, available in the laboratory. The measurement setup is the same as described in 4.2.6.2. The gain pattern of the feed antenna is shown in Fig. 4.40, where the solid line shows the measured gain case and the dashed line shows the best fit case. Like the previous case, the gain is increasing with frequency and at 3.06 GHz the gain of the antenna is 20.3 dBi, which is slightly higher than the original feed antenna case. The radiation patterns of the reflector with this feed are shown in Fig. 4.41 at 3.06 GHz, which includes the feed mismatch and external feed line losses.

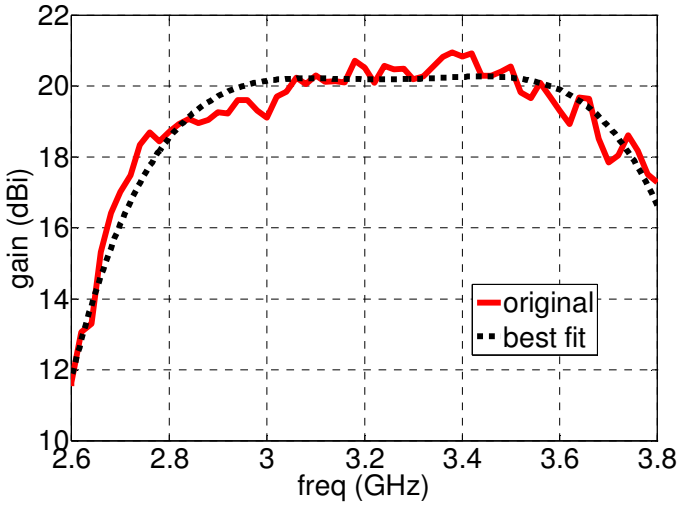

Fig. 4.40 Measured gain of 45 cm reflector with the miniaturized microstirp dipole feed at different frequencies.

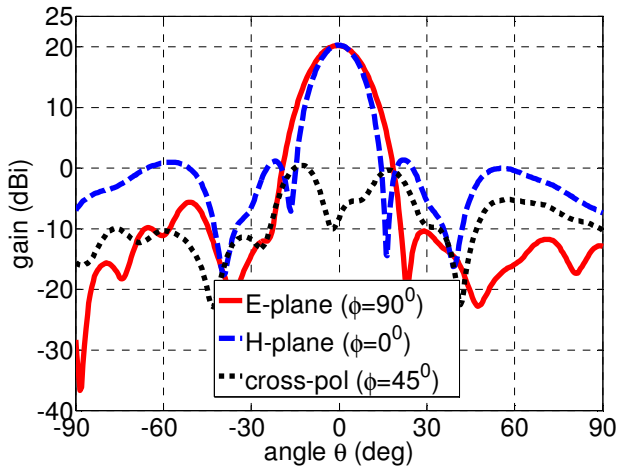

Fig. 4.41 Measured radiation pattern of the miniaturized microstrip dipole feed with the 45 cm reflector at 3.06 GHz.

To calculate the mismatch loss, the feed antenna was also measured with the 45 cm reflector. Fig. 4.42 shows the measured S_{11} of the feed with reflector where the impedance bandwidth is from 2.72 GHz to 3.48 GHz. At 3.06 GHz S_{11} is -17.4 dB, which corresponds to 0.08 dB mismatch loss. The co-axial cable loss is 0.2 dB, which is the same as previous cases. Therefore, the efficiency of the antenna including the mismatch and co-axial cable loss is 55.2% at 3.06 GHz.

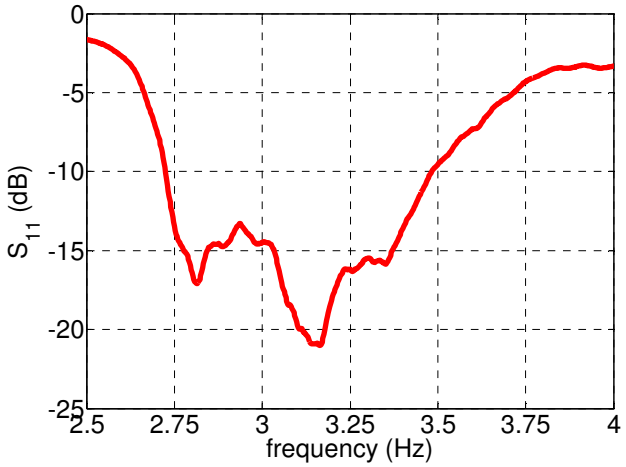

Fig. 4.42 Measured S_{11} of the miniaturized microstrip dipole feed on the 45 cm reflector.

4.6 Dual Frequency Operation of the Dipole Feed

In various radar and communications systems, such as synthetic aperture radar (SAR), dual-band mobile communications systems, and the global positioning systems (GPS), microstrip antennas are used for their low profile, light weight and low cost. Dual frequency antennas provide an alternative solution for these applications. These antennas should operate with similar planar antenna characteristics. However, obtaining these features by using planar technologies is not a simple matter, particularly when the intrinsic structural and technological simplicity of antennas are to be preserved.

Dual-frequency microstrip antennas found in the literature may be divided into orthogonal mode, multi patch or reactively loaded antennas. The simplest way to operate in dual frequencies is to use the first resonance of the two orthogonal dimensions of the rectangular patch [77]. The limitation of this approach is that two different frequencies excite two orthogonal polarizations. Nevertheless, this simple method is very useful in low-cost short-range applications, where polarization requirements are not that important.

The dual frequency operation is also achieved by means of multiple radiating elements, each one supporting strong currents and radiation at its resonance. This category includes the multilayer stacked-patch antennas [78]-[79]-[80], which are of high cost. Another drawback of these antennas is their large sizes, which make them difficult for some applications.

The reactively loaded microstrip patch antenna consists of a single radiating element in which the double resonant behavior is obtained by connecting microstrip stubs [81]-[82] at the radiating edges or two lumped capacitors connected from the patch to the

ground plane [83]. Etching slots on a patch can also be used as reactive loading, where the slot loading modify the resonant mode of a rectangular patch, particularly when the slots cut the current lines of the unperturbed mode. A dual slot-loaded microstrip antenna with dual-frequency operation has been reported in [84]-[85], where two parallel narrow slots are etched in the rectangular patch close to its radiating edges. Other dual-frequency antennas with square-slot or rectangular-slot loading are reported in [86]-[87].

4.6.1 Dual Frequency Dipole Feed Design

The dual frequency microstrip dipole feed is designed by using a simple technique. We know that the operating frequency of a dipole antenna depends on its arms. Hence, introducing two dipole arms with different lengths simultaneously in one feeding structure set two different operating frequencies, and thus a dual frequency operation is obtained.

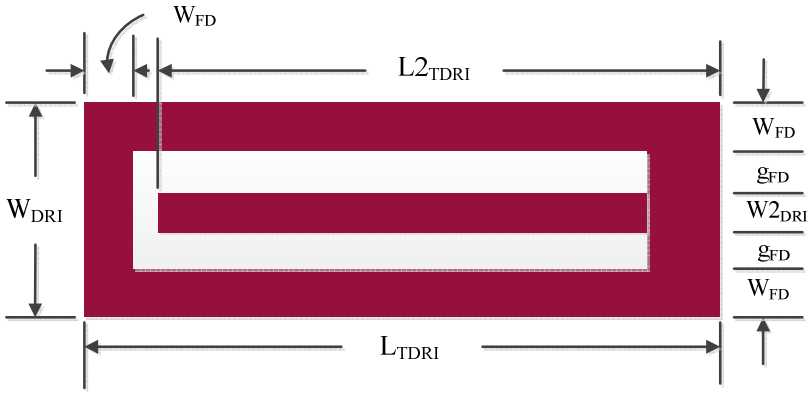

Fig. 4.43 The dipole arms of a dual frequency microstrip dipole antenna. One dipole arm is inside of a folded dipole arm; L_{TDRI} = L_{BDRI} = 22.1 mm, W_{DRI} = 10 mm, $L2_{TDRI}$ = 19.1 mm, $W2_{DRI}$ = 2mm, W_{FD} = 2 mm, g_{FD} = 2 mm, W_{FD} = 2 mm.

Therefore, for the dual frequency operation, we introduce a dipole arm within the original dipole arm. The width W_{DRI} and length L_{TDRI} of the original dipole arm are 10 mm and 22.1 mm, respectively. The dimensions of this dipole arm are designed for operation at 3 GHz. The current density on the surface of the dipole arms is simulated by HFSS ver. 14, and it is observed that most of the surface current is concentrated along the edges of the arms (see Fig. 4.3). Since the majority of surface current is concentrated toward the edges, the performance of the antenna should not be altered significantly in terms of gain, bandwidth and center frequency if most of the metallization is removed from the center. Hence, a slot is etched into the dipole arm, which looks like a folded dipole arms. As the length of the dipole arms is unchanged, the design frequency is also unchanged for this case. Now inside the slot of the dipole arm, another dipole arm is placed whose width and length are smaller than the original dipole arm. The width $W2_{DRI}$ and length $L2_{TDRI}$ of the arm are 2 mm and 19.1 mm respectively. As this dipole arm is shorter than the original dipole arm, its operating frequency is higher than 3 GHz. Therefore, by changing this dipole length, one can design an antenna for different frequencies. Fig. 4.43 shows the dipole arm of a dual frequency feed antenna.

Fig. 4.44 shows the geometry of the dual frequency microstrip dipole feed. The feed is designed similarly as the microstrip dipole feed presented in section 4.1, except the substrate shape is now truncated. The simulation shows that the truncated shape does not affect the input impedance and radiation patterns and therefore, it is selected for the less space requirement.

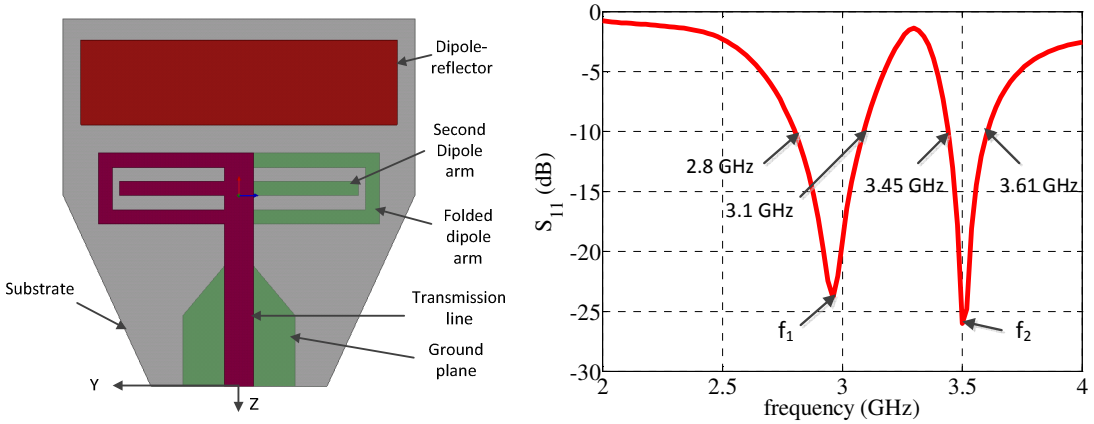

(a) (b)

Fig. 4.44 The dual frequency microstrip dipole feed, dipole parameters: L_{TDRI} = 22.1 mm, W_{DRI} = 10 mm, $L2_{TDRI}$ = 19.1 mm, $W2_{DRI}$ = 2 mm. All other parameters are shown in Table 4.1. (a) geometry, (b) S_{11}.

The simulated S_{11} of the antenna is shown in Fig. 4.44 (b). It is noted that the antenna is matched at two different frequencies. For 3 GHz, -10 dB S_{11} bandwidth is from 2.8 GHz to 3.1 GHz that means the bandwidth is 10.2% and at 3.5 GHz frequency, -10 dB S_{11} bandwidth is from 3.45 GHz to 3.61 GHz, i.e. an impedance bandwidth of 4.6%.

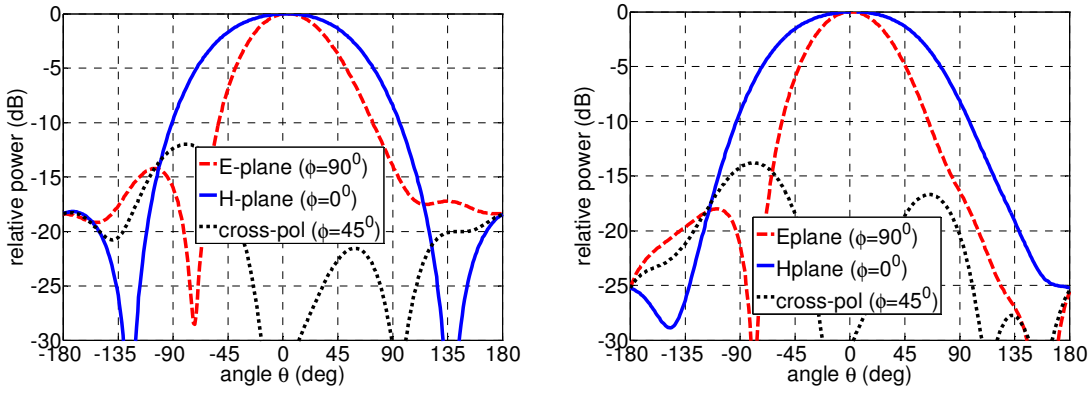

(a) (b)

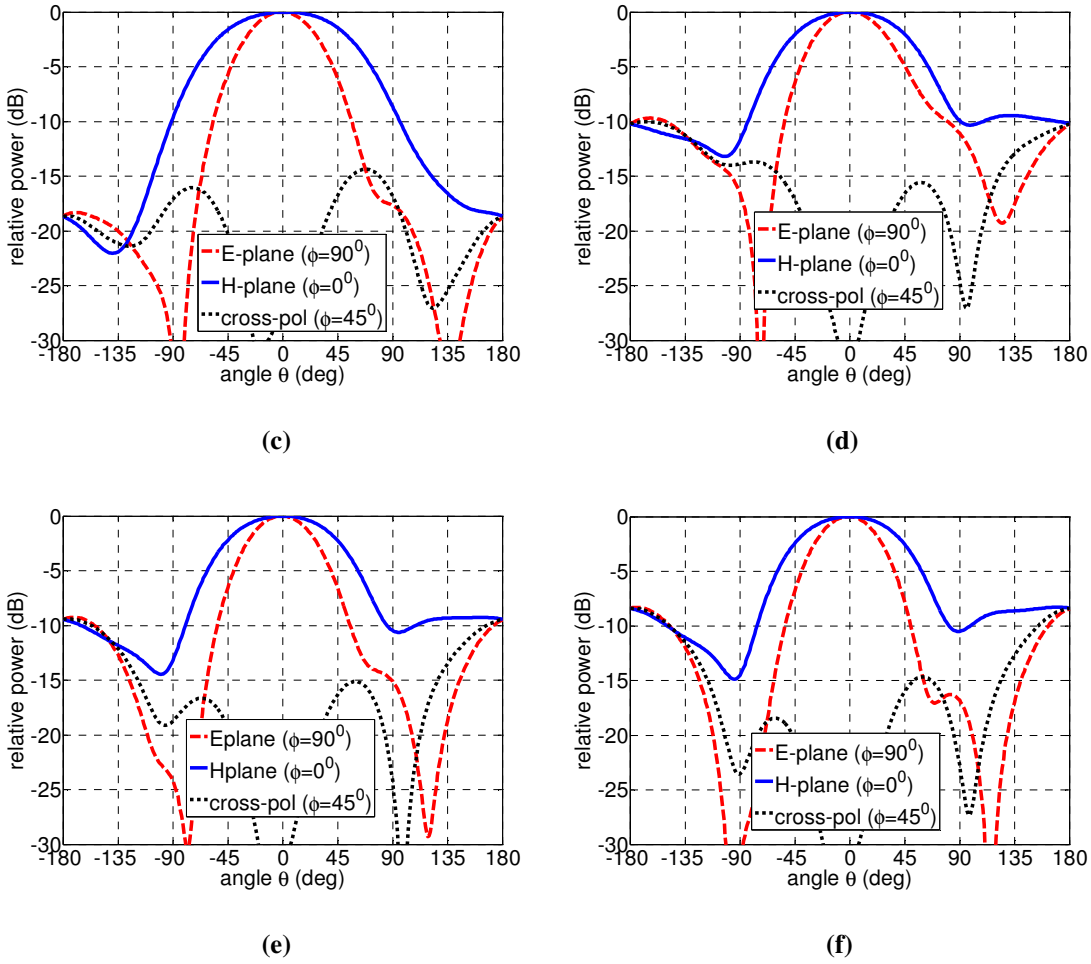

Fig. 4.45 Simulated radiation patterns of the dual frequency microstrip dipole feed at different frequencies; (a) 2.8 GHz, (b) 3 GHz, (c) 3.15 GHz, (d) 3.4 GHz, (e) 3.5 GHz, (f) 3.6 GHz.

The simulated radiation patterns of the feed at different frequencies are shown in fig. 4.45. It is evident from the figure that at low frequencies, the radiation patterns are satisfactory with a back lobe level, below -18 dB. At high frequencies, the radiation patterns are still good, but back lobe levels are high. However, cross-polarization levels are low compare to the low frequency cases. The dual frequency operation can similarly obtained for other frequency band. Table 4.5 shows the effect of inner dipole arm length on dual frequency operation for various cases. It is clearly seen that, with increasing the

inner dipole arm length, the two frequencies are shifted closer to each other, which results in a low frequency ratio.

Table 4.5 Effect of impedance bandwidths on dual frequency operation by changing the inner dipole arm length $L2_{TDRI}$.

Inner dipole arm length $L2_{TDRI}$, mm	First band f_1, bandwidth (GHz, %)	Second band f_2, bandwidth (GHz, %)	Frequency ratio, f_2/f_1
19.1	2.94, 10	3.50, 4.5	1.19
18.1	2.96, 11.5	3.68, 3.3	1.24
17.1	2.96, 12.1	3.90, 2.3	1.32
16.1	2.96, 12.8	4.12, 1.9	1.39

4.6.2 Experimental Verification of Dual Frequency Feed

The dual frequency feed antenna was fabricated in the laboratory on an Arlon Diclad substrate with a thickness of 1.58 mm, dielectric constant of 2.5, loss tangent (tan δ) of 0.002, and an area of 60 × 60 mm^2. All the parameters are selected based on Table 4.1 and Fig. 4.44. Fig. 4.46 shows the fabricated antenna with its top and bottom views.

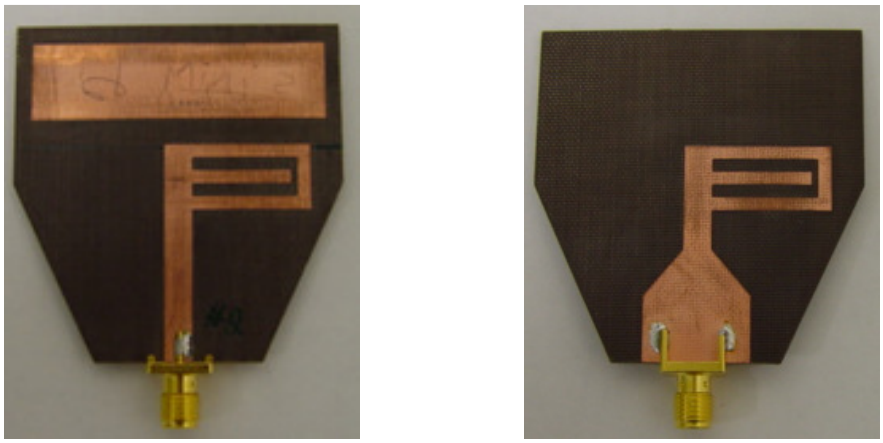

(a) **(b)**

Fig. 4.46 The fabricated dual frequency microstrip dipole feed. All antenna parameters are shown in Table 4.1 except the dipole arms, which is shown in Fig. 4.44; (a) top view, (b) bottom view.

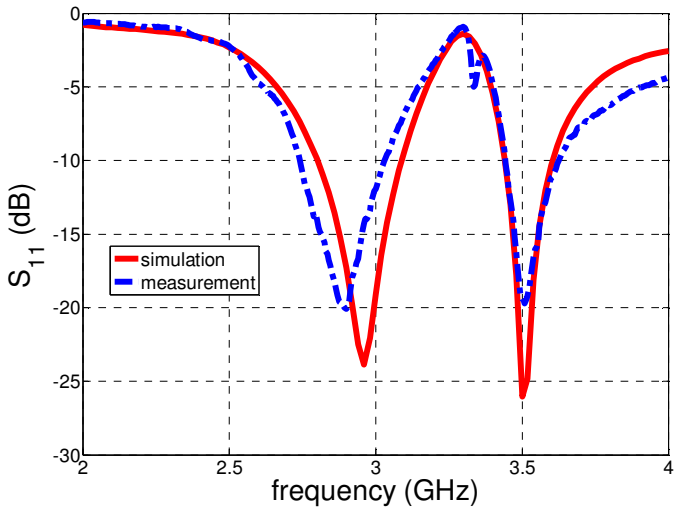

Fig. 4.47 Simulated and measured S_{11} of the dual frequency microstrip dipole feed.

The simulated and measured S_{11} of the antenna are shown in Fig. 4.47, which shows that the antenna is matched at 3 and 3.5 GHz frequency bands. The measured -10 dB S_{11} bandwidth of the antenna at 3 GHz frequency band is from 2.75 GHz to 3.05 GHz and at 3.5 GHz frequency band is from 3.45 GHz to 3.7 GHz respectively. Therefore, both the simulation and measurement results agree with each other. The measured results for the E- and H-plane radiation patterns of the feed have not been included because of the back radiation properties of the feed.

4.6.2.1 Dual Band Feed Performance with Reflector

The dual frequency microstrip dipole feed was also measured with the 45 cm reflector of f/D = 0.25, available in the laboratory. The measurement setup was the same as described in 4.2.6.2. The gain pattern of the feed antenna is shown in the Fig. 4.48 where solid line shows the measured gain case, and the dashed line shows the best fit case. The gain is increasing with frequency from 2.5 GHz to 3 GHz, and decreasing after that.

Again it is increasing from 3.4 GHz to 3.5 GHz and then decreasing. This is because of the feed is matched in this two frequency bands.

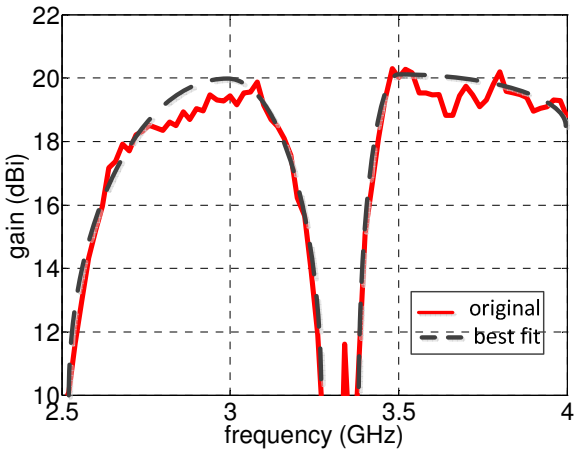

Fig. 4.48 Measured gains of the 45 cm reflector with the dual frequency microstirp dipole feed at different frequencies.

The radiation patterns of the reflector with this feed are shown in Fig. 4.49 at 3.08 GHz and 3.52 GHz, which includes the feed mismatch and external feed line losses. The gain of the antenna at 3.08 GHz is 19.9 dBi and at 3.52 GHz is 20.1 dBi, respectively.

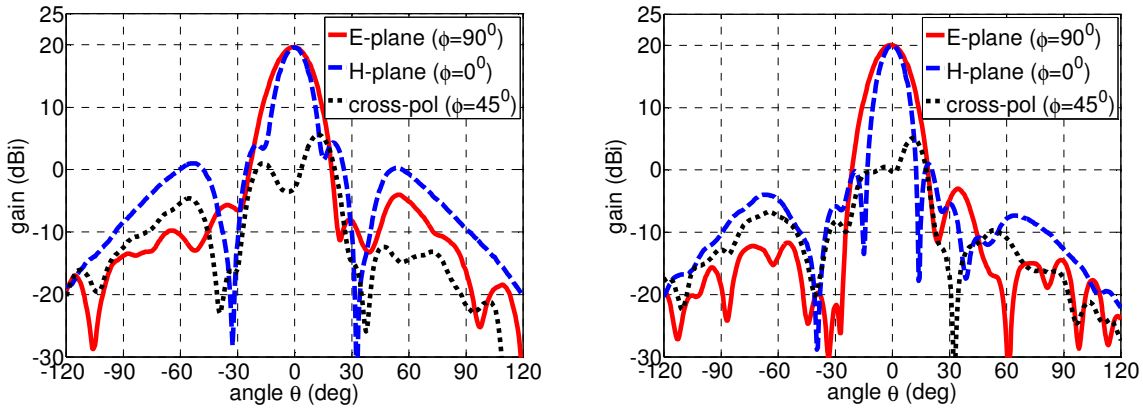

(a) **(b)**

Fig. 4.49 Measured radiation pattern of the 45 cm reflector with the dual frequency microstrip dipole feed; (a) 3.08 GHz, (b) 3.52 GHz.

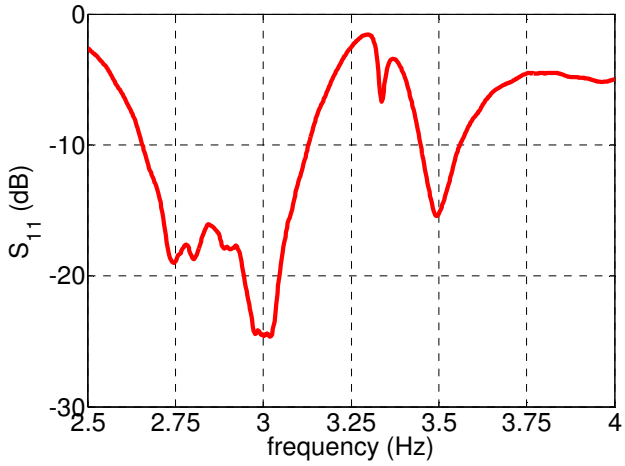

Fig. 4.50 Measured S_{11} of the dual frequency microstrip dipole feed on the 45 cm reflector.

To calculate the mismatch loss, the feed antenna is also measured with the 45 cm reflector antenna. Fig. 4.50 shows the measured S_{11} of the feed on the reflector where the impedance bandwidth is from 2.61 GHz to 3.12 GHz and 3.45 GHz to 3.56 GHz. At 3.08 GHz S_{11} is -15.1 dB, which corresponds to 0.13 dB mismatch loss and at 3.52 GHz, S_{11} is -13.7 dB, which corresponds to 0.19 dB mismatch loss. The co-axial cable loss was 0.2 dB, which is the same as the previous cases. Therefore, the efficiency of the antenna including the mismatch and co-axial cable losses are 55.2% at 3.08 GHz and 55.3% at 3.52 GHz.

4.7 Summary

In this chapter, microstrip fed printed dipole feed antennas with a dipole-reflector, based on the classic Yagi-Uda antenna was presented. In the antenna design, the dipole-reflector and the director were interchanged to provide backward radiation (radiation toward feed line). The microstrip dipole antenna was designed for 3 GHz frequency range

and a parametric study was performed to investigate the effects of various input parameters on its input impedance and radiation patterns. Based on the parametric study, the best parameters were selected and a prototype of the feed antenna was simulated by the finite element method based 3-D full wave simulator, Ansoft HFSS ver. 14 and also tested in the laboratory. It achieved good impedance matching characteristics at 3 GHz frequency range and provided good radiation characteristics with wider H-plane pattern than the E-plane pattern. Furthermore, it produced relatively lower cross-polarization level and also produced a reasonable back lobe level.

The gain factor, spillover and illumination efficiency of the proposed feed antenna were calculated. The gain factor was around 65% at f/D = 0.25, which is a reasonable efficiency in the desirable range. The phase center of the feed antenna was also determined to get optimized secondary patterns. The feed antenna was measured with a 45 cm reflector with f/D = 0.25, available in the laboratory. The gain of the reflector was found to be 20.2 dB at 3.06 GHz, and 55% efficiency was achieved.

The feed antenna suffered from narrow impedance bandwidth. Therefore, the antenna bandwidth was improved by changing the feed line width. It was found that the impedance bandwidth was increased 29% compared to 16.5% of the original case. This wideband feed was also fabricated and measured in the laboratory. The results showed good impedance matching with the simulation results. The original microstirp dipole antenna showed asymmetric pattern especially in the E-plane. The pattern symmetry was achieved by using the unequal dipole arms. It also improved the cross-polarization level of the antenna.

Size reduction of the original feed antenna was also achieved by using slits at the dipole arms and changing shapes of the dipole arms. Further size reduction was achieved by combining these two techniques. The feed was simulated and measured in the laboratory and the simulation and measured results agreed well.

The original feed antenna was then modified for the dual frequency operation. The dual frequency feed was designed for 3 GHz and 3.5 GHz, respectively. The feed was simulated and measured in the laboratory and simulation results matched with the measurement results.

The microstrip dipole feeds presented in this chapter showed unequal E- and H-plane radiation patterns. However, radiation pattern equalization was important for using the feeds with a reflector having a circular aperture. In the following chapter, we will investigate modified microstrip dipole feeds for radiation pattern equalization and discuss some of their properties.

Chapter 5

Modified Microstrip Dipole Feeds for Radiation Pattern Symmetry

5.1 Introduction

Microstrip dipole feeds, discussed in the previous chapter, had several advantages, as a feed for reflectors in simplicity and elimination of struts, as they were supported by a coaxial-feed cable and thus eliminating the blockage from support struts. However, their unequal radiation patterns in the principal planes were unable to illuminate the prime focus reflector effectively, thus caused low illumination efficiencies. Therefore, pattern equalizations of these feeds are important in order to illuminate effectively a prime focus reflector. In this chapter attempts have been made to equalize the E- and H-plane radiation patterns of these feeds.

Microstrip dipole feeds have a wider H-plane radiation pattern than the E-plane radiation pattern. Therefore, for pattern equalization, it is necessary to decrease the beamwidth of the H-plane radiation pattern, so that both beamwidths can become equal. From the geometry and co-ordinate system of the microstrip dipole antenna, it is

observed that the H-plane (XZ-plane) is symmetric with respect to the dipole arms. Therefore, it is assumed that dipole arms have effects on shaping the H-plane radiation patterns of the antenna.

Dipole antennas with straight arms are widely used for their simple geometries, which offer advantages of being relatively easy to analyze even with approximate theories. On the other hand, non-linear dipole antennas suffer from experimental investigations and also their numerical analysis is restricted. Therefore, a limited number of dipole antennas with arbitrary shapes are found in the literature. In [88], the authors showed by changing the dipole arms from a linear to non-linear, the radiation characteristics of the antenna was changed. This is the primary reference of motivation to equalize the E- and H-plane radiation patterns. The basic idea is to search for a feed antenna that will offer equal radiation patterns than comparable straight arm microstrip dipole antennas, by optimizing the dipole arm shape. Due to the computing power increase, it is relatively easy to analysis non-liner arm microstrip dipole structure.

In this chapter, we will use two techniques to equalize the radiation patterns of the microstrip dipole feed antenna. In the first technique, the dipole arms are bent so that H-plane beamwidth is decreased until both the E- and H-plane radiation patterns become equal. In the second technique, dipole arms are meandered and orthogonal stubs are added, so that the current distribution within the arms will be changed and equal E- and H-plane radiation patterns can be achieved.

5.2 Bent Arms with a Single Dipole-Reflector

A bend dipole is simply a dipole antenna that its arms are bent, instead of being straight. The number of ways that a dipole can be bent is limitless, so we can't look at all the possibilities. One way to fit a dipole antenna in a restricted space is to bend the legs horizontally, which is shown in Fig. 5.1. The bent angle depends on the radiation characteristics of the antenna and its arm length and width are adjusted to improve the input impedance at the operating frequency. If the resonant length doesn't change much and the impedance remains close to that for a straight dipole, we would expect a dipole with bent arms will produce improved radiation characteristics.

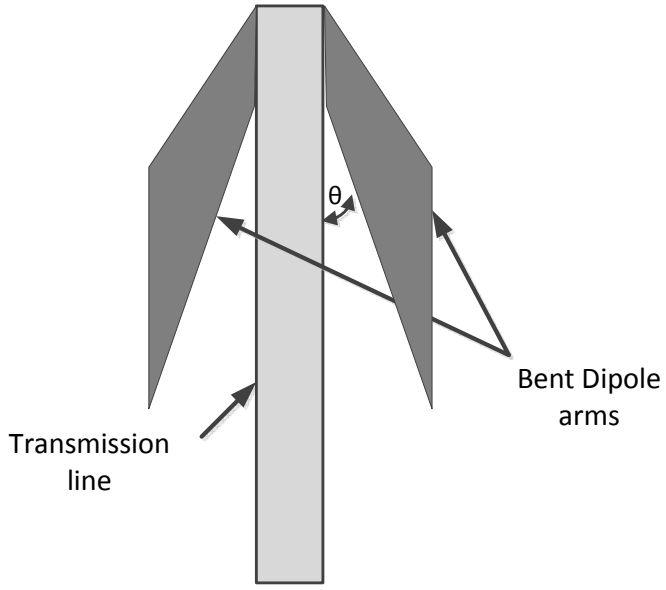

Fig. 5.1 Schematics of a bent dipole arms which are connected to parallel transmission lines. The two arms are on each side of a substrate. The bent angle determines the radiation patterns of the feed.

5.2.1 Bent Arm Dipole Feeds Design

Fig. 5.2 presents the layout of the bent dipole antenna operating at 3 GHz and printed on a substrate of dielectric constant $\varepsilon_r = 2.5$, loss tangent (tan δ) = 0.002 and thickness t = 1.58 mm with metallization on both sides. The antenna is designed the same way as it was presented in the previous chapter, except the dipole arms and the dipole-reflector are bent.

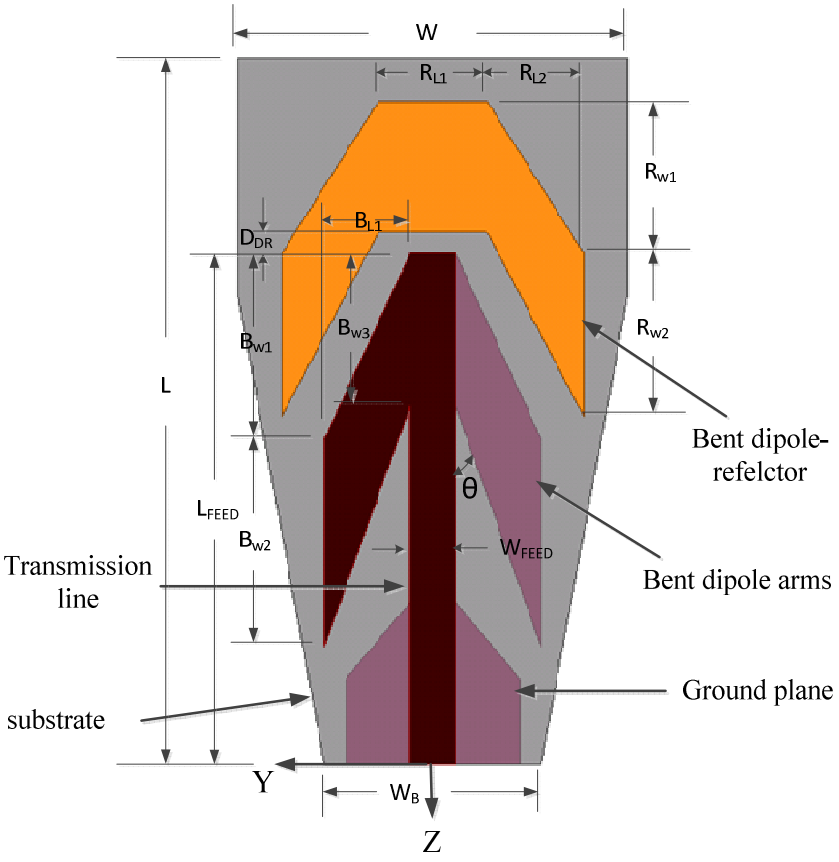

Fig. 5.2 The geometry of the bent arms micostrip dipole feed with a single dipole-reflector; L = 65 mm, W = 36 mm, W_B = 20 mm.

The length of the bent arm is evolved from the original straight dipole arms, which is quarter wavelength at the operating frequency. However, the length is adjusted to the

operating frequency. The width of the bent arms is initially selected as the same width of straight dipole, although finally it was changed along the arm to optimize for good input impedance and radiation characteristics. The bent angle was selected after several iterations. It plays an important role in determining the radiation characteristics of the antenna. By changing the bent angle one may get different impedance matching and radiation patterns.

The dipole-reflector of the feed antenna was also bent similarly. The shape and bent angle of this dipole-reflector also determine the impedance and radiation characteristics of the antenna. For back ward radiation, the horizontal length of the bent dipole-reflector should be higher than the horizontal length of the bent dipole arms. The gap between the dipole arms and dipole-reflector is also important in determining the input impedance and radiation characteristics of the antenna.

The substrate of the antenna is truncated in the direction of radiation, which is shown in the figure. Its shape had small effect on the radiation and impedance characteristics, which are confirmed by the simulation.

5.2.1.1 Effects of the Dipole Angle

We already mentioned that bending the dipole arms affects the impedance and radiation characteristics of the antenna. Therefore, the effects of the bending arms are investigated. Table 5.1 shows the output parameters for three different cases: straight dipole arm case ($\theta = 90^0$), medium bent angle case ($\theta = 47.3^0$) and narrow bent angle case ($\theta = 20.2^0$). It is shown in the table that at 3-dB point, H-plane beamwidths are 124^0, 106^0 and 82^0 at $\theta = 90^0$, 47.3^0 and 20.2^0 respectively. E-plane 3-dB beamwidths are same for

all three cases. Therefore, the H-plane beamwidth decreases by decreasing the bent angle. The cross-polarization level at 45^0 plane is almost the same for all three cases. The back lobe level increases by decreasing the bent angle. That means the beamwidth of the antenna increases. As a result, the spillover losses of the feed will be higher at higher bent angles. The -10 dB S_{11} bandwidth is also affected by the bending angle. It shows that the impedance bandwidth of the antenna decreases by decreasing the bent angle.

Table 5.1 Effects of the bending arms on radiation and impedance characteristics. All parameters are the same as previous sub-section (5.2.1) expect the bent dipole arm and bent angle.

	Straight dipole case B_{L1} = 17.9 mm, B_{W1} = 0 mm , B_{W2} = 12 mm, B_{W3} = 12 mm, $\theta = 90^0$	Medium angle case B_{L1} = 13.9 mm , B_{W1} = 12 mm, B_{W2} = 13 mm, B_{W3} = 12 mm, $\theta = 47.3^0$	Pattern equalize case B_{L1} = 7.9 mm, B_{W1} = 17 mm, B_{W2} = 19 mm, B_{W3} = 14 mm, $\theta = 20.2^0$
-3 dB beamwidth, (E-plane)	76^0	76^0	76^0
-3 dB beamwidth, (H-plane)	124^0	106^0	82^0
Cross-pol at 45^0, ($0< \theta \leq 90^0$)	-14 dB	-15.8 dB	-13 dB
Back lobe level	-14.25 dB	-13.3 dB	-8 dB
-10 dB S_{11} bandwidth	2.78 - 3.26 GHz	2.93 - 3.13 GHz	2.96 - 3.06 GHz

5.2.1.2 Simulation Results of the Bent Dipole Feed

The feed antenna was designed and simulated by Ansoft HFSS ver. 14. The antenna parameters are optimized and selected as R_{L1} = 10 mm, R_{L2} = 9 mm, R_{W1} = 14 mm, R_{W2} = 15 mm, B_{L1} = 7.9 mm, B_{W1} = 17 mm, B_{W2} = 19 mm, B_{W3} = 14 mm, W_{FEED} = 4.2 mm, L_{FEED} = 47 mm, D_{DR} = 2mm. All other parameters are same as the microstrip dipole case, which were already mentioned in the previous chapter. The simulated S_{11} of the feed antenna is shown in Fig. 5.3. It is observed that -10 dB S_{11} bandwidth is from 2.96 GHz to 3.06 GHz. Therefore, the impedance bandwidth of the antenna is only 3.33%, which is

narrow compare to the straight microstrip dipole feed. The reason for this narrow impedance bandwidth of the antenna is the bent arms, which affects the impedance characteristics of the antenna.

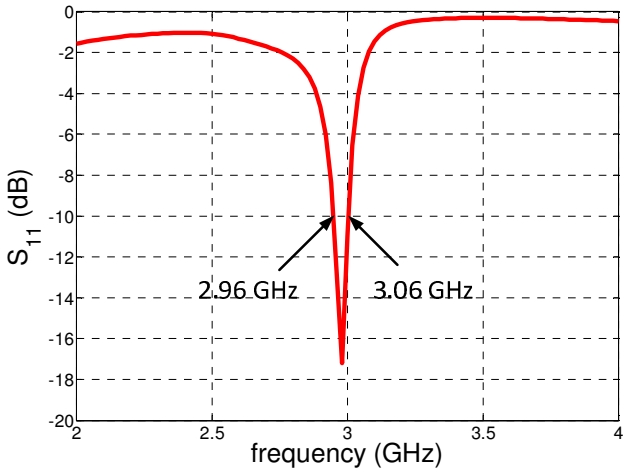

Fig. 5.3 Simulated S_{11} of the bent microstrip dipole feed with a single dipole-reflector.

The simulated radiation patterns of the feed antenna at three different frequencies are shown in Fig. 5.4. At 3 GHz, the E- and H-plane radiation patterns are almost symmetric with respect to the axis, with equal patterns up to 58^0, which corresponds to an f/D = 0.45. After that aperture angle, the E-plane pattern is not symmetric with respect to the axis. The cross-polarization level at 45^0 plane of the antenna is -13 dB and is not symmetric. This is because of the asymmetric nature of the radiation patterns after 58^0 angles. The back lobe level of the antenna is -8 dB, which is high for a feed antenna. This high back lobe level will increase the spillover loss, and decrease the spillover efficiency, which ultimately decrease the gain factor of the antenna. At 2.9 GHz, the E- and H-plane radiation patterns are almost equal with -11 dB cross-polarization level. However, at 3.1

GHz a side lobe appears in the E-plane with asymmetric nature with respect to the axis and that causes higher cross-polarization level.

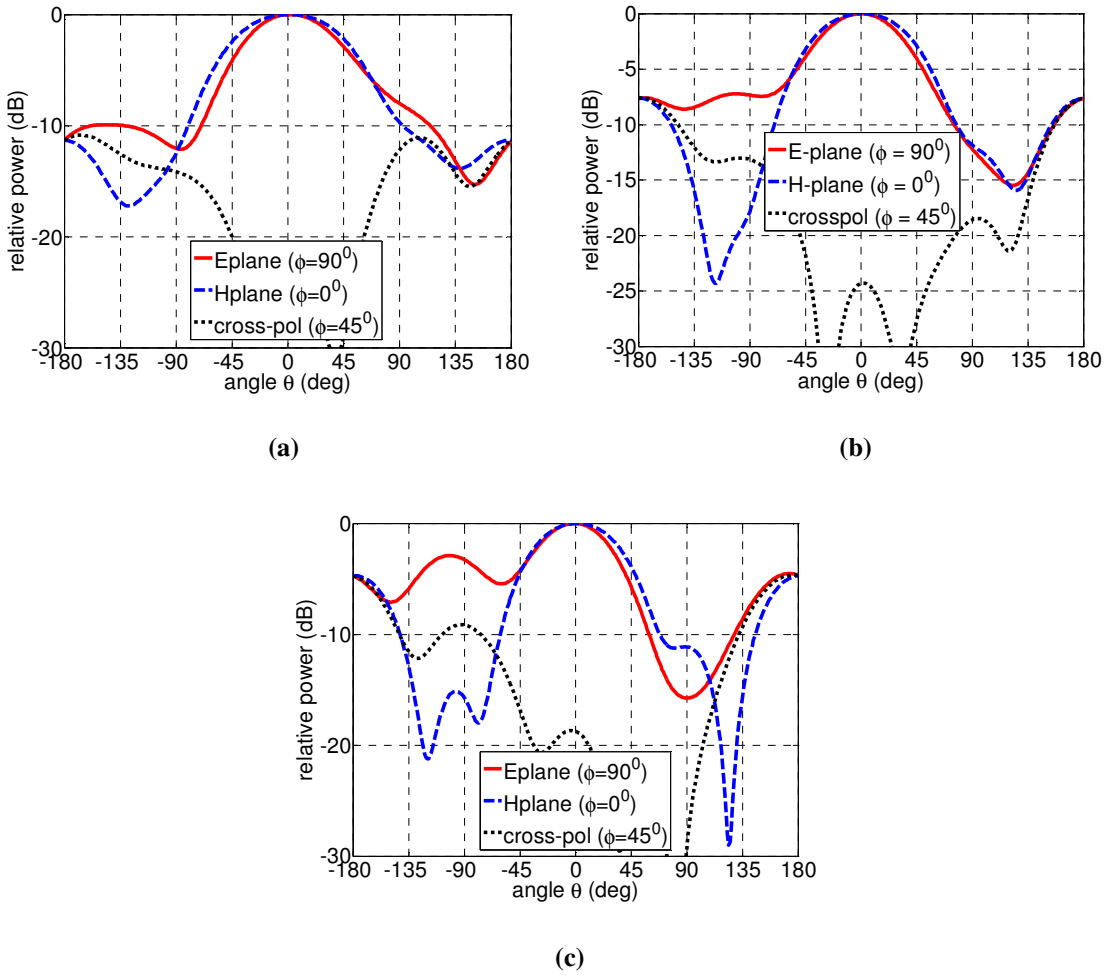

Fig. 5.4 Simulated radiation patterns of the bent microsrip feed with a single dipole-reflector at three different frequencies. (a) 2.9 GHz, (b) 3.0 GHz, (c) 3.1 GHz

Fig. 5.5 shows the surface current distributions of the antenna at 3 GHz frequency. It is observed that strong current exists at the feed line and also at the edge of the dipole arms. There is also current at the edge of the dipole-reflector, which is opposite direction to the current in the dipole arms, indicates the phase reversal at the radiating edge of the dipole-reflector.

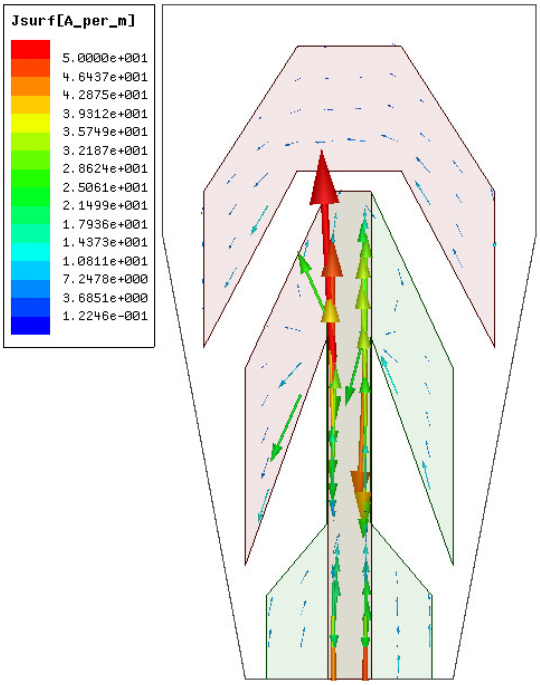

Fig. 5.5 Surface current distribution of the bent microstrip dipole feed with a single dipole-reflector at 3 GHz.

5.2.2 Performance of the Bent Dipole Feed

The performances in terms of the spillover efficiency, the illumination efficiency and the gain factor of the feed are shown at Table 5.2 for various f/D cases. It is noticed from the table that by increasing the aperture angle, the illumination efficiency is increased and the spillover efficiency is decreased, as expected. The maximum gain factor of the feed is 63.2% at f/D = 0.41, which is low compared to the other cases. This is because of the high back lobe level, which causes higher spillover loss, and also large E- and H-plane phase errors.

Table 5.2 Spillover, illumination and gain factor of the bent microstrip dipole with a single dipole-reflector feed for various f/D or aperture angle at 3 GHz.

f/D	Aperture Angle	Spillover efficiency	Illumination efficiency	Gain factor
0.35	71^0	78.7 %	84.1 %	61.4 %
0.375	67^0	76.3 %	87.1 %	62.8 %
0.39	65^0	75.0 %	88.4 %	63.1 %
0.41	63^0	73.5 %	89.7 %	63.2 %
0.43	61^0	71.0 %	91.4 %	63.0 %
0.45	58^0	69.2 %	92.5 %	62.2 %

5.2.3 Phase Center of the Bent Dipole Feed

The phase center location of the feed antenna is important to know as the phase center and reflector focal point coincide with each other. In this feed, radiations are in the Z-direction and therefore, the phase center location is also on the Z-axis. To find the phase center location of the feed, its phase distribution is important to know. The feed itself is not rotationally symmetric about the axis, and therefore it is hard to find similar phase pattern about its axis, for both E-and H-planes. Fig. 5.6 shows the phase variation of the feed antenna within 70^0 angle, with respect to a point 57 mm from the coaxial feed point, which is located at the dipole arms. The figure shows that the E-plane phase variation is not symmetric with respect to the axis and is higher than the H-plane phase variation, which is symmetric. This indicates that the phase center locations of the E- and H-planes will not coincide with each other.

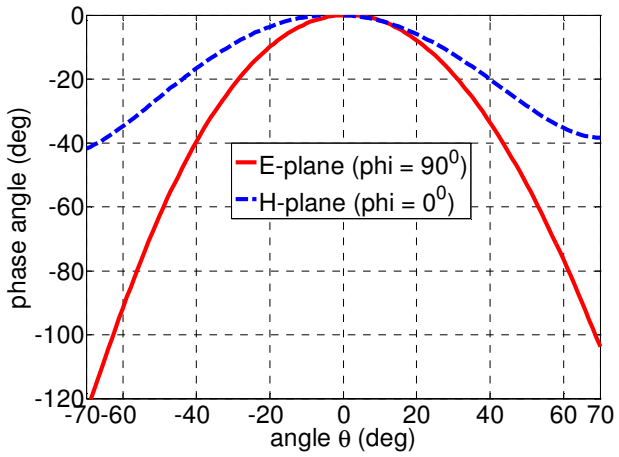

Fig. 5.6 Phase variations of the bent microstrip dipole with a single dipole-reflector feed within θ = 70^0, when the co-ordinate origin is 57 mm from the co-axial feed point.

To find the phase center location of the feed, the phase variations of the E- and H-planes are varied for optimized case by changing its location on the Z axis. As the phase variations are different for the E- and H-planes, the phase center locations are also different for each plane and the optimum phase variations of the E- and H-planes will be the combined phase center location of the antenna. Fig. 5.7 shows the E-plane, H-plane and combined phase center locations for the bent microstrip dipole antenna with one dipole-reflector, which are indicated as d_E, d_H and d_C respectively. In this figure, d = 0 means the phase center location is 57 mm away from the co-axial feed point. The E- and H-plane phase centers vary with aperture angle. However, the E-plane phase center location is further away from the H-plane phase center location, indicating that the phase variation is higher for the former. The combined phase center location is 28 mm from d=0 point at 90^0, compared to 30 mm at 71^0, which indicates higher phase variations at higher aperture angles.

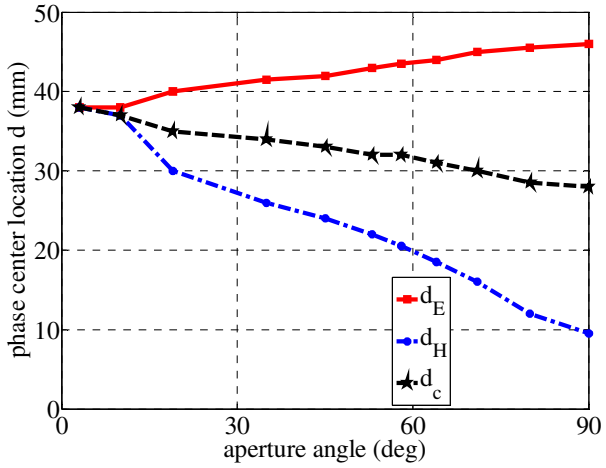

Fig. 5.7 Phase center locations of bent microstrip dipole with a single dipole-reflector feed; d = 0 is located at 57 mm away from the feed point.

5.2.4 Experimental Verification of the Bent Dipole Feed

To verify the simulated results presented in the previous section, the feed antenna was fabricated and tested at the University of Manitoba Antenna Laboratory with a 36 x 65 mm^2 substrate with ε_r = 2.5, loss tangent (tan δ) = 0.002 and thickness t = 1.58 mm. All other parameters are selected based on simulation design. Figs. 5.8 (a) and (b) show the top and bottom view of the fabricated antenna.

Fig. 5.9 shows the measured and simulated S_{11} of the antenna. The measured -10 dB S_{11} bandwidth is from 2.99 GHz to 3.08 GHz that means the impedance bandwidth is 2.98%. Thus there is a good agreement between simulated and measured bandwidth. However, there is a slight difference between the simulated and measured matching of the antenna. This is due to the fabrication tolerances of the antenna as the dipole angle is very sensitive to the matching of the antenna.

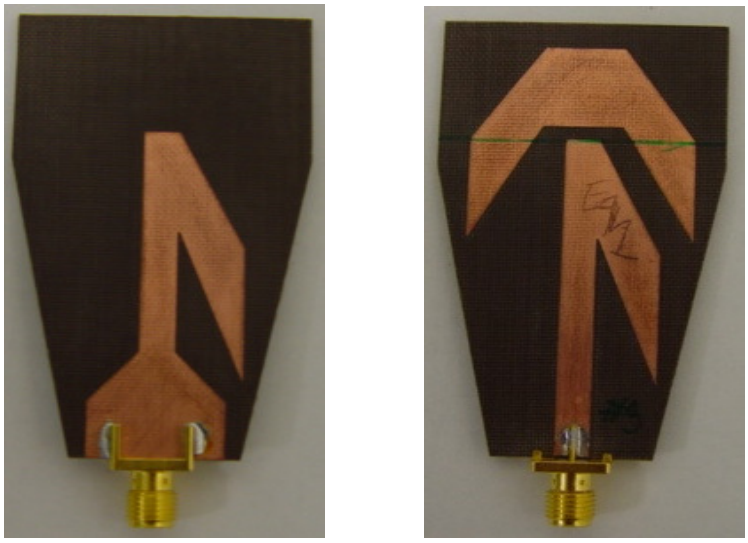

(a) (b)

Fig. 5.8 The fabricated bent microstrip dipole with a single dipole-reflector antenna; (a) top view, (b) bottom view.

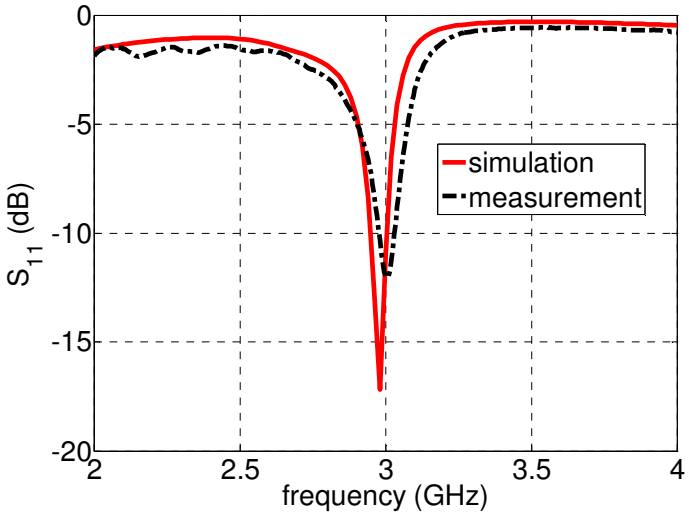

Fig. 5.9 The simulated and measured S_{11} of the bent microstrip dipole with a single dipole-reflector feed.

The measured results for the E- and H-plane radiation patterns of the feed have not been included because of the back radiation properties of the feed.

5.2.4.1 Bent Dipole Feed With a Reflector

The feed antenna was also measured with the 45 cm reflector of f/D = 0.25, available in the laboratory. The measurement setup is same as described in 4.2.6.2. The gain patterns of the feed antenna is shown in the Fig. 5.10, where the solid line shows the original gain case and the dashed line shows the best fit case. The gain is increasing with frequency from 2.5 GHz to 3 GHz and then decreasing thereafter. This is because of the antenna impedance matched characteristics.

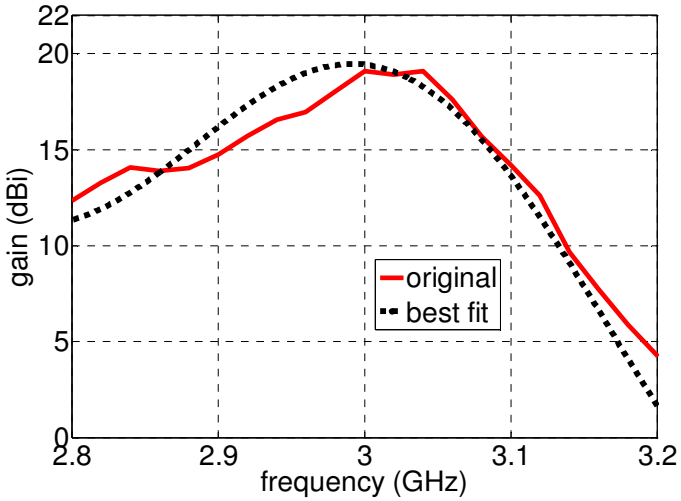

Fig. 5.10 Measured gain of the 45 cm reflector with the bent microstrip dipole with a single dipole-reflector feed at different frequencies.

The radiation patterns of the modified feed antenna with reflector are shown in Fig. 5.11. The figure shows that at 3 GHz, the gain of the antenna is 19.1 dBi with slightly unequal radiation patterns. The E- and H-plane radiation patterns of the reflector-feed should be equal as they were equal in the feed patterns. The main reason for unequal E- and H-plane radiation patterns is due the unequal patterns after 58^0 in the feed antenna.

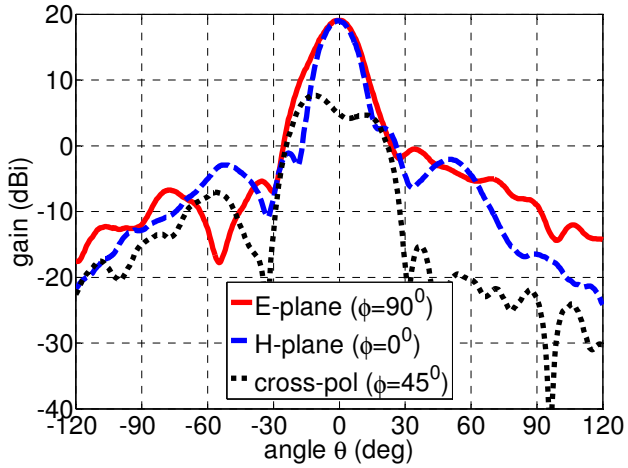

Fig. 5.11 Gain of the bent microstrip dipole feed with a single dipole-reflector with the 45 cm reflector.

Fig. 5.12 shows the S_{11} of the bent microstrip dipole feed with the reflector antenna. The figure shows that the feed with reflector is matched at 3 GHz. The impedance bandwidth of the reflector-feed at -10 dB point is from 3 GHz to 3.05 GHz. So the bandwidth is 1.7% which is very narrow. At 3 GHz, S_{11} is -10 dB, which corresponds to 0.46 dB mismatch loss.

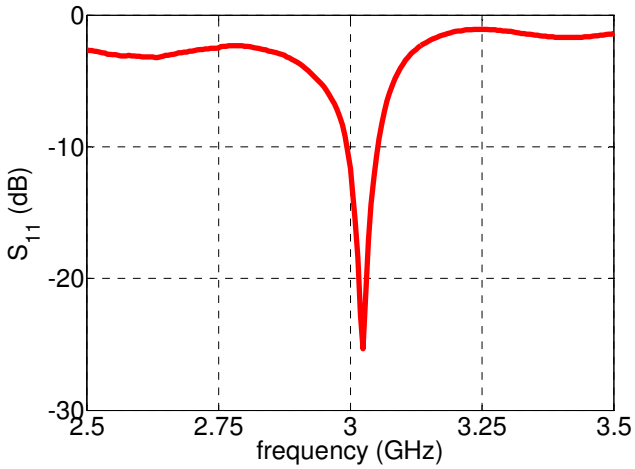

Fig. 5.12 The measured S_{11} of the bent microstrip dipole feed on the 45 cm reflector.

The co-axial cable loss is 0.2 dB, which is the same as previous cases. Therefore, the overall gain of the antenna is 19.76 dBi and the efficiency of the antenna is 52% at 3 GHz.

5.3 Bent Arms with Double Dipole-Reflectors

Bent Microstrip dipole with a single dipole-reflector equalized the E- and H-plane radiation patterns. However, the E- and H-plane radiation patterns were not equal after 58^0 and back lobe level of the antenna was 8 dB, which is high. Therefore, the feed-reflector radiation patterns were not equal. Hence, it is necessary to improve the radiation patterns by improving front to back ratio of the antenna.

5.3.1 Double Dipole-Reflectors Feed Design

To achieve good radiation characteristics with good front to back ratio, an additional dipole-reflector was introduced with the previous antenna configuration. This dipole-reflector acts as an additional reflector for the previous antenna configuration and therefore, the antenna will be more directive towards the Z direction, and hence the radiation patterns and front to back ratio of the antenna will be improved.

Fig. 5.13 shows the bend microstrip dipole with double dipole-reflectors. The feed is operating at 3 GHz and is printed on a substrate of length L = 80 mm, width W = 50 mm, dielectric constant $\varepsilon_r = 2.5$, loss tangent ($\tan \delta$) = 0.002 and thickness t = 1.58 mm with metallization on both sides. Antenna configuration is the same as the single dipole-reflector case except a second dipole-reflector is added with the structure. The second

dipole-reflector parameters are listed as R_{L21} = 15 mm, R_{L22} = 10 mm, R_{W21} = 12 mm, R_{W22} = 15 mm after several simulation. The distance between first and second dipole-reflector D_{DR2} is 2 mm. This distance is selected after some iteration based on optimum results in terms of radiation patterns. The second dipole-reflector is slightly bent to the positive Z axis. This will improve the radiation characteristics of the antenna over that of the straight case. All other parameters are the same as the single dipole-reflector case.

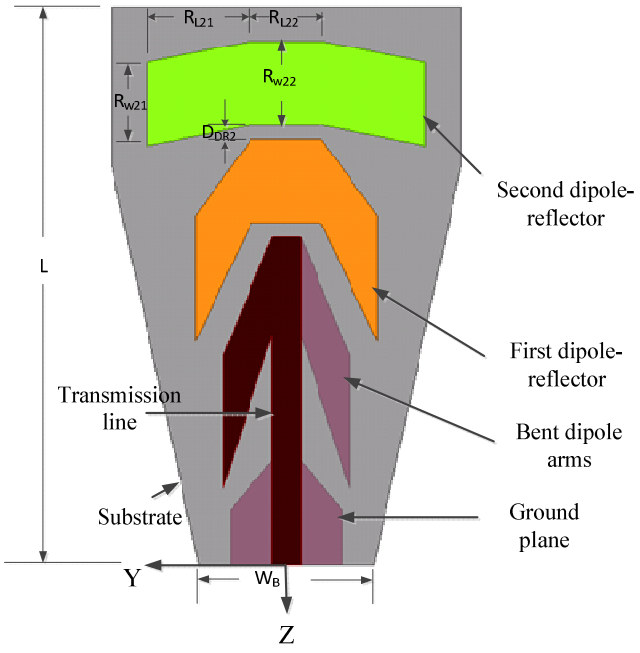

Fig. 5.13 The The geometry of the bent microstrip dipole with double dipole-reflectors; L = 80 mm, w = 50 mm, t = 1.58 mm, ε_r = 2.5.

The feed antenna is designed and simulated by Ansoft HFSS ver. 14 and the simulated S_{11} of the feed is shown in Fig. 5.14. It is observed that -10 dB S_{11} bandwidth is from 2.99 GHz to 3.08 GHz. Therefore, the impedance bandwidth of the antenna is 2.97 %, which is low compare to straight microstrip dipole antenna. The reason for low

S_{11} of the antenna is the bent arms, which affects the impedance characteristics of the antenna.

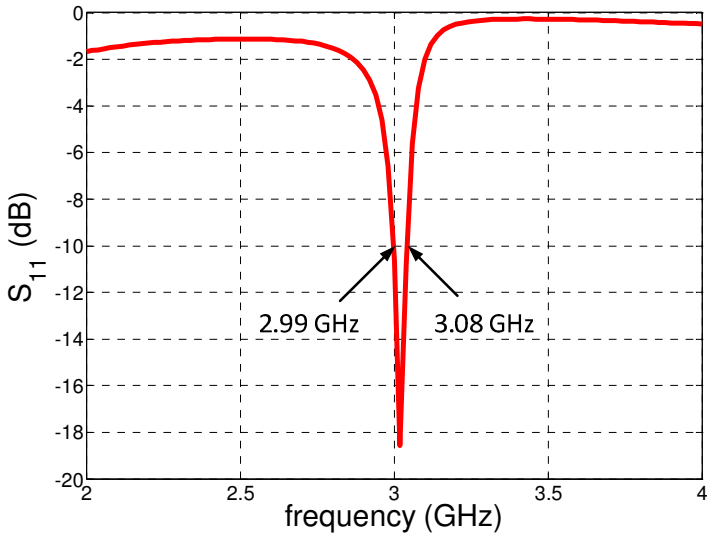

Fig. 5.14 Simulated S_{11} of the bent microstrip dipole with double dipole-reflectors feed.

The simulated radiation patterns of the feed antenna are shown in Fig. 5.15 for three different frequencies. The E- and H-plane radiation patterns at 3 GHz are almost symmetric with respect to the axis with equal pattern up to 71^0, which corresponds to f/D = 0.35. The back lobe level of the antenna is -17.5 dB, which is lower than previous (single dipole-reflector) case. The cross-polarization level of the antenna is -15 dB at $(0 \leq \theta < 90^0)$. It is also observed that E- and H-plane radiation patterns are not equal and also not symmetric to the Z-axis at the lower (2.9 GHz) and higher (3.1 GHz) frequencies. This indicates that the dipole arms are frequency sensitive to the bent angle.

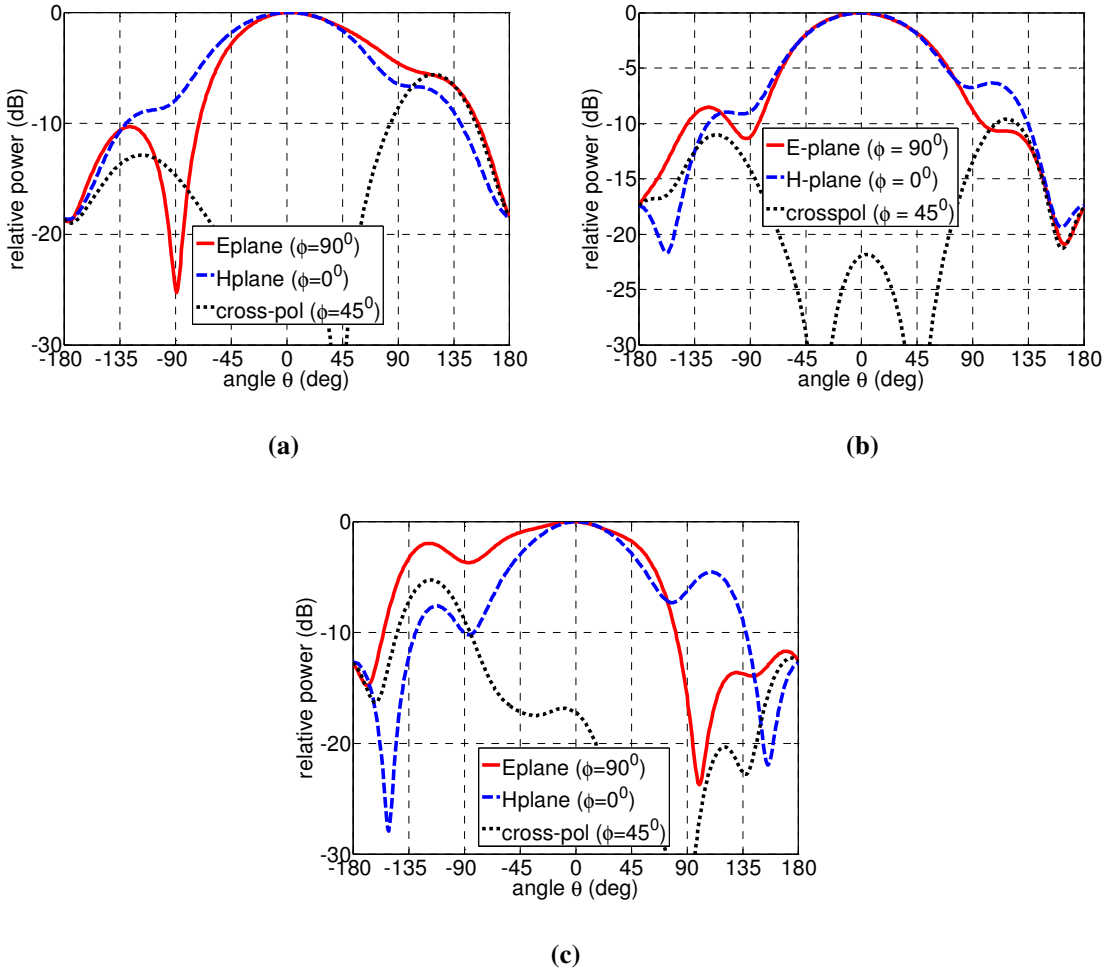

Fig. 5.15 Simulated radiation patterns of the bent microstrip dipole feed with double dipole-reflectors at different frequencies; (a) 2.9 GHz, (b) 3 GHz. (c) 3.1 GHz.

5.3.2 Performance of the Double Dipole-Reflectors Feed

The performance in terms of the spillover efficiency, the illumination efficiency and the gain factor of the bent microstrip dipole with double dipole-reflectors feed is shown in Table 5.3, for various f/D cases. The illumination efficiency is increased and the spillover efficiency is decreased with increasing the aperture angle. The gain factor of the feed is 62.3 % at 76^0 aperture angle or f/D = 0.32.

Table 5.3 Spillover, illumination and gain factor of the bent microstrip dipole with double dipole-reflectors feed antenna for various f/D or aperture angle at 3 GHz.

f/D	Aperture Angle	Spillover efficiency	Illumination efficiency	Gain factor
0.30	80^0	75.6 %	86.8 %	61.9 %
0.31	78^0	74.3 %	88 %	62.2 %
0.32	76^0	72.9%	89.1 %	62.3 %
0.33	74^0	71.5%	90.2 %	62.2 %
0.35	71^0	69.2 %	91.8 %	61.7 %

5.3.3 Phase Center of the Double Dipole-Reflectors Feed

The radiations of this feed are also in the Z-direction and therefore, the phase center location is also in the Z-axis. To find the phase center location of the feed, its phase distribution is important to know. Fig. 5.16 shows the phase variation of the feed antenna within 70^0 angle, with respect to a point 57 mm from the coaxial feed point, which is located at the dipole arms. The figure shows that the E-plane phase variation is not symmetric to the axis and is higher than the H-plane phase variation, which is symmetric to the axis. This indicates that the phase center locations for the E- and H-planes do not coincide with each other.

To find the phase center location of the feed, the phase variations of the E- and H-planes are varied by changing its location on the Z axis. As the phase variations are different for the E- and H-plane, the phase center locations are also different for each plane and the optimum phase variation of the E- and H-planes will be the combined phase center location of the antenna.

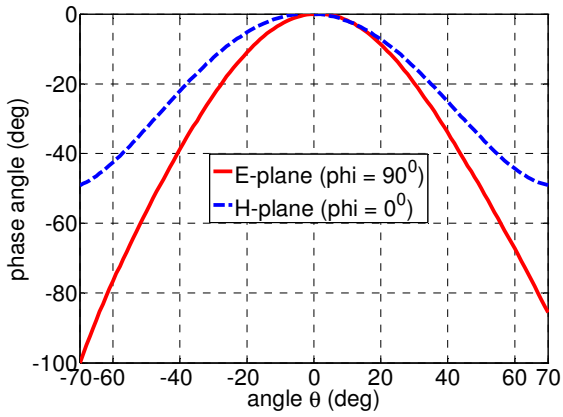

Fig. 5.16 Phase patterns of the bent microstrip dipole feed with double dipole-reflectors feed within θ = 70^0, when the co-ordinate origin is 57 mm from the co-axial feed point.

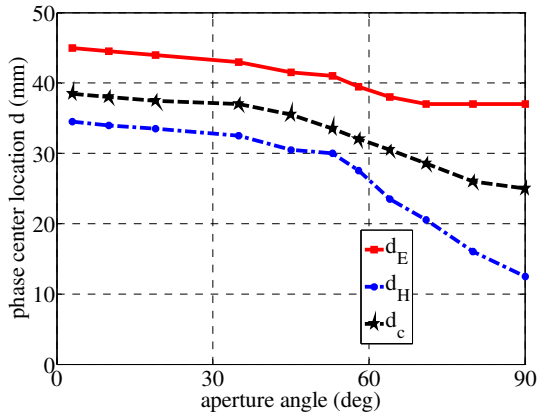

Fig. 5.17 Phase center location of a bent microstrip dipole with double dipole-reflectors; d = 0 is located at 57 mm from feed point.

Fig. 5.17 shows the E-plane, H-plane and combined phase center locations for the bent microstrip dipole antenna with double dipole-reflectors, which are indicated as d_E, d_H and d_C respectively. In this figure, d = 0 means the phase center location is 57 mm away from the feed point. The E- and H-plane phase center varies with aperture angle. However, the E-plane phase center location is further away from the H-plane phase center location indicating that the phase variation is higher for the former. The combined

phase center location is 26 mm from d = 0 point at 90^0, compare to 30 mm at 71^0, which indicates higher phase variations at higher aperture angle.

5.3.4 Experimental Verification of the Feed

To verify the simulated results presented in the previous section, the feed antenna was fabricated and tested at the University of Manitoba antenna laboratory. The dimension of the fabricated double dipole-reflectors feed antenna substrate was 50 x 80 mm^2 with ε_r = 2.5, loss tangent (tan δ) = 0.002 and thickness h = 1.58 mm. All other parameters are selected based on simulation process. Figs. 5.18 (a) and (b) shows the top and bottom views of the fabricated antenna.

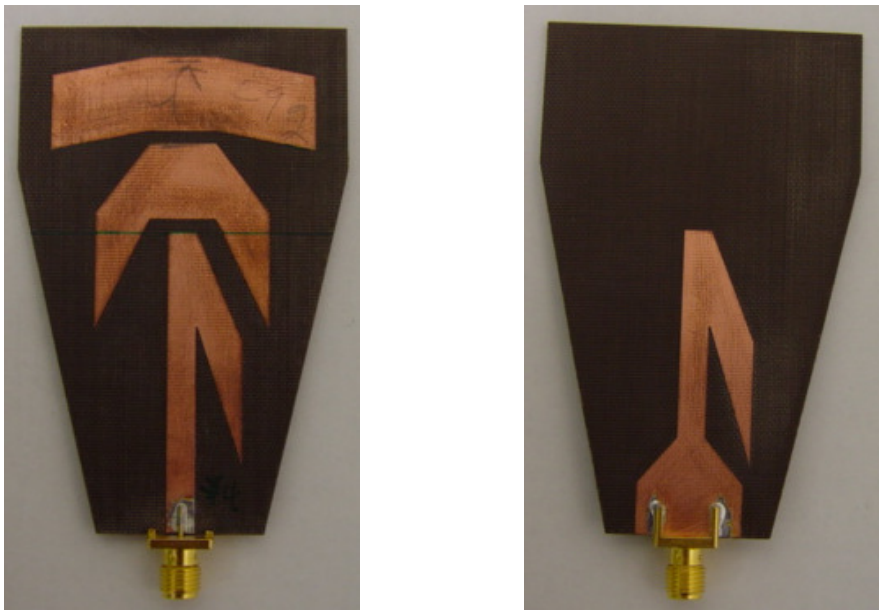

(a) **(b)**

Fig. 5.18 The fabricated bent microstrip dipole with double dipole-reflectors feed; (a) top view, (b) bottom view.

Fig. 5.19 shows the measured and simulated S_{11} of the antenna. The measured -10 dB S_{11} is from 3.05 GHz to 3.12 GHz that means the impedance bandwidth is 2.26%. Thus there is a good agreement between the simulated and measured bandwidths. However, there is slight difference between the simulation and measurement matching of the antenna. This is due to the fabrication tolerance of the antenna as the matching is very sensitive to the dipole angle.

The measured results for the E- and H-plane radiation patterns of the feed have not been included because of the back radiation properties of the feed.

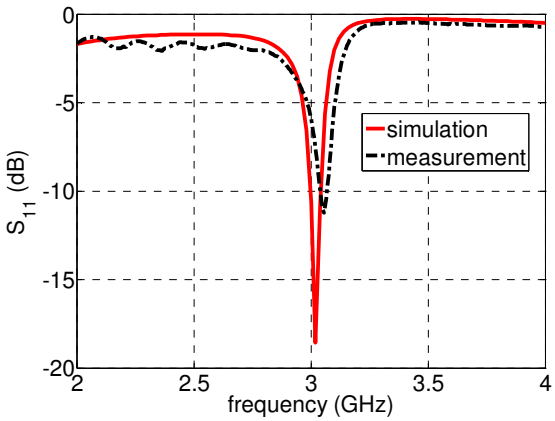

Fig. 5.19 The S_{11} of the bent microstrip dipole with double dipole-reflectors feed.

5.3.4.1 Double Dipole-Reflectors Feed Performance with Reflector

The feed antenna is also measured with the 45 cm reflector of f/D = 0.25 available in the laboratory. The measurement setup is the same as described in 4.2.6.2. The gain pattern of the feed antenna is shown in the Fig. 5.20, where the solid line shows the measured gain and the dashed line shows the best fit case. The gain is increasing with frequency from 2.5 GHz to 3 GHz and thereafter decreasing. This is because the antenna is matched within a narrow frequency band.

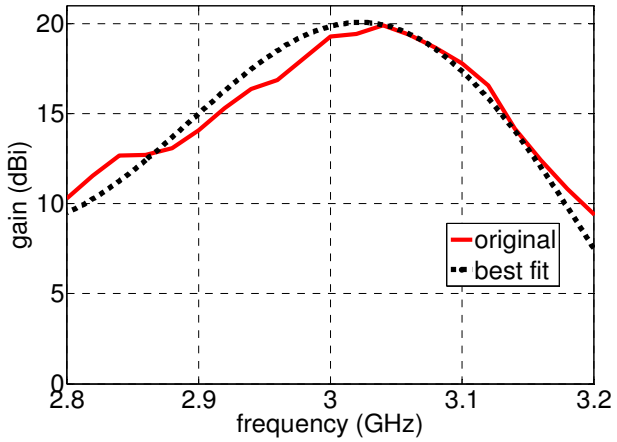

Fig. 5.20 Measured gain of the 45 cm reflector with the dipole with two dipole-reflectors feed at different frequencies.

The radiation patterns of the feed antenna with reflector are shown in Fig. 5.21. The figure shows that at 3.04 GHz, the gain of the antenna is 19.9 dBi, which is almost the same as the microstrip dipole case. The E- and H-plane radiation patterns of the reflector-feed are more equal than the previous case. This is because of the symmetric nature of the feed antenna.

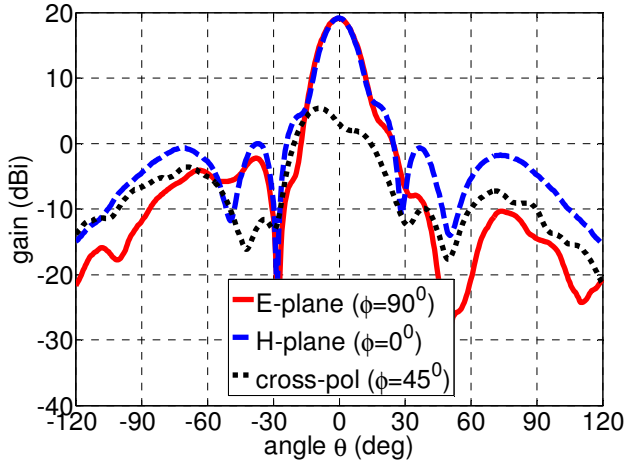

Fig. 5.21 Measured radiation patterns of the 45 cm reflector with the bent microstrip dipole with double dipole-reflectors feed at 3.04 GHz.

Fig. 5.22 shows the S_{11} of the feed with the reflector. The figure shows that the reflector-feed is matched with 3 GHz frequency band. The impedance bandwidth of the reflector-feed at -10 dB point is from 3 GHz to 3.08 GHz. Thus the bandwidth is 2.63%.

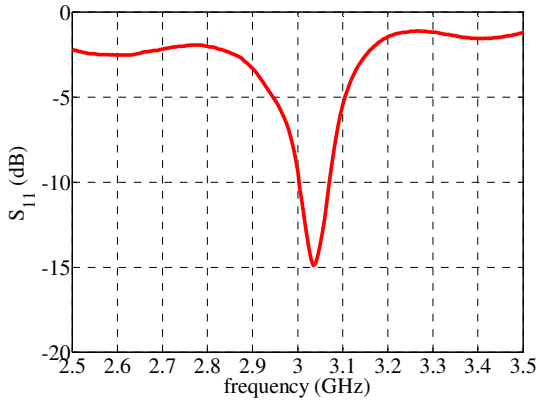

Fig. 5.22 Measured S_{11} of the bent micostrip dipole with double dipole-reflectors feed on the 45 cm reflector.

At 3.04 GHz, S_{11} is -12.1 dB, which corresponds to 0.28 dB mismatch loss. The co-axial cable loss is 0.2 dB, which is the same as previous cases. Therefore, the overall gain of the antenna is 20.4 dBi and the gain factor of the antenna is 55% at 3.04 GHz.

5.4 Corrugated Microstrip Dipole Feed

We already know that microstrip dipole antennas have wider H-plane radiation pattern than the E-plane radiation pattern. Therefore for pattern equalization, it is necessary to decrease the beamwidth of the H-plane radiation pattern faster than the E-plane pattern, so that both beamwidths can become equal. In the previous section, we designed a feed antenna where E- and H-plane radiation patterns were equal. However, its input impedance bandwidth was very narrow. Therefore, improving the input

impedance and retaining the pattern equalization is a challenge and in the following section we will design a feed antenna with these characteristics.

5.4.1 Corrugated Microstrip Dipole Feed Design

Fig. 5.23 shows the layout of the corrugated microstrip dipole feed antenna [89]. The antenna is operating at 3 GHz and is printed on a substrate with a dielectric constant of ε_r = 2.5, loss tangent (tan δ) = 0.002 and thickness t = 1.58 mm, with metallization on both sides. The feed antenna is designed as the same way as it was presented in the previous chapter except the dipole arms are loaded with orthogonal stubs. Therefore, the dipole with these orthogonal stubs can be called as corrugated microstrip dipole feed antenna.

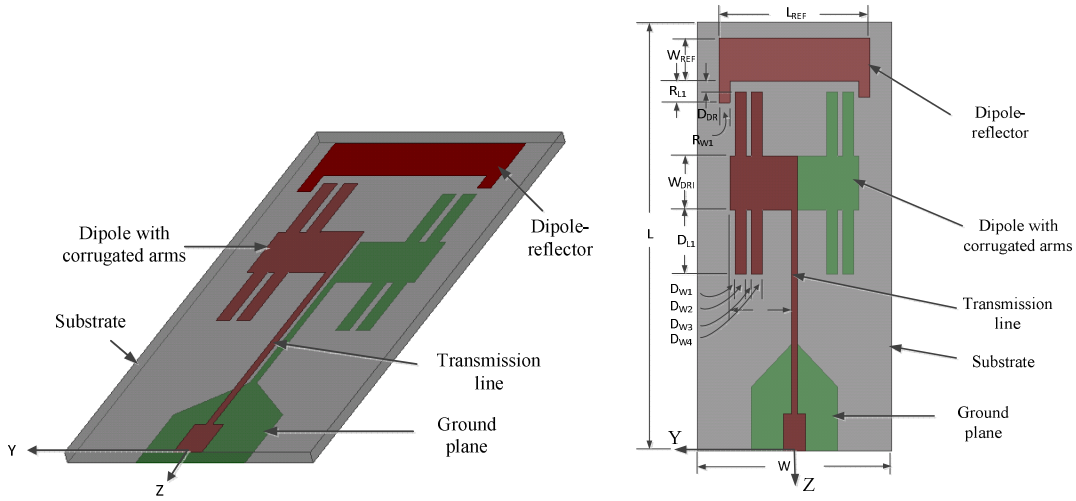

(a) **(b)**

Fig. 5.23 The geometry of the corrugated microstrip dipole feed antenna, (a) 3-D view, (b) top view.

Initially, the length of the dipole arm is set as the quarter wavelength at the operating frequency. Since the dipole is loaded with two orthogonal stubs, the horizontal length of the dipole arm is shortened and adjusted at the operating frequency. This length also

depends on the length of the stubs. If the length of the stubs is large, then the length of the corrugated dipole arm will be small.

The length of the dipole-reflector is slightly larger than the total length of the corrugated dipole arms and its width is set the same as the previous cases. The dipole-reflector is extended vertically on each side to improve the back radiation characteristic of the feed. The gap between the dipole arms and dipole-reflector is optimized for good input impedance and radiation characteristics of the feed antenna.

Table 5.4 Corrugated microstrip dipole feed antenna dimensions (units: mm)

L	80	L_{DRI}	24	L_{FEED}	45
W	36	W_{DRI}	10	L_1	7
L_{REF}	28	D_{L1}	12	L_2	12
W_{REF}	8	D_{w1}	1	L_3	20
R_{L1}	4	D_{w2}	2	W_{FEED1}	4.2
R_{w1}	2	D_{w3}	1	W_{FEED2}	1
D_{DR}	2	D_{w4}	2	W_{GP}	16

The initial design parameters of the antenna are given in Table 5.4, which were selected after several iterations. However, for pattern equalization the most sensitive parameters were found to be those of the corrugated dipole arms and therefore, were selected for the parametric study.

5.4.1.1 Effect of the Loaded stubs

As mention earlier, orthogonal stubs were added to the original dipole arms, to shape its radiations. Therefore, it is important to know the number of stubs and their dimensions as well as locations, for pattern equalization. Fig. 5.24 (a) shows the effects of varying

number of stubs. For all three cases S_{11} is below -10 dB line, but the bandwidth is widest for the two stub case. Fig. 5.24 (b) shows the radiation patterns for three different cases. For all cases the E- and H-plane radiation patterns are almost identical, but -10 dB beamwidth increases with the increase of the number of stubs from 1 to 2, but are almost the same for 2 and 3 stub cases. However, the back lobe level is lowest at -26 dB for the three stub case.

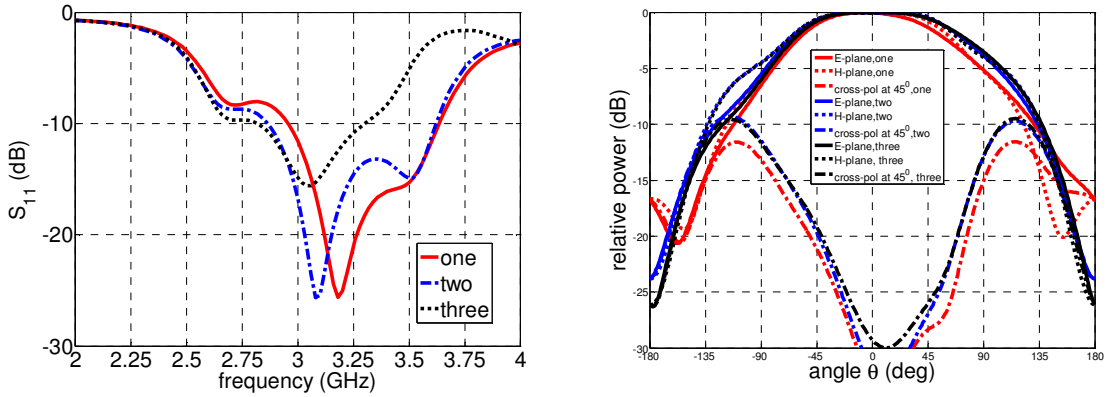

(a) **(b)**

Fig. 5.24 The Effects of changing the number of stubs. (a) S_{11}, (b) radiation patterns at 3 GHz.

The stub length D_{L1} is the most important parameter for pattern equalization. The length of the original dipole arms is 20 mm. However, as D_{L1} is increased, the total length of the corrugated dipole arms is reduced to 12 mm. The gap between adjacent stubs is important for input impedance characteristics of the feed, although it does not affect the radiation characteristics of the feed. If the gap is large, the feed matching becomes weak. Therefore, the gap is selected as 1 mm. Fig. 5.25 (a) shows the effect of varying D_{L1}, on its S_{11}. By varying D_{L1} from 10 to 14 mm, the lower limit of the S_{11} at -10 dB point is decreased from 3 to 2.75 GHz. This is because, as the stub length increases, the overall

dipole length are increased, which ultimately decreased the S_{11} of the antenna. Fig. 5.25 (b) shows the radiation patterns for these cases. At D_{L1} = 10 mm, the radiation patterns are almost identical, but the back lobe level is -11 dB, which is high. The cross-polarization level for this case is low compare to the other cases. At D_{L1} = 12 mm, the radiation patterns are also almost the same, but the back lobe level is decreased to -23.8 dB, which is the lowest. The cross-polarization level of this case is still satisfactory. When D_{L1} =14 mm, the radiation patterns deteriorate, with high back lobe level, and high cross-polarization.

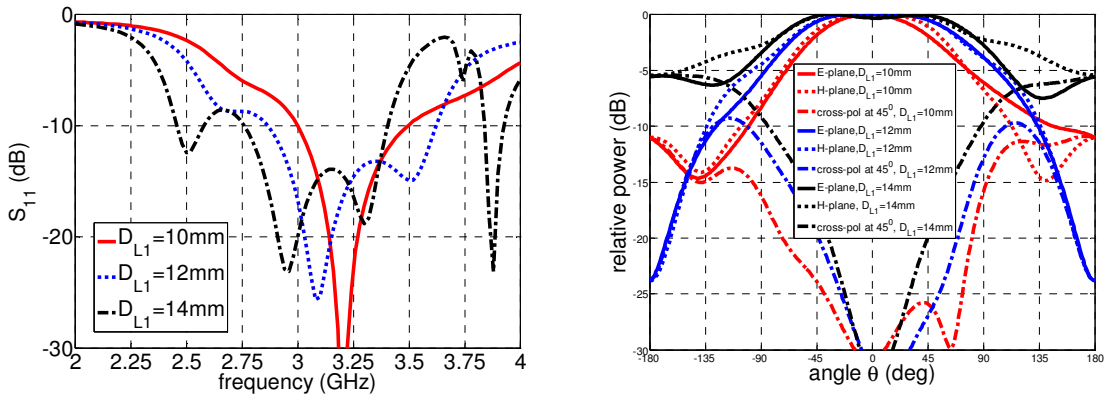

(a) **(b)**

Fig. 5.25 The Effects of changing the stub length D_{L1}. (a) S_{11}, (b) radiation patterns at 3 GHz.

5.4.1.2 Simulation Results of the Corrugated Dipole Feed

The feed antenna is designed and simulated by Ansoft HFSS ver. 14. The antenna parameters are optimized and selected as R_{L1} = 4 mm, R_{L2} = 3 mm, R_{W1} = 2 mm, R_{W2} = 2 mm, D_{L1} = 12 mm, D_{W1} = D_{W3} = 1 mm, D_{W2} = D_{W4} = 2 mm. All other parameters are the same as the microstrip dipole case and also shown in Table 5.4, which were already mentioned.

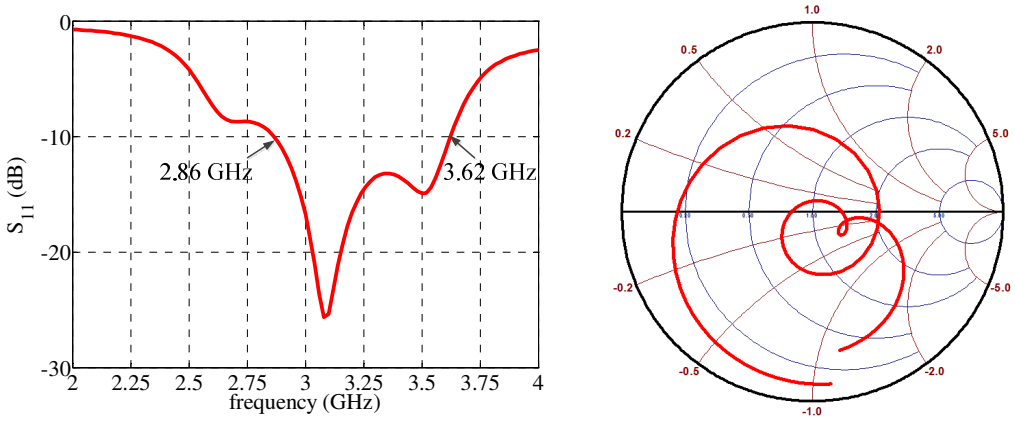

(a) **(b)**

Fig. 5.26 Simulated S_{11} and Smith chart of the corrugated microstrip dipole feed antenna. (a) S_{11}, (b) Smith chart.

The simulated S_{11} of the feed antenna is shown in Fig. 5.26 (a). It is observed that -10 dB S_{11} bandwidth is from 2.86 GHz to 3.62 GHz. Therefore, the impedance bandwidth of the antenna is 23.46%, which is wider than that of the bent microstrip dipole case. Its Smith chart is shown in Fig. 5.26 (b), where it shows that the impedance loop is around 50 Ω circle, indicating a wider bandwidth of the antenna. The reason for wider impedance bandwidth of the antenna is that dipole arms have less effect on the impedance characteristics of the antenna.

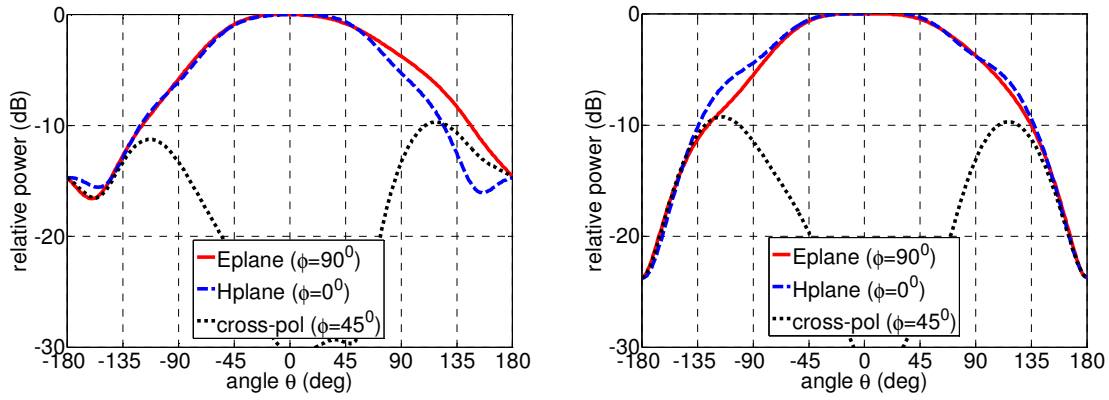

(a) **(b)**

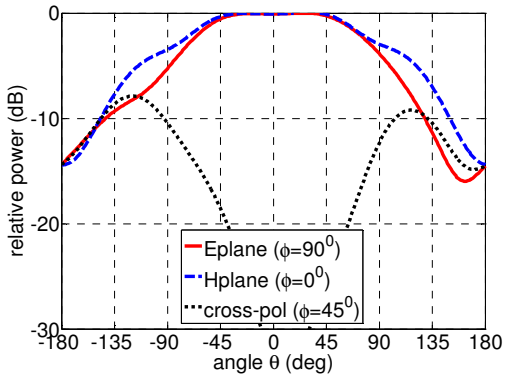

(c)

Fig. 5.27 The radiation patterns of the corrugated microstrip dipole feed antenna at different frequencies. (a) 2.9 GHz, (b) 3.0 GHz, (c) 3.1 GHz.

The simulated radiation patterns of the feed antenna at 3 GHz are shown in Fig. 5.27 for different planes. The patterns show that the E- and H-plane patterns are almost symmetric. The beamwidths of the feed antenna at -10 dB are both 270^0. The cross-polarization level at 45^0 plane of the antenna is -13 dB ($0^0 < \theta \leq 90^0$) and is the same as previous cases. The back lobe level of the antenna is -24 dB, which is lower than the previous cases. This low back lobe level will decrease the spillover loss, and increase the spillover efficiency.

Fig. 5.28 shows the surface current distributions of the antenna at 3 GHz frequency. As can be seen from current distributions, strong currents exist at the feed line and also at the edge of the dipole arms. There is also strong current at the edges of the dipole-reflector, which is in the opposite direction to the current in the dipole arms, indicating the phase reversal at the radiating edge of the dipole-reflector.

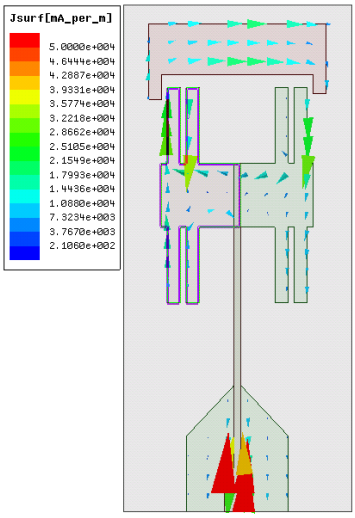

Fig. 5.28 Surface current distribution of the corrugated microstrip dipole feed antenna at 3 GHz.

The corrugated microstrip dipole feed antenna has more metallization on each side of the substrate than the original microstip dipole feed antenna. Therefore, the dielectric loss and copper loss of the antenna are needed to determine, as they affect the radiation efficiency of the antenna. Table 5.5 summarize the results for different cases. The radiation efficiency associated with the conductor loss is only 0.3% and dielectric loss only 1% (loss tangent (tan δ) = 0.002) and the total conductor and dielectric losses are 1.9%. Therefore, the losses associated with the conductor and dielectrics are not significant for the corrugated microstrip dipole feed antenna.

Table 5.5 Different output power and radiation efficiency of the corrugated microstrip dipole feed antenna at 3 GHz.

	Input power	Reflected power	Accepted power	Radiated power	Radiation efficiency
Perfect Conductor, Perfect dielectric	100%	2.1%	97.9%	97.9%	100%
Perfect Conductor, lossy dielectric	100%	2.6%	97.4%	96.4%	99%
Copper Conductor, Perfect dielectric	100%	1.8%	98.2%	97.9%	99.7%
Copper Conductor, lossy dielectric	100%	1.7%	98.3%	96.5%	98.2%

where, radiation efficiency = radiated power/accepted power.

5.4.2 Performance of the Corrugated Dipole Feed

The performances in terms of spillover efficiency, illumination efficiency and gain factor of the feed are shown in Table 5.6 for various f/D cases. The gain factor of the feed increases by the increasing of the reflector aperture angle up to a highest point, where it is maximum and after that point the gain factor is decreasing again. The maximum gain factor is found to be at $\theta_0 = 92^0$ aperture angle, indicating that the feed is suitable for deep reflectors.

Table 5.6 Spillover, illumination and gain factor of the corrugated microstrip dipole feed antenna for various f/D or aperture angle at 3 GHz.

f/D	Aperture Angle	Spillover efficiency	Illumination efficiency	Gain factor
0.21	100^0	86.7%	81.8%	67.9 %
0.23	95^0	83.7%	85.1%	68.8 %
0.24	92^0	81.6%	86.8%	68.9 %
0.25	90^0	80.2%	88.0%	68.7 %
0.30	80^0	72.2%	92.7%	65.3 %

Table 5.7 Performance of the corrugated microstrip dipole feed for three different frequencies; all parameters are shown in section 5.4.1.2.

Frequency	2.9 GHz	3.0 GHz	3.1 GHz
θ_0	92^0	92^0	94^0
η_s	83.2 %	81.6 %	80.2 %
η_i	85.1 %	86.8 %	86.8%
η_g	68.3 %	68.9 %	67.6 %
d_c	56 mm	57 mm	59 mm

where,

θ_0 = aperture angle at which gain factor is maximum,
η_s = maximum spillover efficiency at θ_0,
η_i = maximum illumination efficiency at θ_0,
η_g = maximum gain factor at θ_0,
d_c = phase center location from feed point toward z-axis

The performance of the feed with two other frequencies is also investigated. Table 5.7 summaries the gain factor, the spillover, and the illumination efficiencies for three different frequencies at 2.9 GHz, 3 GHz and 3.1 GHz, respectively. The gain factors of these three different frequencies are found to be 68.3%, 68.9% and 67.6%, respectively, which are almost the same. Therefore, the feed parameters are very stable with frequency, in terms of the gain factor. The phase center location d_c for these frequencies are 56 mm, 57 mm and 59 mm, respectively, from the co-axial feed point, which confirms the phase center stability of the feed.

5.4.3 Phase Center of the Corrugated Dipole Feed

The phase center location of the corrugated dipole feed antenna is important to know as the phase center and reflector focal point coincide with each other. In the corrugated microstrip dipole antenna feed, radiations are in the Z-direction and therefore, the phase center location is also on the Z-axis. To find the phase center location of the feed, its phase distribution is required. The phase of the antenna is also changed with the angle θ in both cases, therefore more than one phase center locations may be found on this axis. Nevertheless, one location is selected where phase variations are small in the E-and H-planes. Fig. 5.29 shows the phase variations of the feed antenna within 70^0 angle, with respect to a point 57 mm from the coaxial feed point, which is located at the dipole arms. The figure shows that phase variation is not symmetric with respect to the axis and also it varies with the angle.

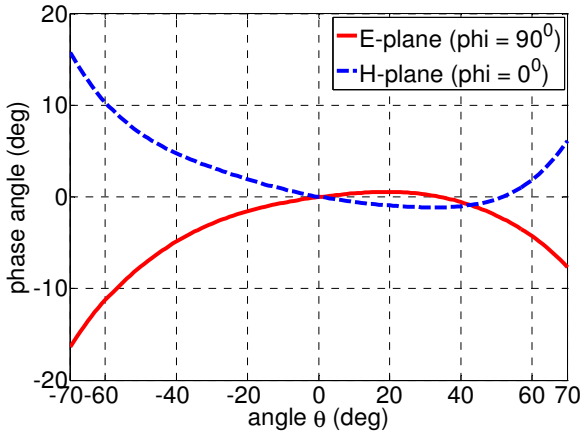

Fig. 5.29 Phase patterns of the corrugated microstrip dipole feed antenna for aperture angle of 70^0, when the co-ordinate origin is 57 mm from the co-axial feed point.

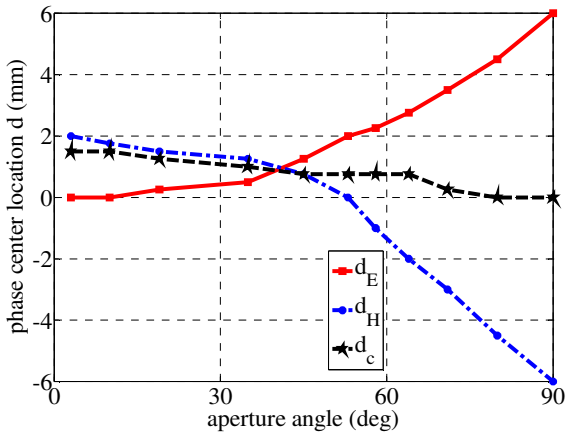

Fig. 5.30 Phase center locations of the corrugated microstrip dipole feed antenna; phase center location d=0 is located 57 mm from the coaxial feed point.

To find the phase center location of the feed, the phase variations in the E- and H-planes are examined, by changing the phase center location on the Z axis. By changing the locations back and forth, the phase center location is selected. Fig. 5.30 shows the E-plane, H-plane and combined phase center locations for the corrugated microstrip dipole antenna, which are indicated as d_E, d_H and d_C, respectively. In this figure, d = 0 means the

phase center location is 57 mm away from the co-axial feed point. The E- and H-plane phase center locations vary with the aperture angle. The combined phase center location is 0 mm from d = 0 point at 90^0, compared to 1 mm at 71^0.

5.4.4 Experimental Verification of the Corrugated Feed

To verify the simulated results presented in previous section, the feed antenna was fabricated and tested at the University of Manitoba antenna laboratory. The dimension of the fabricated antenna substrate was 36 x 80 mm^2 with ε_r = 2.5, loss tangent (tan δ) = 0.002 and thickness t = 1.58 mm. All other parameters are selected as the simulated antenna parameters. Figs. 5.31 (a) and (b) show the top and bottom views of the fabricated antenna.

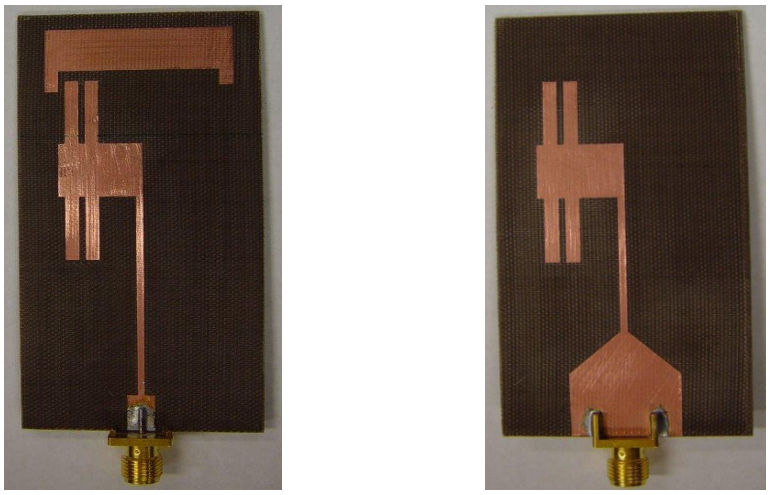

(a) **(b)**

Fig. 5.31 The fabricated corrugated micorstrip dipole feed antenna; (a) top view, (b) bottom view.

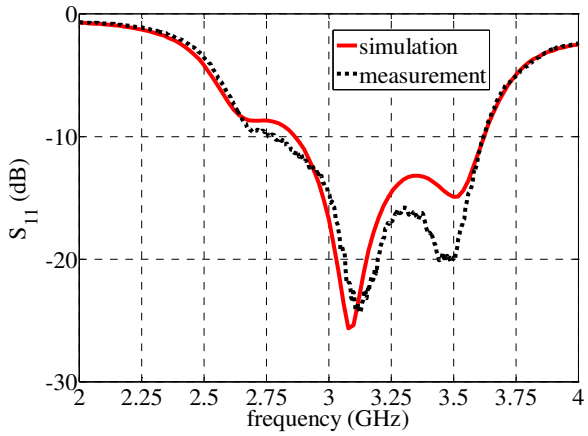

Fig. 5.32 The S_{11} of the corrugated microstrip dipole feed antenna.

Fig. 5.32 shows the measured and simulated S_{11} of the antenna. The measured -10 dB S_{11} bandwidth is from 2.75 GHz to 3.62 GHz that means the impedance bandwidth is 27.3%. The simulated impedance bandwidth of the antenna was 23.5%. Thus there is a good agreement between simulated and measured bandwidths. The measured results for the E- and H-plane radiation patterns of the feed have not been included because of the back radiation properties of the feed.

5.4.4.1 Corrugated Dipole Feed Performance with a Reflector

The feed antenna was also measured with the 45 cm reflector of f/D = 0.25, available in the laboratory. The measurement setup is same as described in 4.2.6.2. The gain pattern of the corrugated dipole feed is shown in the Fig. 5.33, where the solid line shows the measured gain and the dashed line shows the best fit case. The gain is increasing with frequency from 2.6 GHz to 3.2 GHz and then decreasing after that frequency. The figure shows that the maximum gain found at 3.06 GHz is 21.2 dBi, which is almost 1 dB higher than that of the microstrip dipole feed antenna of Fig. 4.19.

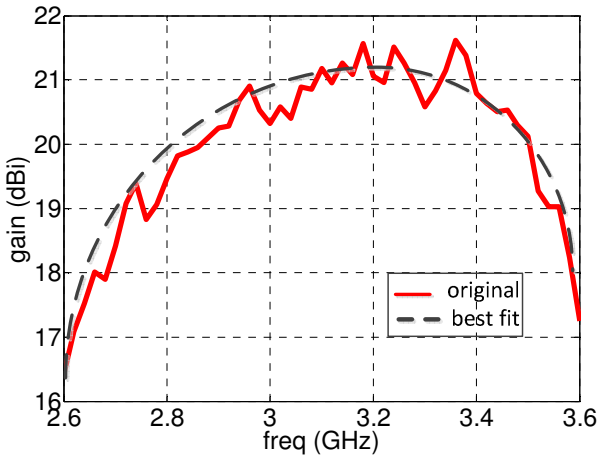

Fig. 5.33 Measured gain of the 45 cm reflector with the corrugated microstrip dipole feed antenna for different frequencies.

The radiation patterns of the reflector at 3.06 GHz are shown in Fig. 5.34. The E- and H-plane radiation patterns of the reflector-feed are almost equal. This is because of the symmetric nature of the feed antenna.

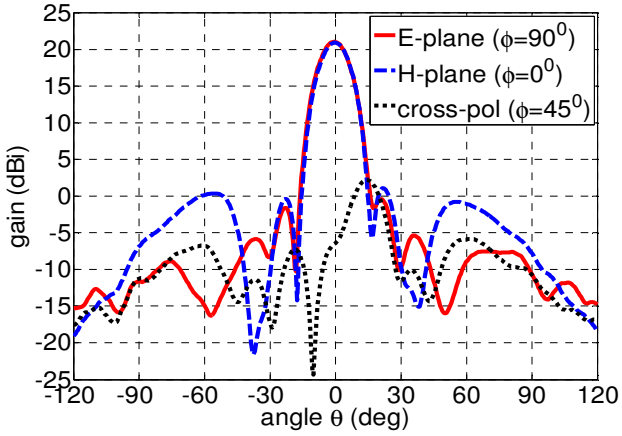

Fig. 5.34 Measured radiation patterns of the 45 cm reflector with the corrugated microstrp dipole feed antenna at 3.06 GHz.

Fig. 5.35 (a) and (b) show the measurement setup and S_{11} of the feed with reflector antenna. The figure shows that the reflector-feed is matched at 3 GHz. The impedance

bandwidth of the reflector-feed at -10 dB point is from 2.6 GHz to 3.52 GHz, i.e. 30%. At 3.06 GHz, S_{11} is -22.1 dB, which corresponds to 0.03 dB mismatch loss.

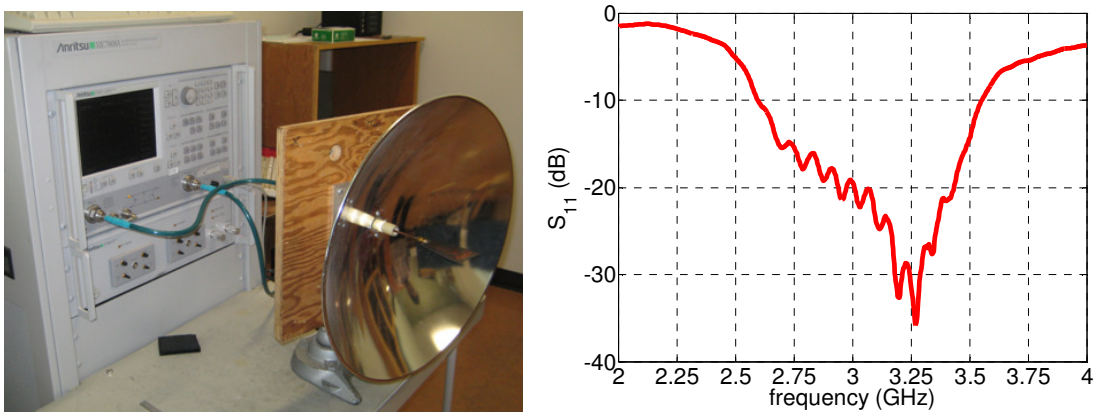

(a) Measurement setup **(b) S_{11}**

Fig. 5.35 Measured S_{11} of the corrugated microstrip dipole feed antenna on the 45 cm reflector.

The gain of the reflector is 21.2 dBi at 3.06 GHz, which includes the feed mismatch and external feed line losses. Excluding these losses the actual reflector gain increases to 21.4 dBi, which corresponds to an efficiency of 66.4%, at the feed input after the SMA connector. Table 5.8 shows the analysis of the reflector gain, and magnitude of various losses for different frequencies. The co-axial cable loss is 0.2 dB. The overall efficiency of the antenna is almost the same for all three frequencies.

Table 5.8 Measured gain, losses and efficiency of the corrugated micostrip dipole feed antenna with a 45 cm reflector at three different frequencies.

	2.9 GHz	3.06 GHz	3.3 GHz
Measured Gain	20.5 dBi	21.2 dBi	21.3 dBi
Mismatch Loss	0.04 dB	0.03dB	0.03 dB
Coaxial Cable Loss	0.2 dB	0.2 dB	0.2 dB
Gain at Feed Input	20.7 dBi	21.4 dBi	21.5 dBi
Antenna Efficiency	62.9%	66.4 %	58.4%

5.5 Summary

In this chapter, modified microstrip dipole feed antennas were designed to equalize the E- and H-plane radiation patterns. Two different techniques, bent micostrip dipole antenna and corrugated dipole antenna were used for this purpose. In the bent microstrip antenna, the dipole arms were bent to the direction of radiation, which changed the surface current distribution, affecting the radiation characteristics and making the pattern equal. The radiation patterns were equal up to 58^0. This antenna provided back lobe level of -8 dB, which was high. To improve the back lobe level, another dipole-reflector was added with the antenna retaining pattern equalization. The improved radiation patterns were equal up to 71^0 with back lobe level of -17.5 dB. In both cases, the efficiency of the antenna was almost the same as the micrsotrip dipole antenna case. The impedance bandwidths of these antennas were narrow and radiation patterns degraded after the center frequency. To improve the input impedance, while retaining pattern equalization, the corrugated microstrip dipole feed antenna was designed. This feed provided 23.5% impedance bandwidth, which was higher than the previous case, and the radiation patterns were equal up to 90^0. As a result, the gain factor of the antenna was improved in this case. The feeds were fabricated in the laboratory and measured with the 45 cm reflector of f/D = 0.25. The gain of the reflector was found to be 21.4 dBi, at 3.06 GHz and the efficiency of the antenna was 66.4%.

Chapter 6

Summary, Conclusions and Future Work

6.1 Summary and Conclusions

In this thesis, two new types of electrically small feeds, slotted circular waveguide feeds and microstrip dipole feeds, were designed and studied. For the slotted circular waveguide feeds, the primary objectives were to design feeds with smaller waveguide diameter (0.7 λ_0), with symmetrical E- and H-plane radiation patterns and improved gain factor. Two different types of slots, the E- and H-plane slots, were used at the open end of the waveguide. As the slots were etched on the waveguide wall, the overall dimensions of the feeds were not changed. To investigate the best possible slot size, slot width was varied and the feed performance was studied. For the E-plane slotted case, at fr = 10 GHz, the optimum results were found, when the slot width was 18 mm and height was 2 mm. In this case, the -10 dB beamwidth for both in E- and H-planes were found to be 158^0. The cross-polarization at 45^0 plane and back lobe levels were -26 dB and -12.9 dB, respectively. For the H-plane slot case, the optimum results were found, when the slot width was 18 mm and height was 4 mm. In this case, the -10 dB beamwidth for the E-

and H-planes were found 146^0. The cross-polarization at 45^0 plane and back lobe levels were -20 dB and -11.1 dB, respectively. The performance in terms of spillover efficiency, illumination efficiency and gain factor of the feeds was evaluated. The gain factor of the E-plane slotted feed was found to be 66.4%, at the aperture angle of 73^0, and for the H-plane slotted feed, it was 70.3% at the aperture angle of 67^0. The results showed the symmetrical radiation patterns with improved gain factor especially for the H-plane. The performance of the feeds with frequency variation, in terms of gain factor was also studied, and it was shown that the feeds had stable performance within a 10% frequency band. The phase center of the antennas was determined and showed that it was inside the waveguide with its location changing with the slot height. Therefore, using slots with the waveguide improved the radiation characteristics, and gain factor of the antenna. A sample feed with slot dimension of w = 18 mm, and h = 2 mm, was fabricated and evaluated in the antenna laboratory. The measured results showed good agreement with the simulation results.

Further improvement in terms of the gain factor was achieved using chokes with the slotted circular waveguide feeds. Slots in the waveguide wall equalized the E- and H-plane radiation patterns, while chokes reduced its cross-polarization and back lobe level. The E- and H-plane slotted feeds with a single choke was designed and simulated. It achieved symmetrical radiation patterns with low cross-polarization. The results showed that -10 dB beamwidths for both E- and H-planes of the E-plane slotted case reduced to 134^0 and for H-plane slotted cases reduced to 135^0. The cross-polarization and back lobe level for the E-plane slotted cases were -33.5 dB and -25.1 dB, respectively, and for the H-plane slotted case -22.4 dB and -13.3 dB, respectively. Therefore, the beamwidths, the

cross-polarization and back lobe levels were all decreased from previous case. As a result, the gain factor of the antenna was improved to 72.8% and 70.5%, respectively for the E- and H-plane slotted cases. The phase center of the antennas was also determined. For the E-plane slot case, it was found to be outside the waveguide aperture, and for the H-plane slot case, it was at the waveguide aperture. After evaluating the results, a feed antenna whose slot dimensions were w = 18 mm and h = 4 mm, and choke dimensions g_1 = 1 mm, ch = 7.5 mm, was fabricated and evaluated in the antenna laboratory, and measured results showed good agreement with the simulation results.

Slotted circular waveguide feeds with a cavity were also investigated. It equalized the E- and H-plane radiation patterns for wider beamwidths. The E- and H-plane slotted feeds with a cavity, whose dimension were ch = 17 mm, g_1 = 18.5 mm were designed and simulated. The -10 dB beamwidths of the E- and H-plane slotted case were 152^0 and 150^0 respectively. The cross-polarization and back lobe levels for the E-plane slotted case were -23.1 dB and -18.3 dB, respectively and for the H-plane slotted case were -27 dB and -16.1 dB, respectively. The feed produced sectorial shape radiation patterns which ultimately increased the beamwidths. The gain factor of the E-plane slotted feed was found to be 77.6% at an aperture angle of 68^0, and for the H-plane slotted case, it was 78.5%, at aperture angle 67^0. The phase center location of the feeds were also determined and showed that, it was 3 mm inside the waveguide aperture for the E-plane slotted case, and 1 mm inside the aperture for H-plane slot case. The back lobe level of the feeds was high. To improve the back lobe level, slotted circular waveguides with a choke in the cavity wall was designed and simulated. The -10 dB beamwidths of the E- and H-plane slotted case remained the same as the previous case. The back lobe level of the E- and H-

plane slotted cases also remained the same. The back lobe level of the E- and H-plane slotted feeds, with chokes in the cavity wall were -25 dB and -21.5 dB, respectively. Therefore, the feeds showed good radiation characteristics with improved back lobe levels.

The second part of the thesis investigated the design and performance of printed dipole feed. For this case the primary objective was to investigate and design a feed for backward radiation. This feature provided a feed with simple mounting mechanism on the reflector by eliminating the strut support. Therefore, microstrip feeds were studied not only for their light weight, but also for the ease of assembly on the reflector system. The feeds were designed on a substrate, based on classic Yagi-Uda antenna, where a dipole-reflector was used to provide the backward radiation (radiation toward feed line). The dipole-reflector, one of the dipole arms and one of the parallel transmission lines were on one side of the substrate. The other dipole arm, ground plane and other transmission line were on the other side of the substrate. The feed antenna was designed for 3 GHz frequency range and a parametric study was performed to investigate the effects of various input parameters on its input impedance and radiation patterns. The study showed that for the dipole arm, the length was important as it determined the operating frequency of the feed. At 3 GHz, the length was 22.1 mm. The dipole width was also important in a way that it affected the S_{11} of the antenna. The best result in terms of S_{11} was found when the width was 12 mm. The length of the dipole-reflector was slightly larger than the driver element. The width of the dipole-reflector was important as it affected the back lobe level of the feed. The length and widths of the dipole-reflector were selected as 45 mm and 10 mm, respectively. The length of the transmission line was set at 23 mm after

several iteration processes. The width of the transmission line was set at 4.2 mm to match with 50 Ω line. The ground plane was located on one side of the substrate, which was tapered / truncated shaped. The optimum size of the ground plane was set at 16 mm. The feed antenna was designed and simulated with a substrate with thickness of 1.58 mm, and $\varepsilon_r = 2.5$. The -10 dB S_{11} bandwidth of the feed was from 2.78 GHz to 3.26 GHz, which meant the impedance bandwidth of the antenna was 16.5%. The -10 dB beamwidth for the E- and H-planes were found to be 129^0 and 214^0, respectively. The cross-polarization at 45^0 plane and back lobe levels were at -11.4 dB and -20 dB, respectively. The phase center of the feed was determined to get optimized secondary patterns. It was found that the phase center location was 23 mm from the co-axial feed point toward the Z-axis. The performance of the feed antenna in terms of the gain factor, spillover and illumination efficiencies was also studied. The gain factor was around 65% at f/D = 0.25 or 90^0 aperture angle, which was reasonable efficiency in the desired range. The performance of the feeds, in terms of frequency was also studied, and shown that the feeds had stable performance within the frequency band. The feed was also fabricated in the laboratory and its S_{11} was measured with the network analyzer. The measured S_{11} was matched with the simulation results. The feed antenna was measured with a 45 cm reflector with f/D = 0.25, available in the laboratory. The gain of the reflector was found to be 20.2 dBi at 3.06 GHz. After adding all losses with the measured gain, its efficiency was calculated to be 55% and was found reasonable for a prime focus reflector.

The antenna bandwidth was improved by modifying the feed line width. The modified feed line width was 1 mm, at the dipole arm end. After improving the input impedance by modifying the feed line, the bandwidth increased to 29%, which was twice

that of the original one. The modified feed was designed and fabricated in the laboratory. The measured S_{11} of the antenna was matched with the simulation results. The feed antenna was then measured with the 45 cm reflector. The gain of the reflector was found to be 20.1 dBi at 3.08 GHz, corresponding to an efficiency of 53%.

The original microstrip dipole antenna showed asymmetric radiation patterns, especially in the E-plane. The pattern symmetry was achieved by using the unequal dipole arms. After some iteration, the length of the dipole arms was selected as 24.6 mm and 19.6 mm, respectively. The antenna was simulated and showed -2.4 dB improvements in the cross-polarization level at 45^0 plane. The effects of the substrate parameters were also studied. It showed that the S_{11} of the antenna depended on the substrate thickness t.

To miniaturize the microstrip dipole feed, two techniques were used: i) using slits at the dipole arms and ii) changing shapes of the dipole arms. Using a single slit in the dipole arm, about 11.17% size reduction was achieved. The -10 dB S_{11} bandwidth of the size reduced antenna was 0.88 GHz or 27.8%. The radiation efficiency was not affected with this size reduction technique. Further size reduction was achieved using more than one slits in the dipole arm. The radiation efficiency was reduced with increasing slits in the dipole arm. However, it remained above 90% for all cases. Another technique for the size reduction was vertically extending the dipole arms. In this technique, the dipole arm length was 17.5 mm and the dipole reflector length was 40 mm. The original dipole-reflector length was 45 mm. Therefore, about 11.1% size reduction was realized for this case. In order to further reduce the size, these two techniques were combined. A miniaturized antenna was designed with two slits in a shaped dipole arm and about 20%

size reduction was achieved. The antenna was simulated and the -10 dB S_{11} bandwidth was 0.94 GHz or 28% impedance bandwidth was achieved. The radiation patterns were also stable at 3 GHz frequency range. The miniaturized feed antenna was fabricated and measured in the laboratory for a comparison with the simulations results. The simulation and measured results agreed well. The feed antenna was measured with the 45 cm reflector and the measured gain of the reflector was 20.3 dBi at 3.06 GHz or the efficiency of the reflector was 55.2%.

The microstrip dipole feed was also modified for the dual frequency operation. The original dipole arms were etched, which looked like a folded dipole arm and another dipole arm was incorporated in this folded dipole arm. Thus a dual frequency operation was achieved. The dual frequency microstrip dipole feed was designed for 3 and 3.5 GHz. The -10 dB S_{11} bandwidth was 10% at 3 GHz and 4.5% at 3.5 GHz. The radiation patterns of the dual frequency feed were also satisfactory in both frequency bands. The frequency of operation could be tuned by changing the length of the inner dipole arm. The dual frequency feed was fabricated and measured in the laboratory. The measured and simulated S_{11} agreed with each other. The dual frequency feed was also measured with the 45 cm reflector and the reflector efficiency was 55.2% at 3.08 GHz and 55.3% at 3.52 GHz, respectively.

The main limitations of microstrip dipole feeds were unequal E- and H-plane radiation patterns which were the cause of low aperture efficiency. The modified microstrip dipole antennas were designed to equalize the E- and H-plane radiation patterns. Two different techniques were used for this purpose. First, the microstrip dipole arms were bent to the direction of radiation, which changed the surface current

distribution affecting the radiation characteristics, making the patterns equal. The feed antenna was designed similar to microstrip dipole feed, except the dipole arms were bent. The simulated -10 dB S_{11} bandwdith was 0.1 GHz or 3.3%. The radiation patterns of the feed antenna were equal up to 58^0 at 3 GHz. The cross-polarization level at 45^0 plane and back lobe level of the antenna were -13 dB and -8 dB, respectively. The performance of the feed in terms of the gain factor, spillover and illumination efficiencies was studied. The gain factor was found to be 63.2% at f/D = 0.41 or at an aperture angle of 63^0. The phase center of the feed antenna was also determined to get optimized secondary patterns. The feed antenna was fabricated in the laboratory. The measured results agreed with the simulation results. The feed was also measured with the 45 cm reflector and the gain was found to be 19.8 dBi at 3 GHz or 52% efficiency was achieved.

To improve the back lobe level, another dipole-reflector was added with the bent dipole antenna, retaining pattern equalization. The simulated -10 dB S_{11} bandwidth of the double dipole-reflector feed was 0.09 GHz or 3% impedance bandwidth was achieved. The radiation patterns were equal up to 71^0 at 3 GHz, with back lobe level of -17.5 dB. The cross-polarization level at 45^0 plane was the same as the previous case. The performance in terms of the gain factor, spillover and illumination efficiencies was studied. The gain factor was 62.3% at f/D = 0.32 or an aperture angle of 76^0. The phase center of the feed was also determined. The double dipole-reflector feed was fabricated in the laboratory. The measured results agreed with the simulation results. The feed was measured with the 45 cm reflector and the gain was found to be 20.4 dBi at 3 GHz, or 55% efficiency was achieved.

The input impedance bandwidth of these bent microstrip dipole antennas was narrow and radiation patterns degrade after the center frequency. To improve the input impedance, while retaining pattern equalization, the corrugated microstrip dipole feed was designed. The -10 dB S_{11} bandwidth of the antenna was 0.76 GHz or 23.5% impedance bandwidth was achieved. The radiation patterns of the feed were equal up to 90^0. The cross-polarization level at 45^0 plane and back lobe levels of the feed were -13 dB and -24 dB, respectively. The radiation efficiency of the feed was also simulated and it was found to be 98.2%. The performance in terms of the gain factor, spillover and illumination efficiencies was calculated. The gain factor was 68.9% at f/D = 0.24 or 92^0 aperture angle. The gain factors for other frequencies were calculated and their value was closed to each other, which indicated the stability of the feed. The phase center of the corrugated dipole feed was also determined. The feed was fabricated in the laboratory. The measured results agreed with the simulation results. The feed was measured with the 45 cm reflector and the gain of the reflector was found to be 21.4 dBi at 3.06 GHz, or the efficiency of the reflector was 66.4%.

6.2 Summary of Contributions

Two different types of feed categories, slotted circular waveguide feeds and microstrip dipole feeds were designed and studied. Slotted circular waveguide feeds were simple, and their diameters were unchanged, so the feeds were easy to fabricate. The potential contributions related to circular waveguide feeds are summarized as follows:

- Slotted circular waveguide feeds (a = 0.35 λ_0) equalized the E- and H-plane radiation patterns and improved their gain factor.
- Slotted circular waveguide feeds with a single choke showed equal radiation patterns with improved gain factor. Multiple chokes were used for further gain factor improvement.
- Slotted circular waveguide feeds with a cavity showed equal radiation patterns with wider beamwidths. This kind of feeds is suitable for deep reflectors.

The performance of slotted circular waveguide is excellent. However, they need struts support and it is hard to integrate them with other circuitry. Therefore, the second categories of feeds, the microstrip dipole feeds, were designed, which were new backward radiating feeds. The primary advantages of these feeds were low profile, simple structure, low cost, ease of fabrication and mount with RF circuits. As the feeds were radiating backward, they were mounted on the reflector using a semi rigid cable and thus eliminated the struts support. The potential contributions related to microstrip dipole feeds are summarized as follows:

- Microstrip dipole feeds were introduced as a new backward radiating feeds, which were designed for reflectors with elliptical apertures.
- Demonstrated the technique for improving the radiation pattern symmetry about the boresight axis of the microstrip dipole feed.
- Designed and investigated the input impedance broadening, size reduction and dual frequency operation of the microstrip dipole feed.

- Modified microstrip dipole feeds were designed and investigated for radiation pattern equalization so that the feeds could be used with circular symmetric reflectors.

6.3 Future Work

This thesis dealt electrically small feed antennas for prime focus reflectors. While the primary findings of these feeds were implemented, there are some areas, which need further investigation. The circular waveguide used in this research had a radius of 0.35 $\lambda_{0,}$ and wall thickness of 1 mm. The effects of the slots with other waveguide diameters and wall thickness were not investigated and therefore can be explored for further study. For slotted waveguide with choke, the waveguide face and choke face were on the same level. However, the effects of choke height with respect to waveguide face can be investigated. In case of multiple chokes, slots were used only with the waveguide. But the effect of slots at choke wall may be studied. The same studies might be done for multiple cavity feed case.

For microstrip dipole feeds the cross-polarization level of the feed was reasonable but not low. Further study can be conducted to design a feed with low cross-polarization. The bandwidth of the microstrip dipole feed antenna was 29%, which might be improved by further study. The asymmetrical E- and H-plane radiation patterns, with respect to the radiation axis, were improved by using unequal dipole arms. Further study is needed to improve the radiation pattern symmetry with axis. At high frequencies, spurious feed line

radiation increased the side lobe level of the feed. Therefore, further study is needed to improve the side lobe level.

Microstrip dipole feed had inherently unequal E- and H-plane radiation patterns. Equalization was possible by modifying the dipole arms. However, there are further scopes to improve the pattern equalization of microstrip dipole feed. For bent microstrip dipole cases, the input impedance bandwidth was very low, which can be improved by further study. For corrugated microstrip dipole feed the cross-polarization level was reasonable, further study is needed to improve the cross-polarization level. For the same feed, the gain factor was high, beyond the aperture angle of 90^0 that means the feed is also suitable for other antennas, such as the back fire antennas. A detail study might be carried out in future on back fire antennas using this feed.

Bibliography

[1] H. Hertz, *Electric Waves*. London, UK: Macmillan, 1983.

[2] Significant Achievements in Space Communications and Navigation 1958-1964, NASA-SP-93, 1966, Retrieved 2010-10-31.

[3] Keyvan Bahadori, *Spaceborne Reflector Antennas for Advanced Remote Sensing Applications*.: BiblioBazaar, 2011.

[4] K. Sarabandi and T. Chiu, "Optimum corner reflectors for calibration of imaging radars," *IEEE Trans. Antennas Propagat.*, vol. 44, no. 4, pp. 1348-1361, Oct. 1996.

[5] I.M. Davis, J.S. Kot, C. Granet, and K. Verra, "Compact shaped dual reflector system for military Ka-Band SATCOM on the Move," in *EuCAP*, Rome, 2011.

[6] A. D. Olver, P.J.B. Clarricoats, A. A. Kishk, and L. Shafai, "Introduction," in *Microwave Horns and Feeds*. New York, NY: IEE Electromagnetic Waves Series 39, 1994, ch. 1, pp. 1-15.

[7] A. W. Love, *Electromagnetic Horn Antennas*. New York, NY: Peter Peregrinus, IEEE Electromagnetic Series 15, 1976.

[8] A. Ludwig, "The definition of cross polarization," *IEEE Transactions on Antennas and Propagation*, vol. 21, no. 1, pp. 116-119, January 1973.

[9] S. Silver, *Microwave antenna theory and design*. London, UK: Peter Peregrinus Ltd, 1984.

[10] Harry R. Anderson, *Fixed Broadband WirelessSystem Design*.: Wiley, 2003.

[11] P. J. B. Clarricoats and G. T. Poulton, "High efficiency micowave reflector antennas - A review," *Proceedings of the IEEE*, vol. 65, pp. 1470-1504, Oct. 1977.

[12] R. E. Collin, *Antennas and Radiowave Propagation*. New York, NY: McGraw-Hill Book Company, 1985.

[13] P.-S. Kildal, *Foundations of Antennas - A Unified Approach*. Lund, Sweden: Studentlitteratur, 2000.

[14] Pattan Bruno, *Satellite systems: principles and technologies*. USA: Springer, 1993.

[15] D. Carter, "Phase centers of microwave antennas," *IRE Transactions on Antennas and Propagation*, vol. 4, no. 4, pp. 597-600, Oct. 1956.

[16] W. V. T. Rusch and P. D. Potter, *Analysis of reflector antennas*. New York, NY: Academic press, 1970.

[17] L. Mania, "The antenna phase center in Satellite Radio-Doppler Geodetic Systems," *IEEE Trans. Geoscien. Remote Sens.*, vol. 20, pp. 536-543, Oct. 1982.

[18] P.- S. Kildal, "Combined E- and H-plane phase centers of antenna feeds," *IEEE Trans. Antennas Propagat.*, vol. 31, pp. 199-202, Jan. 1983.

[19] K. S. Rao and L. Shafai, "Phase center calculations of reflector antenna feeds," *IEEE Trans. Antennas Propagat.* , vol. 32, pp. 740-742, Jul. 1984.

[20] H. Moheb, A. Sebak, and L. Shafai, "Phase centre analysis of array antennas and its significance for microwave landing system," in *Seventh International Conference on (IEE) Antennas and Propagation*, Apr. 1991, pp. 213-216.

[21] A. Helaly, A. Sebak, and L. Shafai, "Phase centre movement in linear phased array antennas," in *Antennas and Propagation Society International Symposium*, May, 1990, pp. 1166-1169.

[22] L. Shafai and A. A. Kishk, "Prime-focus Waveguide Feeds," in *Microwave Horns and Feeds*. New York, NY: IEE Electromagnetic Waves Series 39, 1994, ch. 7, pp. 181-209.

[23] G. L. James and K. J. Greene, "Effect of wall thickness on radiation from circular waveguides," *Electron. Lett.*, vol. 14, pp. 90-91, Feb. 1978.

[24] G. L. James, "The radiation performance of flanged waveguides," CSIRO, Division of Radiophysics Rep, RPP 2033(L), 1978.

[25] C. A. Mentzer, JR., L. Peters, and F.B. Beck, "A corrugated horn antenna using V-shape corrugations," *EEE Trans. Antennas Propagat.*, vol. 23, pp. 93-97, Jan. 1975.

[26] A. A. Kishk, L. Shafai, and A. Ittipiboon, "Performance of a small primary feed with trapezoidal and sinusoidal corrugations," *Electron. Lett.*, vol. 19, pp. 297-298, Apr. 1983.

[27] G. F. Koch, "Coaxial feeds for high aperture efficiency and low spillover paraboloidal reflector antennas," *IEEE Trans. Antennas Propagat.*, vol. 21, pp. 164-169, Mar. 1973.

[28] R. Wohlleben, H. Mattes, and O. Lochner, "Simple small primary feed for large opening angles and high aperture efficiency," *Electron. Lett.*, vol. 8, pp. 474-476, Sep. 1972.

[29] L. Shafai, "Broadening of primary feed patterns by small E-plane slots," *Electron. Lett.*, vol. 13, pp. 102-103, Feb. 1977.

[30] H. Scheffer, "Optimale dimensionierung von koaxialerregern fur parabola antenna," *Nachrichtentech Z.*, vol. 24, pp. 137-142, 1971.

[31] C. Kim and W. Rhoden, "Radiation pattern analysis of coaxial cavity feed horn," in *Antennas and Propagation Society International Symposium*, vol. 64, 1986, pp. 95-98.

[32] A. A. Kishk, "Simple primary focus feeds for deep reflectors," *IEE Proc.H, Microwaves, Antenna and Propag.*, vol. 136, pp. 169-171, Apr. 1989.

[33] S. Silver, "Microwave dipole antennas and feeds," in *Microwave Antenna Theroy and Design*, S. Silver and H. M. James, Eds. London, UK: Peter Peregrinus Ltd, 1984, ch. 8, pp. 239-256.

[34] L. Shafai and A. A. Kishk, "Dipole feeds," in *Microwave Horns and Feeds*. New York, NY: IEE Electromagnetic Waves Series 39, 1994, ch. 13, pp. 419-422.

[35] J. D. Kraus and R. J. Marhefka, *Antennas For All Applications*, 3rd ed.: McGraw-Hill, 2001.

[36] P. D. Potter, "A new horn antenna with suppressed sidelobes and equal beamwidths," *The Microwave Journal*, Jun. 1963.

[37] W. C. Jakes, "Horn Antennas," in *Antenna Engineering Handbook*, H. Jasik, Ed. New York, USA: McGraw-Hill, 1961, ch. 10.

[38] P.-S. Kildal and S. A. Skyttemyr, "Dipole-disk antenna with beam-forming ring,"

IEEE Trans. Antennas Propagat., vol. 30, pp. 529-534, Jul. 1982.

[39] P.-S. Kildal, "A small dipole-fed resonant reflector antenna with high efficiency, low cross polarization and low sidelobes," *IEEE Trans. Antennas Propagat.*, vol. 33, pp. 1386-1391, Dec. 1985.

[40] P. S. Kildal, S. A. Skyttemyr, and A. A. Kishk, "G/T maximization of a paraboloidal reflector fed by a dipole-disk antenna with ring by using the multiple-reflection approach and the moment method," *IEEE Trans. Antennas Propagat.*, vol. 45, pp. 1130-1139, Jul. 1997.

[41] K. Carven and J. Mink, "Microstrip antenna technology," *IEEE Trans. Antennas Propagat.*, vol. 29, pp. 2-24, Jan. 1981.

[42] P. S. Hall and C. J. Prior, "Microstrip feeds for prime focus fed reflector antennas," *IEE Proc.H, Microwaves, Antenna and Propag.*, vol. 134, pp. 185-193, Apr. 1987.

[43] M. Q. Maula and L. Shafai, "Low-cost, microstrip-fed printed dipole for prime focus reflector feed," *IEEE Trans. Antennas Propagat.*, vol. 60, no. 11, pp. 5428-5433, Nov. 2012.

[44] A. A. Kishk and L. Shafai, "Optimization of microstrip feed geometry for prime focus reflector antennas," *IEEE Trans. Antennas Propagat.*, vol. 37, pp. 445-451, Apr. 1989.

[45] A. A. Kishk and L. Shafai, "The effect of various parameters of circular microstrip antennas on their radiation efficiency and the mode excitation," *IEEE Trans. Antennas Propagat.*, vol. 34, pp. 969-976, Aug. 1986.

[46] C. C. Cutler, "Parabolic-antenna design for microwaves," *Proceedings of the IRE*, vol. 35, no. 11, pp. 1284-1294, Nov. 1947.

[47] A. Chlavin, "A new antenna feed having equal E- and H-plane patterns," *Transactions of the IRE Professional Group on Antennas and Propagation*, vol. 2, no. 3, pp. 113-119, Jul. 1954.

[48] C. C. Cutler, "Ring focus antenna feed," patent 3162858, Dec. 22, 1964.

[49] P. Newham, "A high efficiency splashplate feed for small reflector antennas," in *Fourth International Conference on Antennas and Propagation*, 1985, pp. 420-423.

[50] G. T. Poulton and T. S. Bird, "Improved rear-radiating waveguide cup feeds," in *Antennas and Propagation Socity International Symposium*, vol. 24, 1986, pp. 79-82.

[51] M. Q. Maula and L. Shafai, "Performance of small primary feeds with E- and H-plane slots," in *14th International Symposium on Antenna Technology and Applied Electromagnetics & the American Electromagnetics Conference (ANTEM-AMEREM)*, Banff, AB, Canada, 15-18 Feb. 2009.

[52] M. Q. Maula and L. Shafai, "Phase center study of slotted circular waveguide feed," in *IEEE Antennas Propagat. Soc. Int. Symp.*, Toronto, ON, Canada, 11-17 Jul. 2010.

[53] M. Q. Maula and L. Shafai, "E-plane slotted circular waveguide feed with a single choke," in *15th International Symposium on Antenna Technology and Applied Electromagnetics & the American Electromagnetics Conference (ANTEM-AMEREM)*, Ottawa, ON, Canada, 5-8 Jul. 2010.

[54] D. M. Pozar and D. Schaubert, *Microstrip Antennas: The Analysis and Design of Microstrip Antennas and Arrays*. New York, NY: Institute of Electrical Engineers, 1994.

[55] D. Edward and D. Rees, "A broadband printed dipole with integrated balun," *Microwave Journal*, pp. 339-344, May 1987.

[56] N. Kaneda, W. R. Deal, Y. Qian, R. Waterhouse, and T. Itoh, "A broad-band planar quasi-Yagi antenna," *IEEE Trans. Antennas Propagat.*, vol. 50, pp. 1158-1160, Aug. 2002.

[57] G. Zheng, A. A. Kishk, A. W. Glisson, and A. B. Yakovlev, "Simplified feed for modified printed Yagi antenna," *Electron. Lett.*, vol. 40, pp. 464-466, Apr. 2004.

[58] G. Zheng, A. A. Kishk, A. B. Yakovlev, and A. W. Glisson, "A broad band printed bow-tie antenna with a simplified feed," in *Antennas and Propagation Society International Symposium*, vol. 4, 2004, pp. 4024-4027.

[59] A. A. Eldek, A. Z. Elsherbeni, and C. E. Smith, "Wideband modified printed bow-tie antenna with single and dual polarization for C and X-band applications," *IEEE Trans. Antennas Propagat.*, vol. 53, pp. 3067-3072, Sep. 2005.

[60] W. L. Stutzman and G. A. Thiele, *Antenna Theory and Design*, 2nd ed. New York, NY: Wiley, 1998.

[61] D. M. Pozar, *Microwave Engineering*, 2nd ed. New York, NY: Wiely, 1995.

[62] Ansoft HFSS. (2012, December) Ansoft HFSS web site. [Online]. http://www.ansoft.com/products/hf/hfss/

[63] P-S Kildal, "Factorization of the feed efficiency of paraboloids and cassegrain antennas," *IEEE Trans. Antennas Propagat.*, vol. 33, pp. 903-908, Aug. 1985.

[64] D. M. Pozar, "An update on microstrip antenna theory and design including some novel feeding techniques," *IEEE Antennas Propagat. Soc. Newsletter*, vol. 28, pp. 5-9, Oct. 1986.

[65] E. Chang, S. A. Long, and W. F. Richards, "An experimental investigation of electrically thick rectangular microstrip antennas," *IEEE Trans. Antennas Propagat.*, vol. 34, pp. 767-772, Jun. 1986.

[66] C. H. C. H. Chen, A. Tulintseff, and R. M. Sorbello, "Broadband two-layer microstrip antenna," *in IEEE Antennas Propagat. Soc. Int. Symp.*, pp. 251-254, 1984.

[67] G. Kumar and K. C. Gupta, "Directly coupled multiple resonator wideband microstrip antennas," *IEEE Trans. Antennas Propagat.*, vol. 33, pp. 588-593, Jun. 1985.

[68] H. H. Pues, J. J. Bogaers, R. Pieck, and A. Van de Capel, "Wideband quasi-log-periodic microstrip antenna," *Inst. Elec. Eng. Proc.*, vol. 128, pp. 159-163, Jun. 1981.

[69] H. F. Pues and Van de Capelle A. R., "An Impedance-Matching Technique for Increasing the Bandwidth of Microstrip Antennas," *IEEE Trans. Antennas Propagat.*, vol. 37, pp. 1345-1354, Nov. 1989.

[70] M. Q. Maula and L. Shafai, "Broadband rear radiating printed dipole antenna," in

IEEE Antennas Propagat. Soc. Int. Symp., Spokane, Washington, USA, 3-8 Jul. 2011.

[71] T. K. T. K. Lo, C. O. Ho, Y. Hwang, K. K. W. Lam, and B. Lee, "Miniature aperture-coupled microstrip antenna of very high permittivity," *Electron. Lett.*, vol. 33, pp. 9-10, Jan. 1997.

[72] R. K. Mongia, A. Ittipiboon, and M. Cuhaci, "Low profile dielectric resonator antennas using a very high permittivity material," *Electron. Lett.*, vol. 30, pp. 1362–1363, Aug. 1994.

[73] H. Mosallaei and K. Sarabandi, "Magneto-Dielectrics in Electromagnetics:Concept and Applications," *IEEE Trans. Antennas Propagat.*, vol. 52, pp. 1558-1567, Jun. 2004.

[74] H. Mosallaei and K. Sarabandi, "Antenna miniaturization and bandwidth enhancement using a reactive impedance substrate," *IEEE Trans. Antennas Propagat.*, vol. 52, pp. 2403-2414, Sep. 2004.

[75] J. H. Lu and L. Wong, "Slot-Loaded, Meandered Rectangular Microstrip Antenna with Compact Dual-Frequency Operation," *Electron. Lett.*, vol. 34, pp. 1048-1050, May 1998.

[76] M. Q. Maula and L. Shafai, "Size reduction of a rear radiating microstrip fed printed dipole antenna," in *IEEE Antennas Propagat. Soc. Int. Symp.*, Chicago, IL, USA, 8-14 Jul. 2012.

[77] J-S. Chen and K- L. Wong, "A single-layer dual-frequency rectangular microstrip

patch antenna using a single probe feed," *Microwave Opt. Technol. Lett.*, vol. 11, pp. 83-84, Feb. 1996.

[78] S. A. Long and M. D. Waton, "A dual-frequency stacked circular disc antenna," *IEEE Trans. Antenn. Propagat.*, vol. 27, pp. 281–285, Mar. 1979.

[79] J. S. Dahele, K. F. Lee, and D. P. Wong, "Dual-frequency stacked annular-ring microstrip antenna," *IEEE Trans. Antennas Propagat.*, vol. 35, pp. 1281–1285, Nov. 1987.

[80] J. Wang, R. Fralich, C. Wu, and J. Litva, "Multifunctional aperture-coupled stacked antenna," *Electron. Lett.*, vol. 26, pp. 2067–2068, Jun. 1990.

[81] W. F. Richards, S. E. Davidson, and S. A. Long, "Dual-band reactively loaded microstrip antenna," *IEEE Trans. Antennas Propagat.*, vol. 33, pp. 556–560, May 1985.

[82] S. E. Davidson, S. A. Long, and W. F. Richards, "Dual-band microstrip antenna with monolithic reactive loading," *Electron. Lett.*, vol. 21, pp. 936–937, Sep. 1985.

[83] S. S. Hong and Y. T. Lo, "Single-element rectangular microstrip antenna for dual-frequency operation," *Electron. Lett.*, vol. 19, pp. 298–300, Aug. 1983.

[84] S. Maci, G. Avitabile, and G. B. Gentili, "Single-layer dual frequency patch antenna," *Electron. Lett.*, vol. 29, pp. 1441–1443, Aug. 1993.

[85] S. Maci, G. B. Gentili, P. Piazzesi, and C. Sa, "Dual-band slot-loaded patch antenna," *IEEE Proc. Microw. Antennas Propag.*, vol. 142, pp. 225–232, Jun. 1995.

[86] W. S. Chen, "Single-feed dual-frequency rectangular microstrip antenna with square

slot," *Electron. Lett.*, vol. 34, pp. 231-232, Mar. 1998.

[87] K. Wong and W. Chen, "Compact microstrip antenna with dual-frequency operation," *Electron. Lett.*, vol. 33, pp. 646–647, Aug. 1997.

[88] F. M. Landstorfer and R. R. Sacher, *Optimisation of Wire Antennas*. Letchworth, Hertfordshire, England: Research Studies Press Ltd., 1995.

[89] M. Q. Maula and L. Shafai, "A corrugated printed dipole antenna with equal beamwidths," *Submitted in IEEE Trans. Antennas Propagat.*